Electrostatics at the nanoscale in aqueous solutions: a field theory approach

Hélène Berthoumieux

PSL UNIVERSITÉ PARIS

HABILITATION À DIRIGER DES RECHERCHES

DE L'UNIVERSITÉ PSL

Préparée à ESPCI–PSL

Mémoire d'habilitation à diriger les recherches
Electrostatics at the nanoscale in aqueous solutions: a field theory approach

Habilitation soutenue le

Le 29 Novembre 2023

par

Hélène Berthoumieux

Spécialité

Physique

Composition du jury :

Marie-Laure BOCQUET Directrice de Recherche, ENS Paris		*Examinatrice*
Matej KANDUČ Professeur, Jožef Stefan Institute, Ljubljana		*Rapporteur*
Manoel MANGHI Maître de Conférences, U. Paul Sabatier, Toulouse		*Rapporteur*
Susan PERKIN Professeur, University of Oxford		*Examinatrice*
Benjamin ROTENBERG Directeur de Recherche, Université Sorbonne		*Rapporteur*

ESPCI PARIS | PSL

Contents

Chapter 1

Overview

Water is the most abundant fluid on Earth and a prerequisite for life on this planet. Water as a solvent plays an essential role in assisting a broad range of nanometric machines in their functions, proteins[1, 2] or nanocapacitors [3] to name a few. It is also a puzzling liquid presenting, despite the simplicity of its molecule - two atoms of Hydrogen and one atom of Oxygen, many anomalous properties. Its expansion on freezing and its density maximum at 4 °C are probably the most famous. A network of Hydrogen bonds net structures the fluid. The strength of these interactions and the cavities created by the spacial organization they generate is one of the origins of these anomalous properties [4].

In this work, I focus on the dielectric properties of water at normal temperature and pressure. The electrostatic interactions between weakly charged objects separated by tens of nanometers can be described by the relative dielectric permittivity of water, $\epsilon_b \approx 80$. Still, things get more complicated for highly charged objects separated by nanometric distances. At molecular scales, water possesses peculiar dielectric properties that result from the hydrogen-bond network structuring the fluid and correlating water dipole orientations over about one nanometer [5]. These properties are encoded in the non-local (*i.e.* q-dependent) dielectric tensor $\epsilon_{ij}(\vec{q})$ - where $\vec{q}$ is the wave number - which determines the response of the liquid to charges at distances characteristic of the water surface. Moreover, under high electrostatic excitation, the polarization response of water tends to saturate [6]. Water's nonlocal and nonlinear dielectric properties are crucial to describe interfacial aqueous systems. Note that nonlocal electrostatics for polar fluid is an old field, and many questions have been developed in the seventies and eighties [7, 8, 9]. However, interest in these approaches has waned, partly because of the lack of experimental results at these scales and because the development of simulations of aqueous systems supplemented it.

The experimental study of confined electrolytic systems is currently expanding rapidly. In the last decades, important experimental obstacles have been overcome, making it possible to design a slab of water confined between surfaces with atomic precision for the slab thickness [10, 11, 12]. New spectroscopy methods now give access to the molecular orientation of water in such systems [13, 14]. This has led to recent and unexpected results reporting anomalous structural and dynamical properties of confined electrolyte systems. These results renewed interest in the nonlocal electrostatic field that could be a simple analytical tool to analyze such experiments. In recent years, I have developed functionals of polarizations for systems increasing complexity to answer the questions: What governs electrostatic interactions at the nanoscale in aqueous electrolytes? How does confinement affect the dielectric properties of these systems?

The manuscript is organized as follows. In the first chapter, I briefly present my scientific career. In the second chapter, I focus on the description of bulk water as a linear correlated medium. I describe the main features of the dielectric correlations in water and present functionals of varying complexity that allow us to capture them. In the third chapter, I describe the effects of the nonlinear dielectric properties of the fluid and show how to include them in a field theory. In the fourth chapter, I describe the response of water to inclusion and focus on the

response to ions. The sixth chapter is devoted to describing the dielectric permittivity of bulk electrolytes. In Chapter 7, I consider water and aqueous electrolytes confined between solid surfaces and describe the coupling between structure and confinement. I present a perspective of this work in chapter 9. In appendices, you can find my other topics of research, briefly described; a complete list of publications; my supervision activities; my teaching activities; and finally, my involvement in research organization.

Chapter 2

Scientific career

I did my PhD in the Department of Chemistry of Ecole Normale Supérieure in Paris, under the supervision of Ludovic Jullien. I was co-supervised by Annie Lemarchand, a researcher in the LPTMC - the lab of theoretical physics of condensed matter at the University of Sorbonne Sciences University. One of our goals was to design new protocols to analyze complex reactive mixtures. We considered a mixture of DNA strands of varying sequences. We proposed theoretical methods to quantify a given couple characterized by its binding/unbinding rate constants, and we validate this method experimentally [15, 16].

After my PhD, I did a one-year postdoctoral stay in Gulliver, ESPCI, in Paris, under the supervision of Anthony C. Maggs. I worked on the Van der Waals interactions in atomic fluids. Moreover, under the influence of Anthony, I started to be interested in the dielectric properties of water[17]. Then, I spent two years in the Max Planck 'Physics of Complex Systems' of Dresden, Germany, under the supervision of Frank Jülicher. During this stay, I worked with the biologists Jean-Léon Maître and Carl-Philip Heisenberg on the impact of cell adhesion in cell differentiation and cell sorting during development of embryos [18]. I also worked with Guillaume Salbreux on the theoretical modeling of active surfaces. In particular, we studied the deformation driven by active moments in cell shells [19].

In October 2011, I got a CNRS position as a "chargée de recherche," and I joined Annie Lemarchand's team at LPTMC, Sorbonne Sciences. After a few years and two maternity leaves - Otto in 2014 and Camille in 2016 - I started to work on my own research project: the dielectric properties of water and electrolytes at the nanoscale [20]. Thanks to a small CNRS grant, I invited Alexei Kornyshev, professor at Imperial College, London, to a visit in Paris, and we started to collaborate on the dielectric properties of confined water. At the same time, I was awarded the Emergence Sorbonne Grant, and I hired a postdoctoral student, Geoffrey Monet, whom I co-supervised with Alexei Kornyshev for 16 months [12, 21]. I currently co-supervise a PhD student of Alexei Kornyshev, Jonathan Hedley, with whom I worked on hydration forces in electrolytes [22]. I also collaborated with Ralf Blossey on modeling water under high electrostatic fields [23]. In parallel, I started to work on active membranes. With Anne-Florence Bitbol, (EPFL, Lausanne) we modeled theoretically mithocondria membrane [24, 25]. I supervised two interns (Nirbay Patil, M1 ENS) and Toni Mendes, M2 in this project. Today I supervise a PhD student Yorgos Chatziantoniou on this topic (2023-2026).

In 2021-2022, I spent one sabbatical year in the group of Roland Netz, in the Freie Universitat, Berlin. A Humboldt experienced researcher grant financed this stay. I kept working on the modelisation of electrolytes at the nanoscale, but I focused on the simulations of these systems. I met there Marie-Laure Bocquet, with whom I work on a description of ion-surface interaction [26].

In September 2022, back to Paris, I joined the lab of Gulliver as a permanent researcher, I was awarded of the CNRS emergence grant and could hire Darka Lavavić as a postdoc to work on the charge-surface interaction. I started to work with Vincent Démery, assistant professor

in Gulliver, on the transport of ions in aqueous electrolytes. We investigate the effects of water structure on ion transport [27].

Chapter 3

Water as a continuous correlated medium

3.1 Introduction

Because of its importance, water is the most studied liquid. This has led to a wide variety of models for simulating this system. Always-more-sophisticated classical atomistic models of water are developed, giving access to many microscopic details for the system. In this manuscript, we use SPC/E and the family of TiPnP models [28]. They represent water molecules as rigid bodies and describe electrostatic interactions between effective atomic point charges via Coulomb potentials. The repulsive and dispersion interactions are modeled as Lennard-Jones (LJ) potentials. The number, position, and values of the charges and LJ centers vary from one model to another. There exists more complex classical models for water, including polarizability and/or flexibility of the molecules, that we do not use or discuss here [29]. The rigid models give very good results for bulk ambient water. However, they lead to an uncontrolled lack of precision when modeling atoms as Lennard-Jones centers discarding its intimate electronic structure. This could be of particular importance for interfacial water, which couples with electronic degrees of freedom of the confining surface [30].

The ab initio molecular dynamics (AIMD) gives access to the electronic density of the system. The most common approach in this context is the density functional theory (DFT) with the Born-Oppenheimer approximation. The many-body particle problem can thus be reformulated into a many-body electronic problem and expressed as the electronic density [31]. This approach necessitates important computational resources that could be lightened with the use of machine learning algorithm [32]. As for classical simulations, these approaches give a "brute force" solution to one specific problem and should be run again for a different one as they do not furnish a "master" equation governing the properties of an ensemble of systems.

Classical continuous models for water using density as an order parameter, based on Landau-Ginzburg expansion of the energy [33] or writing the free energy as a density functional [34] have brought an important contribution to the field of the physics of liquids, clarifying the structural response of the fluid to microscopic and macroscopic inclusions by taking into account short and long-range density fluctuations [35, 36, 37]. However, these models focus on density effects, not electrostatic interactions. Thus, They are not the ideal starting point for developing a continuous model for electrolytes.

Description of water as a continuous nonlocal dielectric medium was first envisaged by A. Kornyshev and coworkers, which proposed a Landau-Ginzburg functional of the density and the polarization for the energy of the fluid [7, 8, 38]. A decade later, Anthony Maggs focused on polarization [39] and proposed a functional that catches the main features of the charge structure factor of water. Finally, Borgis and coworkers are developing a functional of density and polarization (MDFT) for the free energy of water but based on a numerical approach [40].

This chapter aims to construct and characterize a platform of phenomenological Landau-Ginzburg functionals of polarization and of the polarization and the density that describe the dielectric properties of water at the nanoscale. We restrict the discussion in this chapter to the Gaussian regime. These functionals are built with an increasing complexity but remain always analytically tractable. The goal is to identify the essential blocks leading to a comprehensive description of the structural properties of water at the nanoscale. They will be used in the following as starting points to study the dielectric properties of more complex systems such as electrolytes or confined water.

This chapter is organized as follows. After a quick reminder of electrostatics in a dielectric medium, we present the seminal functional of the polarization that captures the key features of water dielectric properties with as few parameters as possible [39]. Then, we introduce a second model based only on the polarization, but we consider here two polarization fields associated with different ranges of correlation lengths. Finally, we present a model considering both density and polarization field. The last part is devoted to the conclusion.

3.2 Electrostatics in water

3.2.1 Electrostatics in a simple medium

We begin here with a quick reminder of the properties of linear dielectric media. In vacuum, a punctual ion of charge e and located in $\vec{r} = 0$, associated with the charge distribution $\rho(\vec{r}) = e\delta(\vec{r})$, generates a radial electrostatic field: $\vec{E} = e/4\pi\epsilon_0 r^2 \vec{u}_r$. In a dielectric material, the electrostatic field induced by a charge can be written as:

$$\vec{E} = \frac{\vec{D}}{\epsilon_0} - \frac{\vec{P}}{\epsilon_0}. \tag{3.1}$$

The electrostatic displacement $\vec{D}$ is associated with the response of the vacuum, and the polarization field $\vec{P}$ is associated with the response of the material. A local (non-correlated) linear medium is characterized by a constant relative permittivity ϵ_b. In this case, the electrostatic field generated by a punctual ion obeys: $\vec{E} = e/4\pi\epsilon_b\epsilon_0 r^2 \vec{u}_r$ and the polarization $\vec{P}$ and the excitation $\vec{D}$ are related via the following scalar response functions:

$$\vec{D} = \epsilon_0\epsilon_b\vec{E} \tag{3.2}$$
$$\vec{P} = \chi\vec{D} \tag{3.3}$$

with χ the dielectric susceptibility of the medium:

$$\chi = 1 - 1/\epsilon_b. \tag{3.4}$$

Gauss' law gives the relation between these fields and the free (ionic) and bond (polar solvent) charges in the medium as follows:

$$\nabla \cdot \vec{D} = \rho_{\text{ions}}, \nabla \cdot \vec{P} = -\rho_b \tag{3.5}$$

where ρ_{ions} is the density of free charges and ρ_b the density of bond charges.

Most of the models we are going to introduce in this manuscript are based on a functional of polarization. We thus briefly derive the widely used Poisson-Boltzmann equation and its linearized form, the Debye-Hückel equation, as functions of the field $\vec{P}$ [41]. We write the three coupled equations that correspond to the Poisson-Boltzmann equation, expressed as a function of $\vec{P}$:

$$\frac{\epsilon_b}{\epsilon_b - 1}\nabla\vec{P} = ec, \quad c = c_0 e^{-\beta e\phi}, \quad \vec{P} = -\epsilon_0(\epsilon_b - 1)\vec{\nabla}\phi \tag{3.6}$$

where c is the local volumic concentration of free charges, c_0 its mean value, e the charge of a free charge, β the inverse of the temperature. Linearizing the system, we obtain the Debye-Hückel equation as follows:

$$\epsilon_b \vec{\nabla}\left(\nabla \cdot \vec{P}\right) = \frac{\beta e^2 c_0}{\epsilon_0}\vec{P}. \tag{3.7}$$

For molecular media like liquid water, things get more complicated. Indeed, as the fluid is associated via intermolecular interactions as strong as H-bond, the polarization response in a point $\vec{r}$, $\vec{P}(\vec{r})$, is not directly proportional to the excitation in this point $\vec{D}(\vec{r})$, but depends on the excitation throughout the medium as follows:

$$\vec{P}(\vec{r}) = \int d\vec{r'}\chi(\vec{r},\vec{r'})\vec{D}(\vec{r'}). \tag{3.8}$$

The susceptibility $\chi(\vec{r},\vec{r'})$ is a tensor, as $\vec{P}$ and $\vec{D}$ are vectors and depends on the two points $\vec{r}$, $\vec{r'}$. It is possible to derive this tensor via experimental data or using MD simulations, as we present in the next section.

3.2.2 Dielectric susceptibility of water

The dielectric properties of bulk water are thus encoded in the two-point susceptibility tensor. It is related to the permittivity as follows: $\chi(\vec{r},\vec{r'}) = \delta(\vec{r}-\vec{r'}) - \epsilon^{-1}(\vec{r}-\vec{r'})$, see Eq. (3.4). This nonlocal kernel can be expressed through the correlations of the polarization $\vec{P}$ using the classical approximation for the fluctuation-dissipation theorem[1],

$$\chi(\vec{r},\vec{r'}) = \frac{\langle \vec{P}(\vec{r})\vec{P}(\vec{r'})\rangle}{\epsilon_0 k_B T}. \tag{3.9}$$

with k_B the Boltzmann constant and T the temperature. The polarization can be decomposed in a longitudinal part $\vec{P}_{\parallel}(r)$ and a transverse part $\vec{P}_{\perp}(r)$ defined as follows:

$$\vec{P} = \vec{P}_{\parallel} + \vec{P}_{\perp}, \quad \nabla \cdot \vec{P}_{\perp}(r) = 0, \quad \nabla \times \vec{P}_{\parallel}(r) = \vec{0}. \tag{3.10}$$

Using the translational invariance of the medium, the susceptibility can be decomposed in Fourier space in a longitudinal part $\chi_{\parallel}(q)$ and a transverse part $\chi_{\perp}(q)$ as follows:

$$\chi_{ij}(q) = \chi_{\parallel}(q)\frac{q_i q_j}{q^2} + \chi_{\perp}(q)\left(\delta_{ij} - \frac{q_i q_j}{q^2}\right) \quad \text{where } (i,j) \in \{x,y,z\}^2. \tag{3.11}$$

The longitudinal correlations $\langle \vec{P}(\vec{r})\vec{P}(\vec{r'})\rangle$ can be decomposed in terms of the experimentally measured partial HH, OH, OO structure factors of water[43] under the assumption of simple charge distribution in the molecule [5].

It is also possible to compute both the transverse and longitudinal correlation functions for the polarization using classical molecular dynamics simulations of neat water [5, 38, 40, 44]. The figure 3.1 shows the longitudinal $\chi_{\parallel}$ and transverse $\chi_{\perp}$ susceptibility in Fourier space (panel a and b, blue markers) derived from classical molecular dynamics (MD) simulations with the 3 point charge water model TIP4p/ϵ [45]. The simulation methods are detailed in ref. [46]. Note that this kernel has been computed for other rigid explicit models (SPC/E, Tip3p, etc.), leading to qualitatively similar response functions. The $q-$dependence of the susceptibility in Fourier space illustrates the nonlocal nature of water. The $q = 0$ susceptibility, corresponding to long-range properties, is associated with the bulk permittivity ϵ_b as follows

[1] There is a more general formulation taking into account quantum corrections[42] that is not considered here for due to the model simplicity.

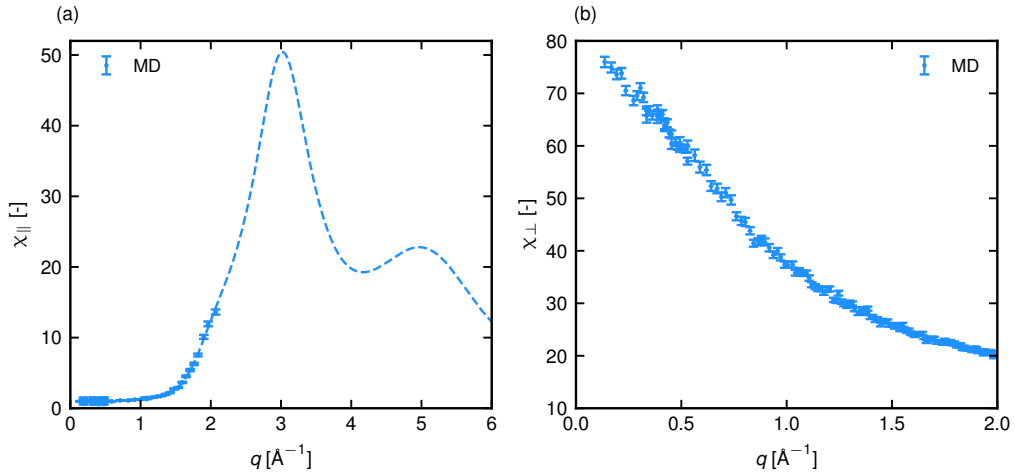

Figure 3.1: **MD simulated susceptibilities for bulk water.** (a) Longitudinal susceptibility (b) transverse susceptibility in Fourier space with TIP4p/ϵ [45] model.

$\epsilon_b = 1/(1-\chi_\parallel(0))$. MD data show an "overresponse" of the system, which corresponds to $\chi_\parallel^{\mathrm{w}}(q) > 1$, around q=3 Å^{-1}. This leads to a q-region associated with a negative permittivity - as $\epsilon(q)$ obeys $\epsilon(q) = 1/(1-\chi_\parallel^{\mathrm{w}}(q))$. This phenomenon is named "overscreening" [5] and was discussed for the first time about 30 years ago. It can be attributed to the H-bond network structuring water at short range [38]. Two ions of the same/opposite charges separated by a small distance could feel an attractive/repulsive force to reach a distance corresponding to a non-disrupting H-bond network between them.

The transverse susceptibility (Fig. 3.1 (b)) shows a spectrum of simpler shape as it monotonously decays.

3.3 Nonlocal electrostatic model for water

In collaboration with Anthony Maggs.

We have seen in the last sections that at the nanoscale, water is not a simple fluid characterized by a constant permittivity but presents correlation modes that are going to play a role in electrostatics at the nanoscale. We present here the seminal phenomenological model for water that we are going to use as a reference in the rest of this manuscript. This model was first introduced by Anthony C. Maggs and Ralf Evarers [39]. It encodes the polarization correlations of water at the nanoscale and is analytically tractable.

We start by writing an electrostatic energy for the fluid as a functional of the polarization as follows:

$$\mathcal{U}_{\mathrm{el}}[\vec{P}] = \frac{1}{2}\int d\vec{r}d\vec{r}' \frac{\nabla\cdot\vec{P}(\vec{r})\nabla\cdot\vec{P}(\vec{r}')}{4\pi\epsilon_0|\vec{r}-\vec{r}'|} + \mathcal{U}_{\mathrm{conf}}[\vec{P}]. \tag{3.12}$$

The first term corresponds to the bare Coulomb interaction between the partial charges $-\nabla\cdot\vec{P}(\vec{r})$ and $-\nabla\cdot\vec{P}(\vec{r}')$ of the fluid. The second term corresponds to the configurational energy of the fluid. To model the nonlocal properties of water, we use a Landau-Ginzburg approach to give an explicit expression of $\mathcal{U}_{\mathrm{conf}}[P]$ [39]. This functional contains only terms quadratic in $\vec{P}$. In the following, we will call it the "Gaussian" model as the associated partition function is Gaussian in $\vec{P}$ or "linear" model, as the polarization response to a perturbation is proportional to the perturbation (see Chapter 4 for examples). A Landau-Ginzburg expansion is based

on a gradient expansion for the energy density. We first write a term quadratic in the field, $K\vec{P}^2$. Then, we include two terms quadratic in the first spatial derivative of the fields. We write $\kappa_l(\boldsymbol{\nabla}\cdot\vec{P})^2$, which includes the derivative of the longitudinal contribution of the field and $\kappa_t(\boldsymbol{\nabla}\times\vec{P})^2$ which includes the derivative of the transverse contribution. The coefficients κ_l and κ_t are named Landau-Ginzburg coefficients. They are homogeneous to $[L^2]$, and we thus see that these terms introduce characteristic lengths in the model of the system. Finally, we add a quadratic term in the second derivative of the longitudinal polarization, $\alpha(\boldsymbol{\nabla}(\boldsymbol{\nabla}\cdot\vec{P}))^2$. The corresponding expression,

$$\mathcal{U}_{\rm conf}[\vec{P}] = \frac{1}{2\epsilon_0}\int d\vec{r}\Big[K\vec{P}(\vec{r})^2 + \kappa_l(\nabla\cdot\vec{P}(\vec{r}))^2 + \kappa_t(\boldsymbol{\nabla}\times\vec{P}(\vec{r}))^2 + \alpha(\nabla(\boldsymbol{\nabla}\cdot\vec{P}(\vec{r})))^2\Big] \quad (3.13)$$

can capture the main features of dielectric properties of water at the nanoscale [17, 21]. The polarization susceptibility χ, defined as follows

$$\mathcal{U}_{\rm el}[\vec{P}] = \frac{1}{2}\int d\vec{r}\int d\vec{r'}\vec{P}(\vec{r})\cdot\chi^{-1}(\vec{r},\vec{r'})\cdot\vec{P}(\vec{r'}), \quad (3.14)$$

is obtained by inversion of Eq. (3.12) and can be decomposed in Fourier space in a longitudinal $\chi_\parallel$ and a transverse $\chi_\perp$. Their expressions follow from Eq. (3.13) as

$$\chi_\parallel(q) = \frac{1}{1+K+\kappa_l q^2+\alpha q^4}, \quad \chi_\perp(q) = \frac{1}{K+\kappa_t q^2}. \quad (3.15)$$

As one sees, the susceptibilities are now functions of the wavenumber q, illustrating the nonlocality of the modeled medium. For the longitudinal susceptibility, we consider the case ($\kappa_l < 0$, $\alpha > 0$), which is associated with a maximum as a function of q. The value of the parameters K, κ_l, and α, are adjusted to fit the bulk value, $\chi_\parallel(0)$, the position and the value of the maximum of $\chi_\parallel(q)$ (q =3 Å^{-1}) of the the MD simulated response. Note that the secondary peak observed for q >4 Å^{-1} corresponds to intramolecular correlations and to length scales that are not addressed in this study. The parameter κ_t is chosen to fit the decay of MD data. Fig. 3.2 shows the response functions given in Eq. (3.15) (panels a and b, black line) for the values of the parameters given in the caption. The longitudinal susceptibility $\chi_\parallel(q)$ is associated with two correlation lengths: a longitudinal decay, λ_d, and an oscillation length λ_o, defined as the imaginary and real part of the inverse of the poles of the function. The transverse susceptibility $\chi_\perp(q)$ is associated with a decay length λ_t, which is the inverse of its pole. We can express these lengths as functions of the phenomenological parameters of the problem. Their expressions obey:

$$\lambda_d = \frac{2\sqrt{\alpha}}{\sqrt{2\sqrt{\alpha(1+K)}+\kappa_l}}, \quad \lambda_t = \sqrt{\frac{\kappa_t}{K}}, \quad \lambda_o = \frac{4\pi\sqrt{\alpha}}{\sqrt{2\sqrt{\alpha(1+K)}-\kappa_l}}. \quad (3.16)$$

Using the estimated values of the parameters, we get a longitudinal decay length λ_d=4.7 Å, an oscillating length λ_o=2.1 Å, and a transverse decay length, λ_t=1.05Å.

When comparing the MD data and the model in Fig. 3.2, one sees that they quantitatively differ. However, the bulk permittivity and the "overscreening" effects are well captured by field theory. Note that a Landau-Ginzburg expansion of the electrostatic energy at larger order in the polarization derivatives would allow for a better reproduction of MD data without bringing any supplementary technical difficulties.

Using this framework, we can now derive an analytical expression for the correlations of the polarizations. We use Eq. (3.9), and calculate the Fourier transform of the susceptibility tensor. Details of the calculations are furnished in ref. ([17]). We write the longitudinal and transverse correlation functions as follows:

$$\langle P(r)P(0)\rangle_\parallel = \frac{1}{2\pi K(K+1)r^3}\left(1+h_\parallel(r)\right), \quad \langle P(r)P(0)\rangle_\perp = -\frac{1}{4\pi K(K+1)r^3}\left(1+h_\perp(r)\right). \quad (3.17)$$

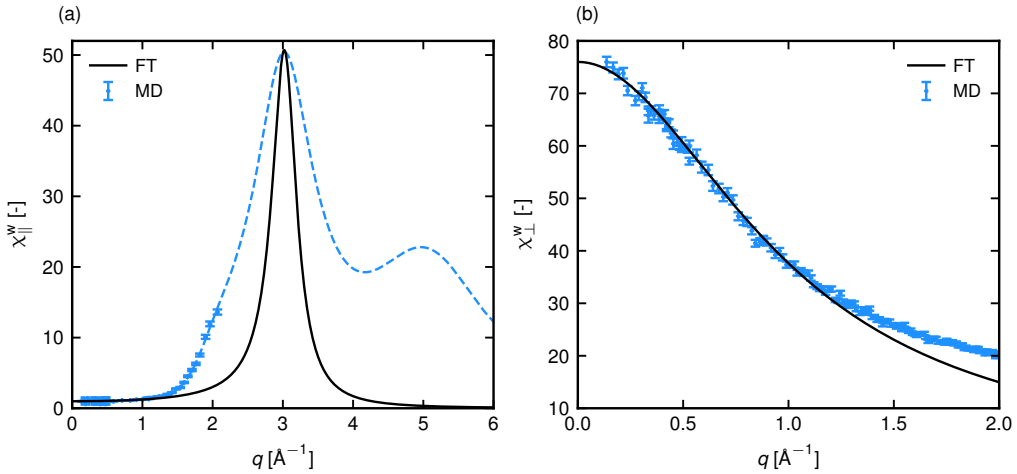

Figure 3.2: **Susceptibilities obtained with FT model.** The parameter values of the FT model are K= 1/76, κ_l= -0.218 Å^2 , α=0.012 Å^4 and κ_t=0.013 Å^2.

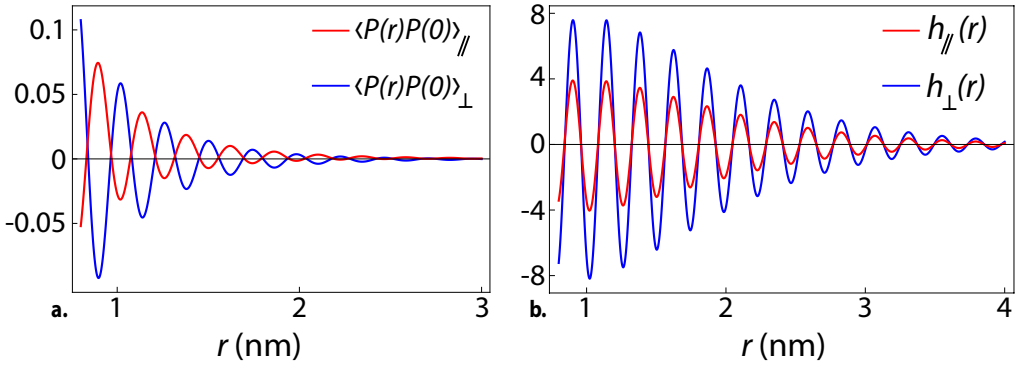

Figure 3.3: Longitudinal $\langle P(r)P(0)\rangle_{\parallel}$ and transverse $\langle P(r)P(0)\rangle_{\perp}$ correlation functions as functions of r (nm). **b.** Longitudinal $h_{\parallel}(r)$ and transverse $h_{\perp}(r)$ short-range correlation terms as a function of the distance r (nm). These functions are plotted for the set of parameters: $\alpha = 0.021$ Å^4, $\kappa_l = -0.29$ Å^2, $\kappa_t = 0.065$ Å^2, $K = 1/70$ [17]

The functions $h_{\parallel}(r)$ and $h_{\perp}(r)$ are functions encoding the correlation lengths of the water at the nanoscale. Their expressions are given in ref. ([17]). For a local medium, the correlations are obtained for $h_i(r) = 0$.

Figure 3.3 shows the longitudinal and the transverse correlations and the functions h_i, (i=$\parallel, \perp$) for a fluid associated with λ_d=0.5 nm and λ_t=0.25 nm (The parameters are here fitted on the MD simulated susceptibility for SPC/E water, in the same manner as described previously). The functions $h_{\parallel}(r)$ and $h_{\perp}(r)$ are oscillating and decaying. The oscillations correspond to the molecular nature of the material and the typical distance between charges at the molecular scale. This structure appears over a few λ_d, the correlation range of the fluid. After this range, a local description is recovered ($h_i(r) \approx 0$). Note that experiments and simulations indicate that for water, the correlations extend on a range of 1 nm [47].

The figure 3.4 (b) compares the longitudinal dipolar correlations obtained from MD simulations and the ones computed using the Gaussian model (Eq. (3.12-3.13)). They can be written as $\langle \mu(0)\mu(r)\rangle_{FT} = \langle P(0)P(r)\rangle_{\parallel}/\mu_D^2\rho_0^2$, with μ_D the dipole moment of water ρ_0 its density. The inset shows the results for a parameterization of the susceptibility as indicated in Fig. (3.2). We see an overestimation of the correlation range. The model does not reproduce the charge

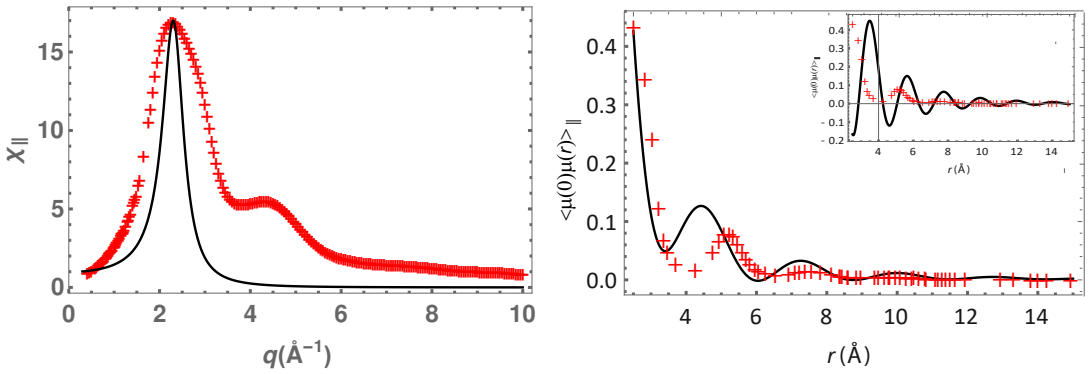

(a) (b)

Figure 3.4: (a) Dipolar correlation function. The red cross is the result of molecular dynamics simulations that are reproduced by Zhang C. *et* al., J. Chem. Phys. **141**, 084504 2014. The black curve is plotted using the expression $\langle\mu(0)\mu(r)\rangle_{FT} = \langle P(0)P(r)\rangle_{\parallel}/\mu_D^2\rho_0^2$, with μ_D=2.2 D, ρ_0=0.033 Å^{-3} and the parameters given in Fig. 2. The insert represents the dipolar correlation obtained for parameters K=1/70, $\kappa_l = -0.22$ Å^2, $\alpha = 0.012$ Å^4 corresponding to a reproduction of the SPC/E susceptibility. (b) Longitudinal susceptibility was derived with molecular dynamics simulations and field theory model. The simulated response is obtained for a dipolar model constructed from SPC/E water simulations (see ref. ([48]). The susceptibility is obtained from the Field theory framework for $K = 1/70$, $\kappa_l = -0.36$ Å^2, $\alpha = 0.034$ Å^4.

layering around a reference point as the extrema of the correlation functions are shifted when compared to the MD data.

The FT susceptibility possesses a peak at 3 Å^{-1}, which is more narrow than the MD simulated system as seen in Fig. (3.2) (a). This narrow "overresponse" zone corresponds to a medium correlated over a larger scale than the simulated one, and this explains the observed discrepancy in the inset of 3.4 (b). This can be improved by adjusting the fitting procedure for the determination of (α, κ_l, K)...

To solve this problem, . we perform simulations of SPC/E water that we treat as a dipolar fluid. Fig. 3.4 (a) shows the corresponding susceptibility (red markers) and the FT one constructed from this input (black line). Details are given in ref. [48]. The correlations for this model are plotted in the main plot of Fig. 3.4. The agreement with MD data is much better.

However, the projection on a simpler molecular model (here a dipole) is not necessary to get a quantitative agreement for correlation lengths between MD simulations and field theory calculations. In another work [21], we have fitted the aspect ratio of the peak at q=3 Å^{-1} - it i.e. its broadness at half height. We have shown that, in this case, the correlation lengths agree with MD data. We detail this case in Chapter 7.

As a brief conclusion of this section, we have shown that nonlocal electrostatics can furnish an analytically tractable framework to describe the polarization correlations in water at the nanoscale.

3.4 Two polarization field model

In collaboration with A. Kornyshev and J. Hedley.

This section focuses on the low-q behavior of the longitudinal dielectric susceptibility. This regime is fundamental as it encodes the correlation of water at a long range. It plays a central role in the description of the electrostatic interactions between macroscopic objects separated by a few nanometers. The model discussed in the last section reproduces the "overscreening"

phenomenon in water but fails to reproduce the behavior at low q. Figure 3.5 represents the simulated susceptibility (top) and the permittivity (bottom) for SPC/E water (blue markers and red plot). In both cases, the inset zooms on the low-q behavior and shows a constant (or going throw a minimum?) susceptibility and a decaying permittivity. This behavior is not reproduced by the model given in Eq. 3.13, which leads to an increasing $\chi_{\|}(q)$ at low q. This section briefly shows how to modify the initial model to capture these properties. We consider the polarization $\vec{P}$ purely longitudinal as we focus on $\chi_{\|}$. In the spirit of Ref.[38], we here assume that the polarisation $\vec{P}$ is a sum of three contributions, $\vec{P} = \vec{P}_1 + \vec{P}_2 + \mathbf{P}_*$. where $\vec{P}_1$ and $\vec{P}_2$ describe contributions from the reorientation of water molecules, and $\mathbf{P}_*$ describes contributions from the polarisability of the molecules themselves. Introducing a three-component model allows us to account for the different possible modes and spatial scales of polarisation fluctuations. The intramolecular modes ($\mathbf{P}_*$) include contributions such as fluctuations of electron density and intramolecular vibrations. However, we assume here that these modes give purely local polarisability, independent of the wavevector, q, and so we do not include them in our model functional. The other orientational modes could correspond to reorientation of molecules that results in rearrangements of the hydrogen-bonding network, or oscillations about an average position preserving the hydrogen bond network. We avoid specifically assigning these modes here, and instead consider a model described by two different orientational modes $\vec{P}_1$ and $\vec{P}_2$, one of which ($\vec{P}_1$) we expand to the second derivative term in the Landau-Ginzburg expansion, and the other ($\vec{P}_2$) to just the first derivative also known as the 'Lorentzian approximation,'

$$\begin{aligned}\mathcal{U}_{conf}[\vec{P}_1, \vec{P}_2] = &\int_V \frac{d\vec{r}}{2\epsilon_0}\left\{K_{11}\vec{P}_1^2 + K_{12}\left(\nabla\cdot\vec{P}_1\right)^2 + K_{13}\left(\nabla(\nabla\cdot\vec{P}_1)\right)^2\right\} \\ &+ \int_V \frac{d\vec{r}}{2\epsilon_0}\left\{K_{21}\vec{P}_2^2 + K_{22}\left(\nabla\cdot\vec{P}_2\right)^2\right\},\end{aligned} \tag{3.18}$$

where the set of phenomenological model parameters is given by $\{K_{ij}\}$. This two-polarisation model allows us to build up a kernel that mimics the simulated nonlocal dielectric properties of bulk water at low q. This model of two orientational polarisation modes, correlated differently in space, one, $\vec{P}_1$, of higher wavenumber with decaying oscillations (described in the last section) and the other one, $\vec{P}_2$, of lower wavenumber that decays exponentially, is also phenomenologic. It matches some simulation data [**?**] as well as several consequences of the nonlocal dielectric response of water [49, 50]. This concept has been discussed in detail in [49] in the context of the interplay between temporal and spatial correlations of polarization fluctuations. This splitting of the polarisation density reminds the attempts to fit the time-frequency Debye spectrum of the frequency-dependent dielectric permittivity of water with two different relaxation times [51, 52, 53, 54, 55], one fast and one slow. These two times are often associated with librations of individual molecules and reorientations of their larger clusters, respectively. However, this does not mean that water should literally be considered as a coupled system of two liquids, each with its own relaxation processes, although new arguments have been put forward to validate such a picture [56, 57] in the context of the recently discussed "low" and "high" density clusters in water. But all these should better be interpreted in the language of collective modes [58, 49]. The dielectric susceptibility associated with the model given in Eq. (3.18) can be computed (see ref. [22]) and parameterized to reproduce the low-q behavior of water. This is shown in Fig. (3.5). The top panel presents the susceptibility and the bottom panel the permittivity, obtained via the relation: $\epsilon(q) = 1/(1 - \chi_{\|}(q))$.

The relevance of this model will be highlighted when we consider confined systems in a later chapter.

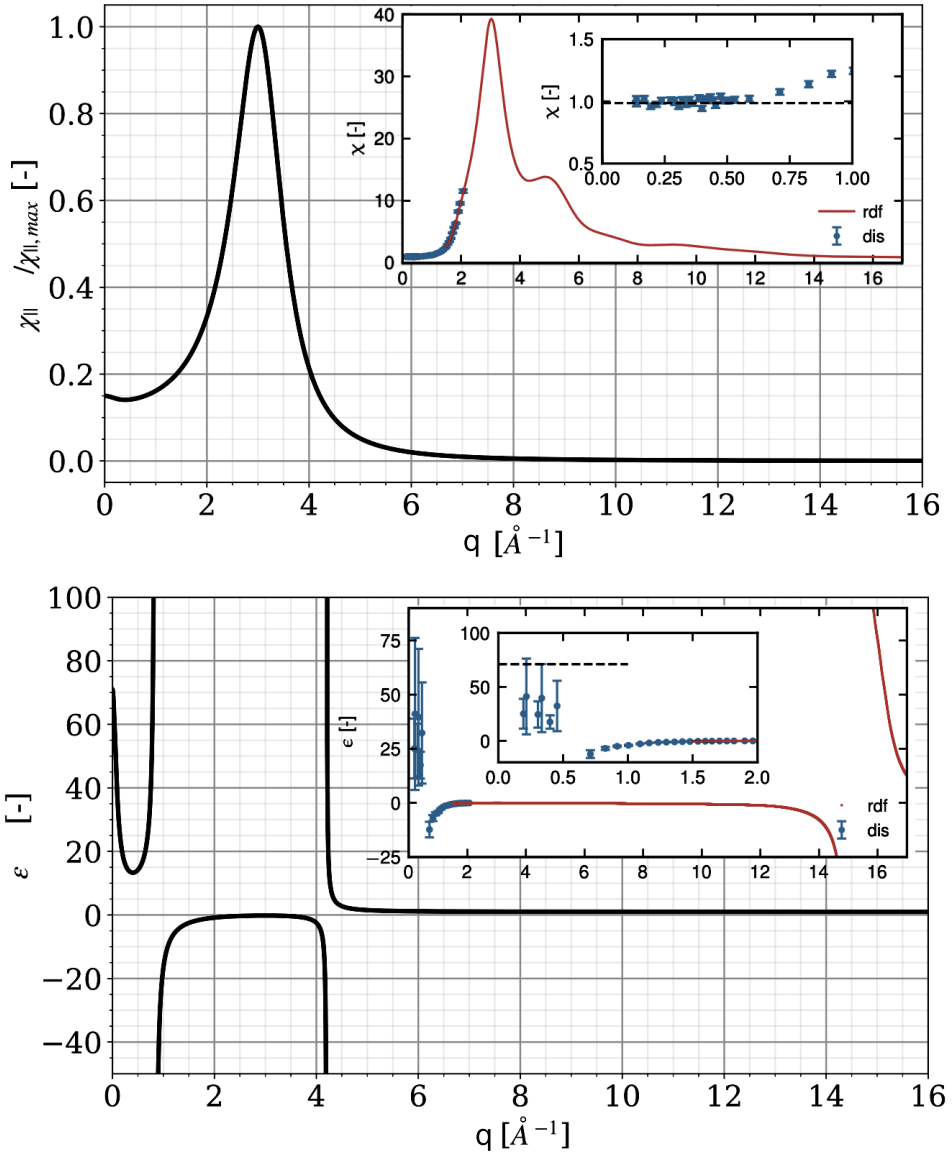

Figure 3.5: Dielectric response function (a) and dielectric function (b) of bulk water. Insets are computed from SPC/E simulations of water. Main Curves have been calculated from Eqs. and with $K_{11} = 0.140125$, $K_{12} = -0.207118$ Å^2, $K_{13} = 0.01129$ Å^4, $K_{21} = 0.015908$, $K_{22} = 2.00394$ Å^2.

3.5 Functional of density and polarization

Until now, we have considered polarization as a unique, relevant field to describe electrostatics in water. This approach goes against the history of liquid theory, which has primarily developed density functionals for the energy, or free energy, of the system [34]. And, indeed MD simulations of water have shown that density and polarization fluctuations are coupled [44]. A perturbation of the water density induces a variation in the polarization. For example, the solvation of a neutral atom (modeled as a Lennard-Jones sphere) produces a perturbation of the density field around it, but also a mean polarisation for the solvent. This suggests that a complete description of the dielectric properties of water must include a density term.

In this section, we construct a phenomenological Gaussian model of two coupled fields, the density, and the polarization, that we apply to study water [59].

Density correlations in water

The density of the fluid, $\rho(r)$, is written as the sum of its mean density ρ_0 and of a fluctuation field $\delta\rho(r)$ as follows: $\rho(r) = \rho_0 + \delta\rho(r)$. In the present Gaussian limit, we assume the density fluctuations are small, $\delta\rho/\rho_0 \ll 1$. We consider water in normal temperature and pressure conditions, which sets ρ_0 =0.033 Å^{-3}. The spatial correlations of the fluctuation of the density are characterized by the structure factor $S(q)$ of the fluid as follows: $S(q) = \langle\delta\rho(q)\delta\rho(-q)\rangle/\rho_0$. Figure 3.6 shows the structure factor in Fourier space measured experimentally using x-ray spectroscopy [60]. We focus here on the low q part of the spectrum $q \ll 4$ Å^{-1} as we target the properties of water at a nanometric and larger scale and not its atomic description. The structure factor in q=0, $S(0)$, is associated with the macroscopic compressibility of water as follows $S(0) = \chi_T/\chi_T^0$, where χ_T is the compressibility of fluid and $\chi_T^0 = 1/k_BT\rho_0$ is the compressibility of a perfect gas of density ρ_0. In real space, the fluctuations of the density are characterized by the well-known pair distribution function through the relation:

$$g(r) = 1 + \frac{\langle\delta\rho(r)\delta\rho(0)\rangle}{\rho_0^2}. \tag{3.19}$$

We now write the energy of the fluid as a Gaussian model of two coupled fields $\delta\rho$ and $\vec{P}$. As one field is a scalar field and the second one a vectorial field, we couple either $\nabla\delta\rho$ and $\vec{P}$ or $\delta\rho$ and $\nabla\cdot\vec{P}$. Both are equivalent to infinite bulk systems. Note that for symmetry reasons, the coupling affects only the longitudinal part of the polarization field. We thus propose for the energy:

$$\mathcal{U}[\delta\rho,\vec{P}] = \mathcal{U}_{el}[\vec{P}] + \frac{k_BT}{2\rho_0}\int d\vec{r}d\vec{r}'\delta\rho(\vec{r})\chi_\rho^{-1}(\vec{r},\vec{r}')\delta\rho(\vec{r}') + c\frac{k_BT}{\mu_0\rho_0}\int d\vec{r}\nabla\delta\rho(\vec{r})\cdot\vec{P}(\vec{r}). \tag{3.20}$$

The first term of the energy, $\mathcal{U}_{el}[\vec{P}]$, is the electrostatic energy, a functional of $\vec{P}$ that we already discussed. Here, we take the expression given in Eqs. (3.12,3.13). The second term corresponds to the energy of excess density introduced in this form by D. Chandler [33] and involves the structure factor $S(q)$ as the kernel for the density correlations. We propose here an explicit expression for the density term using a Landay-Ginzburg expansion:

$$\int d\vec{r}d\vec{r'}\delta\rho(\vec{r})\chi_\rho^{-1}(\vec{r}-\vec{r'})\delta\rho(\vec{r}') \;=\; \int d\vec{r}\Big[K_\rho\delta\rho(\vec{r})^2 + \lambda\left(\nabla\delta\rho(\vec{r})\right)^2 + \nu\left(\nabla\cdot\nabla\delta\rho(\vec{r})\right)^2\Big].$$

The parameters K_ρ ([−]), λ ([L^2]) and ν ([L^4]) are Landau-Ginzburg parameters. We first choose the parameter values such that $\chi_\rho(q)$ reproduces the bulk properties of $S(q=0)$ and possesses a peak around q=3 Å^{-1} which mimics roughly the low q behavior of the structure factor $S(q)$ shown in Fig. 3.6. Finally, the last term in Eq. (3.20) $c\frac{k_BT}{\mu_0\rho_0}\int d^3r\nabla\delta\rho(r)\cdot\vec{P}(r)$ encodes the coupling. μ_0 is the permanent dipole of water, c is the coupling constant, and has

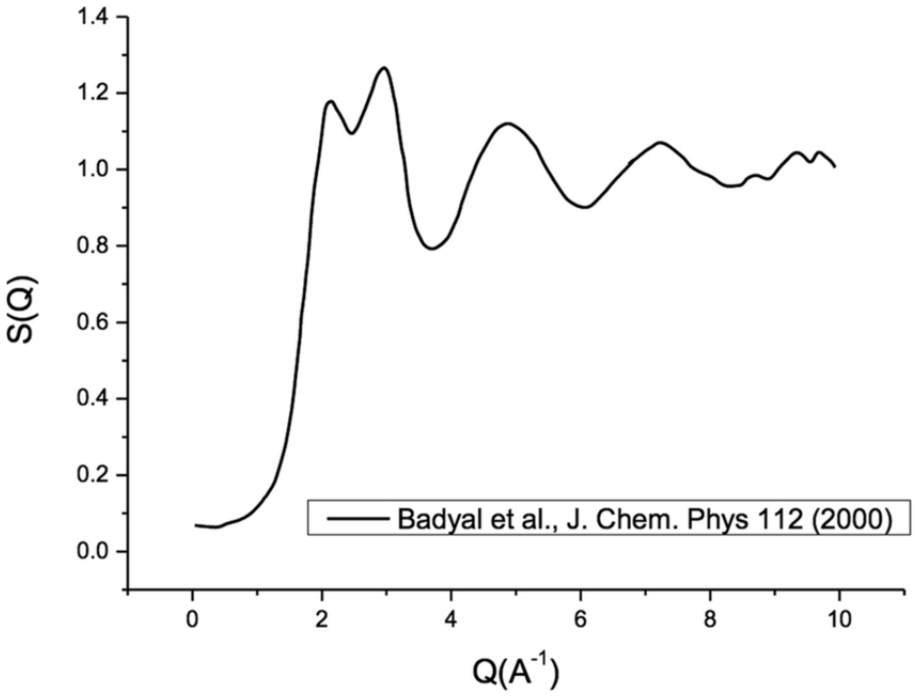

Figure 3.6: **Structure factor of water.** We reproduce the x-ray structure factor of water given in ref. [60]. It has been measured under ambient conditions

the dimension of a length. The total energy of the system can be written in Fourier space as follows:

$$\mathcal{U}[\delta\rho, \vec{P}] = \frac{1}{2}\int d\vec{q}\left(\delta\rho(q), \vec{P}(q)\right)\chi_c^{-1}(q)\begin{pmatrix}\delta\rho(-q)\\ \vec{P}(-q)\end{pmatrix}. \tag{3.21}$$

The susceptibility of the system, $\chi_c(q)$ is a 4x4 antisymmetric matrix obtained by inversion of Eq.(3.20). Its analytical expression is given in ref. [59]. It is a function of c^2 and does not depend on the sign of the coupling constant. The coupling effect is investigated by increasing the value of c^2: it enhances the range of the correlations for $\vec{P}$ and $\delta\rho$. We choose the free parameters of this model (α, κ_l, ν, λ, c) so that we can reproduce the positions and values of the maxima of the SPC/E water susceptibilities. The results are plotted in Fig. 3.7.

It presents the structure factor (a), the longitudinal susceptibility (b), and the coupled susceptibility (c) obtained via MD simulations (dashed lines) or adjusted field theory (black line). The agreement between the two remains qualitative. However, the coupled Hamiltonian presented in Eq .(3.21) gives an analytically tractable framework to estimate the coupled density and polarization response to inclusion in water.

3.6 Conclusion

In this chapter, I have presented three Gaussian models to describe the correlations of the polarization in water. I started with the minimal functional of the polarization that can describe the "over-screening" property of water, see Eq. (3.13). The second and third models illustrate how we can easily adjust this framework to reproduce other interesting properties of the fluid. We built a model based on two polarization fields, Eq. (3.18), which could be thought of as two distinct reorientation modes of water. It can better reproduce the low-q region of the longitudinal susceptibility, which encodes the correlations at a scale larger than a few molecular sizes. Finally, we build a coupled model of the density and the polarization, Eq. (3.20), that qualitatively reproduces the simulated response function water and takes into account the interplay

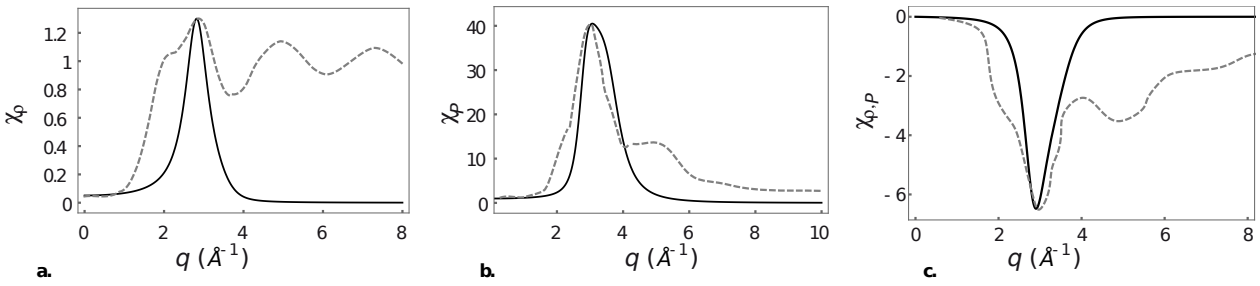

Figure 3.7: Response functions for a water model compared to response functions of SPC/E water. **a.** Density susceptibility $\chi_\rho(q)$ (solid line) and density susceptibility of SPC/E water (dashed line) as a function of q . **b.** Dielectric susceptibility $\chi_P(q)$ (solid line) and dielectric susceptibility of SPC/E water (dashed line) as a function of q. **c.** Cross susceptibility $\chi_{\rho,P}(q)$ (solid line) as a function of q and cross susceptibility of SPC/E water (dashed line). The values of the parameters are given ref. [59]. The molecular dynamics results are reproduced and adapted with permission from ref[40, 44].
.

between mass and charge density. However, these three examples developed here remain in the linear response regime. In the next chapter, we show how to overcome this limit.

Chapter 4

Nonlinear dielectric effects in water

4.1 Introduction

The last section presents phenomenological nonlocal Gaussian polarisation functionals that capture the dielectric properties of water at the molecular scale. While the qualitative behavior obtained with these models is in general agreement with the results of MD simulations, the amplitude of the structuring effects is often overestimated in the linear models.

Water polarizes in response to an electrostatic field by increasing its density and accumulating molecules around the source of the field - an electrode, a charged molecule; moreover, the molecular polarization of one molecule increases by deforming its electronic cloud. However, both of these mechanisms are bounded. Finally, the response of the fluid to a high electrostatic field saturates. The polarization stays constant for a field of increasing strength. This saturation corresponds to a vanishing permittivity.

The permittivity of water submitted to a constant static electrostatic field has been measured with MD simulations (see the sketch in the inset of Fig. 4.1). Figure 4.1 shows the permittivity as a function $|\vec{E}|$ obtained for different water models. As one sees, the permittivity decays with an increase of $|\vec{E}|$, illustrating this saturation effect. It is divided by 2 for $|\vec{E}|$ $\approx$0.05 V.Å^{-1}. The electrostatic field generated by a monovalent ion is larger than this value over a sphere of $r \approx$15 Å, in vacuum and over a sphere of $r \approx$2 Å in a medium associated with ϵ_b=80. The first estimation overestimates the size of the nonresponsing shell as water starts to screen the ion field. The second underestimates it, as the first shell cannot screen the field as efficiently as the bulk. In this chapter, we build tools to model and quantify the nonlocal nonlinear response of water to high fields.

We consider functionals for the energy and the free energy of the system that include non-Gaussian terms [61, 39, 62, 63]. In contrast to non-local models, which have been developed phenomenologically, one can construct nonlinear functionals for the free energy of polar fluids starting from microscopic models [62, 64]. We start by briefly discussing these models and present their properties. We then explain how we implement nonlinear properties in the nonlocal models presented in the previous chapter. We characterize the properties of such models. The last part is devoted to the conclusion.

4.2 Microscopic models of polar fluids

In collaboration with Ralf Blossey

In this section, we present two generalized continuum models for water electrostatics that were developed by Henri Orland, David Andelman and coworkers [62, 64, 65, 63]. They are based on a microscopic description of water: a punctual dipole represents a molecule of the fluid (see sketch in Fig 4.2).

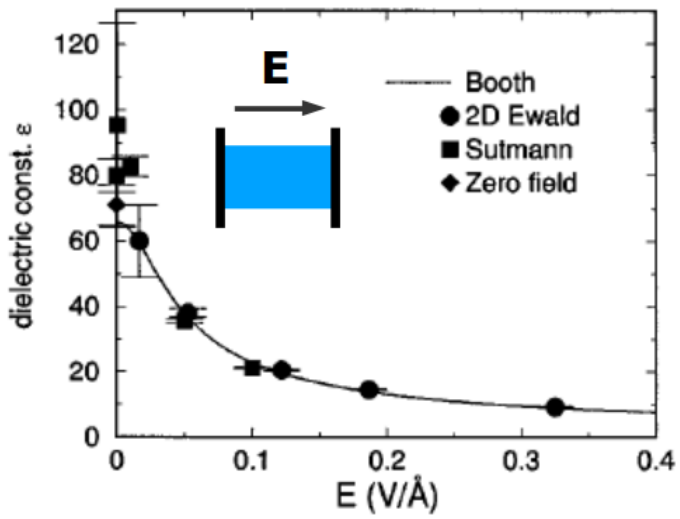

Figure 4.1: Permittivity of water under constant electrostatic field measured with MD simulations. This figure is a reproduction of Fig. 11 of Yeh I.-C. et al., J. Chem. Phys. **110** 7935-7942, 1999. presenting the permittivity for different explicit water models.

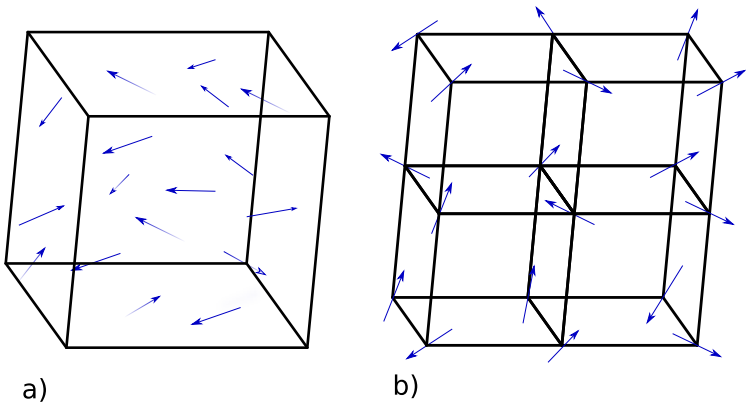

Figure 4.2: Microscopic models for water as a dipolar system. a) the dipole Poisson model (D) is a gas of punctual dipoles. b) the dipolar Poisson Langevin model (DL) is made of punctual dipoles on a lattice [62].

Water is composed of N dipoles. In the first model, which we name here the dipolar Poisson model (D), molecules are modeled as a gas of dipoles -see sketch (a) of Fig. (4.2). In the second model, named dipolar Poisson Langevin (DL), the dipoles are placed on a lattice - see sketch (b) of Fig. (4.2). Note that these models are refereed in the literature under the name of dipolar-Poisson–Boltzmann–(Langevin) models as they are used to study electrolytes, but since we focus here on neat water, we suppress the "Poisson–Boltzmann" notion clarity.

The charge density for the system thus writes as follows: $\rho_{\text{dipole}} = \sum_i -p_0 \cdot \nabla\delta(\vec{r}-\vec{r_i})$, where p_0 is the dipole moment, and r_i the position of the vector i. In both cases, the dipoles are interacting via the Coulomb potential. The partition function and the free energy of the system can be written by taking into account the degrees of freedom of the dipoles. For the D model, the position and rotation of the dipole vary as the density of the dipole is not constrained. For the DL model, the dipoles are pinned on a grid, the system is incompressible, and only the dipole orientations vary. One can compute analytically the free energies U_i (i=D, DL). They can be written as nonlinear functionnals of the electrostatic potential, ϕ, and of microscopic variables of the system p_0, the dipole moment of one molecule, and $1/a^3$ the density of dipoles. Note that for the DL model a is the size of the mesh of the lattice. The free energy expressions are derived in refs. [62, 63]. One gets for the D model:

$$U_{\text{D}} = \int d^3\mathbf{r} \left[-\frac{\epsilon_0}{2}(\nabla\phi)^2 - \frac{1}{\beta a^3}\frac{\sinh(\beta p_0|\nabla\phi|)}{\beta p_0|\nabla\phi|)} \right] + \frac{1}{\beta a^3}\,, \tag{4.1}$$

and for the DL model:

$$U_{\text{DL}} = \int d^3\mathbf{r} \left[-\frac{\epsilon_0}{2}(\nabla\phi)^2 - \frac{1}{\beta a^3}\log\left(\frac{\sinh(\beta p_0|\nabla\phi|)}{\beta p_0|\nabla\phi|}\right) \right]. \tag{4.2}$$

These models introduce the molecular nature of the solvent at the microscopic scale and describe systems associated with a nonlinear response regime. In the D model, the local density of dipoles can increase without any energetic cost„ and the dipole orientation aligns with the external field. The DL model is incompressible, and once all the dipoles are perfectly aligned on an external field, the system stops responding.

These models have a few disadvantages. The free energy density is a local function of $\nabla\phi$. Nonlocal terms could expand it as in the models previously discussed. But, the polarization $\vec{P}$ corresponds to the material response, and the Landau-Ginzburg terms in $\nabla\cdot\vec{P}$ that we have introduced for nonlocality can be seen as a local organization of the molecules. It is more difficult to give a molecular interpretation of a Landau-Ginzburg expansion of the energy of the system with $-\nabla\phi$ as an order parameter. Moreover, the energy density is a concave function of $-\nabla\phi$ (*i.e.* it goes through a maximum and not a minimum), and a nonlocal configurational expansion would have to be convex, making the use of such combined functionals more difficult as discussed in refs. [66, 67].

4.3 D- and DL- model in P-space

In this section, we will characterize these models as functionals of the polarization fields. We discuss the behavior of the D and DL models in the limits of low and high polarization. MD simulations for an SPC/E-water slab in the presence of an external field allows us to parameterize the Dipolar-Langevin model quantitatively .reductionist nature.

Our starting point is the free energy for the two systems expressed as functionals of the electrostatic field $\vec{E}$ that is obtained from the functionals of the electrostatic potentials (see Eqs.(4.1-4.2)) by introducing the excitation field $\vec{D}$ as a Lagrange multiplier as follows :

$$U_i = \int d\vec{r} \left[-\frac{\epsilon_0}{2}\vec{E}^2 - h_i(\vec{E}) + \vec{D}\cdot(\nabla\phi - \vec{E}) \right], \tag{4.3}$$

where $h_i(\vec{E})$ abbreviates: with

$$h_{\rm DL}(\vec{E}) = \frac{1}{\beta a^3}\log\left(\frac{\sinh(\beta p_0|E|)}{\beta p_0|E|}\right), \quad h_{\rm D}(\vec{E}) = \frac{1}{\beta a^3}\frac{\sinh(\beta p_0|E|)}{\beta p_0|E|}\,. \tag{4.4}$$

We perform a Legendre transform to express these energies as functionals of $\vec{P}$. We introduce $\tilde{h}_i(\vec{P})$ the Legendre transformation [66, 67] of $h(\vec{E})$ defined as

$$\tilde{h}_i(\vec{P}) = \vec{P}\cdot\vec{E} - h_i(\vec{E}), \quad \text{and} \quad \vec{P} = \frac{dh_i(\vec{E})}{d\vec{E}} \tag{4.5}$$

to express the free energy of the system as a functional of the conjugated field $\vec{P}$. It gives, for $i = (\mathrm{D}, \mathrm{DL})$,

$$U_i \;=\; \int d^3\mathbf{r}\Big[-\frac{\epsilon_0}{2}\vec{E}^2 + \tilde{h}_i(\vec{P}) - \phi\nabla\cdot\vec{D} + \vec{E}\cdot(\vec{D}-\vec{P})\Big]\,. \tag{4.6}$$

Varying U_i depending on the electrostatic field $\vec{E}$ leads to the relation $\vec{D} = \epsilon_0\vec{E} + \vec{P}$ and thus identifies $\vec{P}$ as the polarization field. By replacing $\vec{E}$ by its mean-field value $\epsilon_0\vec{E} = \vec{D} - \vec{P}$, we obtain the functional in the P-space:

$$\tilde{U}_i = \int d^3\mathbf{r}\left[\frac{(\vec{D}-\vec{P})^2}{2\epsilon_0} + \tilde{h}_i(\vec{P}) - \phi\nabla\cdot\vec{D}\right]\,. \tag{4.7}$$

In the following, we consider only excitations $\vec{D}$ that satisfy the Gauss relation ($\nabla\cdot\vec{D} = 0$ in the absence of free charge) and therefore drop the term $\sim\phi$ in the free energy density.

The nonlinear Dipolar-Langevin (DL) and Dipolar (D) models can thus be studied in either E- and P-space and we now investigate their properties in these spaces. We first compare the two E- and P-functionals with the corresponding linear continuum dielectric medium. To do so, we expand the dipole energy densities h_i (i = D, DL), Eq.(4.3)) to second order in $\vec{E}$, Using Eq. (4.5), one obtains the quadratic Hamiltonian in the P-space [23]. The harmonic approximations of the free energy densities in E-space, $f_i(\vec{E}) = -\epsilon_0\vec{E}^2/2 - h_{i,2}(\vec{E})$, and in P-space, $\tilde{f}_i(\vec{P}) = \vec{P}^2/2\epsilon_0 + \tilde{h}_{i,2}(\vec{P})$, can be written as functions of the macroscopic response functions, -$\epsilon_0\epsilon_b\vec{E}^2/2$, where ϵ_b is the relative dielectric permittivity and $P^2/2\epsilon_0\chi$. By identification, one obtains the expressions

$$\epsilon_b \equiv 1 + \frac{\beta p_0^2}{3\epsilon_0 a^3}\,, \quad 1 + \epsilon_0\frac{3a^3}{\beta p_0^2} \equiv \frac{1}{\chi} \tag{4.8}$$

as functions of the microscopic variables (p_0, a) of the D- and DL-models. We note particularly that the relations $h_{i,2}(\vec{E})$ and $\tilde{h}_{i,2}(\vec{P})$ are not only dual in the field variables $\vec{E}$ and $\vec{P}$, but also in the model parameters, in the temperature dependence β^{-1} and in ϵ_0.

In Fig.(4.3), the functions $-h_{\rm DL}(\vec{E})$ (dashed black curve) and $-h_{\rm D}(\vec{E})$ (green curve) and their harmonic approximation $-h_{\rm DL,2}(\vec{E})$ (blue curve) are plotted in panel **a**. The corresponding functions for P-space are represented in panel **b**. As parameter set to reproduce the properties of water were used: $p_0 = 1.8$ D corresponds to the dipole moment of one molecule and $a = 0.17$ nm is adjusted to fix the relative dielectric permittivity ϵ_b to 78 corresponding to water. We note that it differs from the mesh size giving rise to the density of water which is given by $a_w = 0.3$ nm. As one sees, for both the D- and DL-model the functions are concave in $\vec{E}$ and convex in $\vec{P}$. We compare the value of the dipole energy density for the harmonic approximation in E- and P- space. In the DL model, $\tilde{h}_{\rm DL}(\vec{P})$ increases faster than the quadratic expansion in the P-space and saturates for large values of $\vec{P}$. On the contrary, $h_{\rm DL}(\vec{E})$ decreases more slowly than $h_{\rm DL,2}(\vec{E})$. We observe the opposite trend for the Dipolar model (green curve). A given excitation, $\vec{D}_0$, imposed on a medium described by the DL-functional will thus induce an under-response in P and an over-response in E compared to the corresponding linear medium. On the

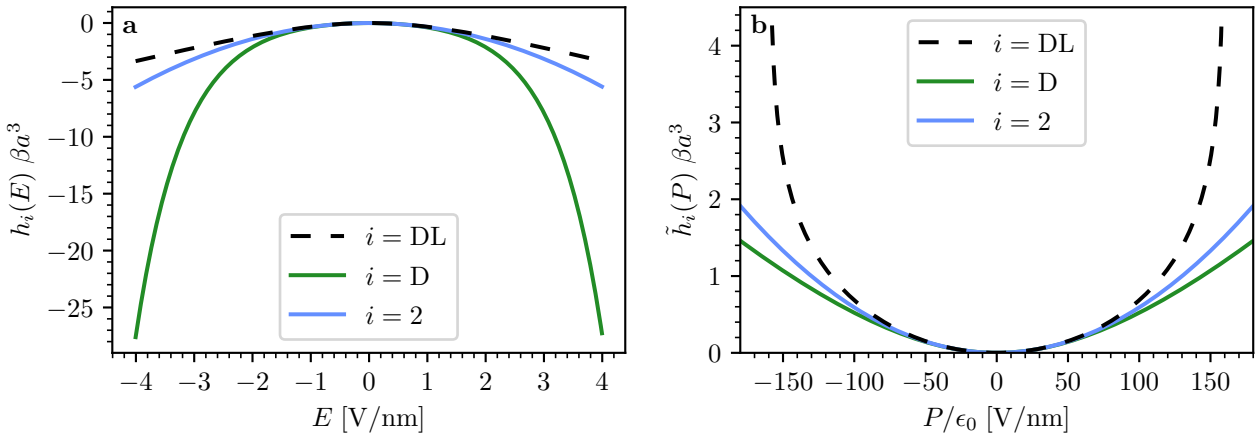

Figure 4.3: Free energy of the dipoles for the Dipolar and Dipolar Langevin models in E- (**a**) and P-space (**b**). The dimensionless functions $h_{\mathrm{D}}(\vec{P})\beta a^3$ and $h_{\mathrm{DL}}(\vec{P})\beta a^3$ are plotted using Eq. (4.5). The parameter values are $a = 0.17$ nm, $p_0 = 1.8$ D, $T = 300$ K.

contrary, a medium described with the D-functional over-responds in P and under-responds in E.

These observations can be understood using the constitutive relation of electrostatics $\vec{D} = \epsilon_0\vec{E} + \vec{P}$, which imposes that beyond the linear regime an over-response in P or E to an external field D_0 will be compensated by the saturation of E or P.

We focus here on the DL model in P-space because it seems to be the most suitable for modeling water. We derive expanded expressions the polarization in response to low or high electrostatic field to obtain an analytical expression of the response to an ion field over the full spatial range. For the sake of simplicity, we drop the vectorial notations for the fields.

Using Eqs.(4.2), the polarization as a function of the electrostatic field can be written as

$$P(E) = \frac{p_0}{a^3}\left(\coth(\beta p_0 E) - \frac{1}{\beta p_0 E}\right). \tag{4.9}$$

This expression can be expanded as a polynomial of E^2 in the low-field regime, around $E = 0$. It can also be expanded in the large-field regime, where the polarization is almost constant and saturated. For this regime the coth-function in Eq.(4.9) can be replaced by 1. The range of validity of the second regime can be estimated by considering $e^{-\beta p_0|E|} = 0.01e^{\beta p_0|E|}$, *i.e.*, $E \geq 1/2\beta p_0 \log(100) = 1.4$ V.nm^{-1} for water ($p_0 = 1.8$ D).

We start with the low-field regime and expand Eq.(4.9) around $E = 0$. We have derived the dipolar free energy density $\tilde{h}_{\mathrm{DL},4}(P)$ to fourth order in the polarization [23] and obtained

$$\tilde{h}_{\mathrm{DL},4}(P) = \frac{1}{2\epsilon_0}\frac{1}{\epsilon_b - 1}P^2 + \frac{9}{20p_0\beta}\left(\frac{a^3}{p_0}\right)^3 P^4. \tag{4.10}$$

The correction in P^4 induces an increase of the free energy density for a given polarization P compared to the linear model.

In the high-field regime, the expression of P as a function of E is simply obtained by approximating the coth-function by 1 in Eq.(4.9) so that

$$P_{\mathrm{sat}}(E) = \frac{p_0}{a^3} - \frac{1}{a^3 E\beta}, \tag{4.11}$$

The polarization saturates to the value $p_{\mathrm{sat}} = p_0/a^3$, which is obtained when all the dipoles p_0

are aligned with the field. The dipole energy density in this regime $\tilde{h}_{\rm sat}(P)$ is written as

$$\tilde{h}_{\rm sat}(P) = \frac{1}{\beta a^3}\left(\log\left(\frac{2p_0/a^3}{p_0/a^3 - P}\right) - 1\right). \tag{4.12}$$

The linear and saturated regimes in response to an excitation are included in the Dipolar-Langevin model which could be a good candidate to model the dielectric properties of water over a wide range of excitation amplitude. The question we address now is whether we can propose a parameterization for the microscopic values (p_0, a) that reproduces quantitatively these behaviors for simulated water.

4.3.1 MD simulation-fit of the model

To enable an independent parameterization of the model, we performed molecular dynamics simulations of water confined between two graphene sheets in a slab geometry as illustrated by the simulation snapshot in Fig.(4.4) **a**. The slab walls are perpendicular to the z-direction and are made up of carbon atoms. The atoms are frozen, neutral and arranged in a hexagonal lattice. The two walls are separated by L =5 nm. We use the SPC/E model for water. It is associated with a relative permittivity of 71. A z-directed excitation field $\vec{D}_{\rm MD,0} = D_{\rm MD,0}\vec{E}_z$ is applied between the two surfaces. The details of the simulations are given in ref. [23].

We measure the response of the system for increasing amplitude of the excitation from 0 V.nm^{-1} to 64 V.nm^{-1}. The symmetry of the system imposes a z-directed response, $\vec{P}_{\rm MD} = P_{\rm MD}\vec{E}_z$, with

$$P_{\rm MD}(z) = \int_{-L/2}^{z} \rho_{\rm c,MD}(z) \tag{4.13}$$

where $\rho_{\rm c,MD}(z)$ is the charge density of the fluid. In Fig.(4.4) **b.**, the water mass density $\rho_{\rm MD}(z)$ (top panel) and the polarization, $P_{\rm MD}(z)$ (bottom panel) are plotted for different values of $D_{\rm MD,0}$. For small excitations (up to 32V.nm^{-1}), $\rho_{\rm MD}(z)$ reaches the bulk density and $P_{\rm MD}(z)$ a constant value on a distance of the range of the correlation length of water (1.5 nm). For large $D_{\rm MD,0}$, density and polarization oscillate with a period corresponding to the width of one molecule. This corresponds to an alignment to the Oxygen atoms in (xy) plane that could be induced by the surfaces. We estimate the spatial mean of the polarization P_m in the bulk, *i.e.* excluding the interfacial water of width l_i = 1.5 nm [68], as

$$P_m = 1/(L - 2l_i)\int_{-L/2+l_i}^{L/2-l_i} P_{\rm MD}(z)dz. \tag{4.14}$$

In Fig.(4.4) **c.**, P_m is plotted as a function of D_0 and one sees that the polarization is a linear function of D_0 at small values and reaches a plateau at large excitations. This highlights the linear and saturated regime of the dielectric properties of SPC/E water.

The linear and the saturated behaviors are captured by the DL-model. We fit the values of microscopic parameters a and p_0 so that the DL model quantitatively reproduces MD by measuring the slope $\chi_{\rm MD}$ of the linear part of $P_m(D_0)$ its saturation value $p_{\rm sat,MD}$. We obtain adjusted values of p_0 = 9.62 D and a = 0.51nm. By comparison, an SPC/E water molecule with $p_{\rm SPC/E}$ = 2.3 D is associated with a mesh size $a_w = a_{\rm SPC/E}$ =0.3 nm where a^3 is defined as the mean volume occupied by a water molecule.

Thus, the dipolar fluid reproducing the bulk permittivity and the saturation polarization of SPC/E water is composed of point dipoles with dipole moments 4 × larger and a density 7 × lower than SPC/E water.

Using this parameterization, the asymptotic free energy densities $\tilde{h}_4(P)$ (low polarization, pink plot) and $\tilde{h}_{\rm sat}$ (high polarization, yellow plot) are plotted in Fig.(4.5). They are compared to the exact model $\tilde{h}_{DL}(P)$ (dashed black curve) and to the quadratic expansion $\tilde{h}_2(P)$ (blue

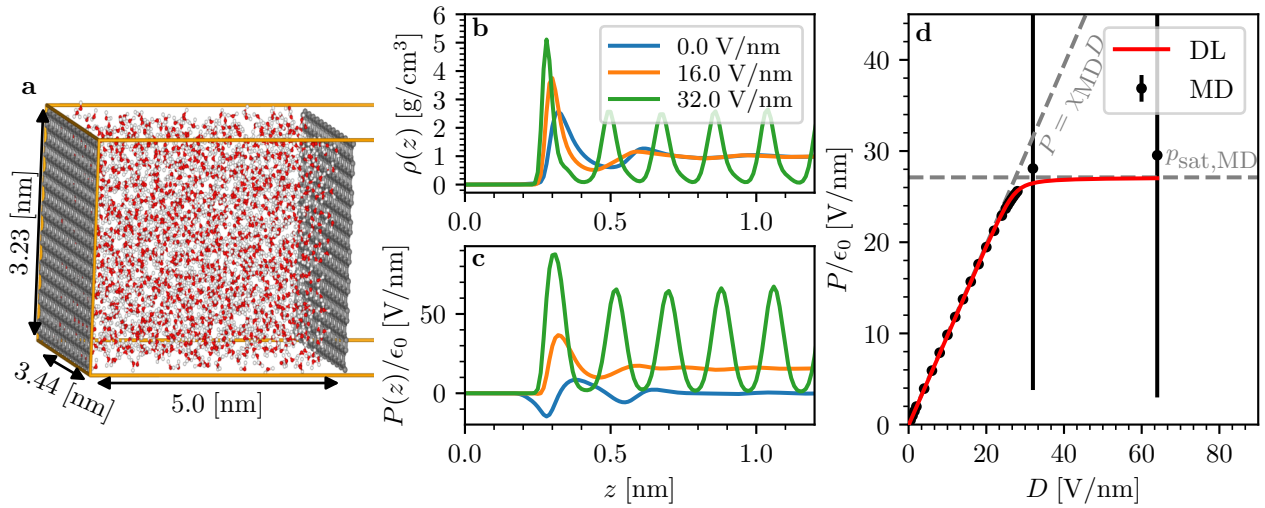

Figure 4.4: Molecular dynamics simulations of SPC/E water under exciation field. **a.** Snapshot of the system composed of water molecules between two graphene sheets. Mass density (**b.**) and polarization (**c.**) for three different excitation fields $D_0/\epsilon_0 = 0$ V.nm^{-1} (blue plot), $D_0/\epsilon_0 = 16$ V.nm^{-1} (yellow plot), $D_0/\epsilon_0 = 32$ V.nm^{-1} (green plot). **d.** Polarization response as a function of the excitation field: MD simulations (black points); exact DL model (red plot); linear regime (dashed grey line), $P = \chi_{\rm MD} D_0$; saturation polarization (horizontal dashed grey line) $P = p_{\rm sat}$.

curve). The fourth-order expansion in the polarization and the high-field expansion allow us to cover the whole range of field values with very good precision. For the low-fields regime, the fourth-order expansion brings a quantitative improvement when compared to the harmonic expansion that catches qualitatively the trend of the exact functional. For the high-field regimes, the polynomial expansions move away from $\tilde{h}_{DL}(P)$, and the harmonic functional cannot be seen as a valid approximation anymore.

To conclude this section, we have studied a nonlinear functional of the polarization reproducing dielectric properties of water when submitted to a constant excitation. This functional derives from a microscopic model that allows to express the coefficients of the polarization expansion - Eq. (4.10) - as functions of the molecular properties.

4.4 Nonlocal non Gaussian functional for water

In collaboration with Fabien Paillusson

In this section, we complete the nonlocal model given in Eq. (3.12) by nonlinear terms to get a better description of the dielectric properties of water at the nanoscale. The term $\int d\vec{r}(\vec{P}^2)^2$ is the first nonlinear contribution to be considered as we just saw.

Thus, we write a non Gaussian nonlocal functional of $\vec{P}$ as follows:

$$\begin{aligned}\mathcal{U}[\vec{P}] &= \frac{1}{2\epsilon_0}\int d\vec{r}\Big[\gamma(\vec{P}(\vec{r}))^4 + K(\vec{P}(\vec{r}))^2 + \kappa_l(\nabla\cdot\vec{P}(\vec{r}))^2 + \kappa_t(\nabla\times\vec{P}(\vec{r}))^2 \\ &\quad +\alpha(\nabla\nabla\cdot\vec{P}(\vec{r}))^2\Big] + \frac{1}{2\epsilon_0}\int d\vec{r}d\vec{r}'\frac{\nabla\cdot\vec{P}(\vec{r})\nabla\cdot\vec{P}(\vec{r}')}{4\pi|\vec{r}-\vec{r}'|}. \end{aligned} \tag{4.15}$$

For $\gamma \neq 0$, the term scaling like $\vec{P}^4$ in the configurational energy in Eq. (4.15) will induce nonlinear response of the medium. When submitted to a strong electrostatic field $\vec{E}$, the

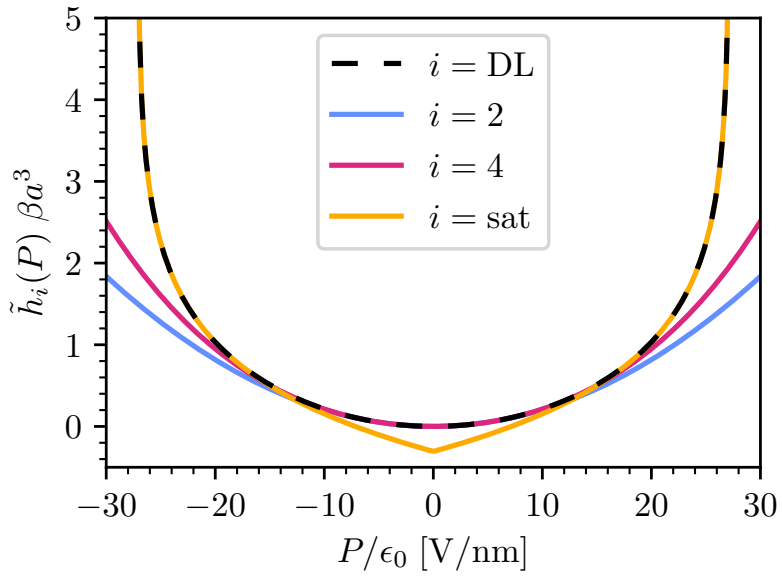

Figure 4.5: Dipolar free energy density in the low- and high-field regime for the DL-model. The fourth-order expression $\tilde{h}_{4,\mathrm{DL}}(P)$ (Eq. (4.10), pink curve)) and the large polarization expansion $\tilde{h}_{\mathrm{sat,DL}}(P)$ (Eq. (4.12), yellow curve) of the dipolar free energy density are compared to the exact density $\tilde{h}(P)$ (dashed black curve) and its harmonic expansion (blue curve). The cusp in $P = 0$ for $\tilde{h}_{\mathrm{sat,DL}}(P)$ is outside of the validity zone of the expansion and has no physical meaning. The parameters used are obtained from SPC/E water simulations: $p_0 = 9.62$ D, $a = 0.51$ nm.

polarization no longer scales linearly with $\vec{E}$ but as $\vec{E}^{1/3}$ [69, 70, 65, 20]. Such a functional can reproduce the response of water under strong fields [20] and presents a threshold saturation, $P_0 = \sqrt{K/2\gamma}$, between a linear response ($|\vec{P}| \ll P_0$) and a saturation response ($|\vec{P}| \gg P_0$) regime. The parameter γ remains the only degree of freedom tuning the saturation threshold. It can be expressed as a functions of microscopic details of the medium using the work done in the last section. See Eq.(4.10).

We now want to characterize the nonlinear effects owing to the Hamiltonian in Eq. (4.15). We consider a stationary external field $\vec{D}_0$ of the form $\vec{D}_0(\vec{r}) = D_0 \cos(qx)\mathbf{u}_x$, with x a Cartesian coordinate and $\mathbf{u}_x$ the associated unit vector and q a given wavenumber. In the linear regime, the response polarization of the form $\vec{P} = P(x)\mathbf{u}_x$ satisfying

$$\begin{aligned} P(x) &= \int dx'\, \chi_{\parallel}(x - x') D_0 \cos(qx') \\ &= \chi_{\parallel}(q) D_0 \cos(qx), \end{aligned} \tag{4.16}$$

with the susceptibility $\chi_{\parallel}$ is given in Eq. (3.15). We generalise the definition of the susceptibility to nonlinear nonlocal medium by defining the Fourier transform of an effective longitudinal susceptibility $\chi_{\parallel\, eff}$ associated to a general polarisation $\vec{P}[D_0 \cos(qx)]$:

$$\chi_{eff}(q, D_0) \equiv \left. \frac{\partial P(x)}{\partial D_0} \right|_{x=0} \tag{4.17}$$

The nonlinear polarization $P(x)$, response to a static oscillating field $D_0 \cos(qx)$, can be expressed as an expansion in D_0. In the third order, we get:

$$P(x, q) = D_0 \chi_{\parallel}(q) \cos(qx) - c_{\mathrm{nl}}(\gamma, K) D_0^3 \left(3\chi_{\parallel}(q)^4 \cos(qx) + \chi_{\parallel}(q)^3 \chi_{\parallel}(3q) \cos(3qx) \right). \tag{4.18}$$

The response is thus the sum of the linear response and a corrective term proportional scaling in D_0^3. The nonlinear coefficient introduced here $c_{\mathrm{nl}}(\gamma, K)$ is a positive function of K and γ.

The expression is given in ref. ([20]). The nonlinear correction thus decreases the value of the response for any wavenumber excited. The corresponding effective susceptibility can readily be obtained from Eq. (4.17). It is plotted in fig. (4.6) for two different excitation -blue and red curves - with a comparison with the Gaussian susceptibility given -dashed gray plot. The model reproduces qualitatively the results obtained with molecular dynamics simulations by Kornyshev and coworkers with the BJH model of water [71, 61].

The first effect of saturation effects appearing at low excitation concerns the wavenumbers associated with the susceptibility maximum. The peak is flattened reducing the nonlocal character of the medium and this effect increases with the amplitude the excitation of as illustrated in Fig. (4.6) a. The Figure 4.6. b. shows the bulk permittivity as a function of the field for MD simulations [6] and with the theoretical model presented here :

$$\epsilon_b(E_0) = 1/(1 - \chi_{eff}(0, \epsilon_0 E_0)). \tag{4.19}$$

The plots are obtained for increasing of γ from blue to purple. As one sees in Fig. 4.6. b), the functional reproduces qualitatively the simulation results.

4.5 Conclusion

In this chapter, we have gone beyond pure Gaussian models for the dielectric properties of water. Saturation of the dielectric response of water occurs for excitations in the range of fields generated by monovalent ions. A model for electrolytes must therefore include this aspect. We have first considered a microscopic model - the DL model - that ignores the nonlocal correlations between particles but has the advantange to be associated with an analytical expression of the free energy as a functional of $\nabla\phi$. We studied the different regimes of this model in the polarization P-space and showed that it reproduces the behavior of simulated water for effective microscopic parameters. We have then studied a nonlocal nonlinear model for water by introducing the lowest nonlinear term P^4. We have shown that the perturbative nonlinear nonlocal response function for this model can reproduce MD results.

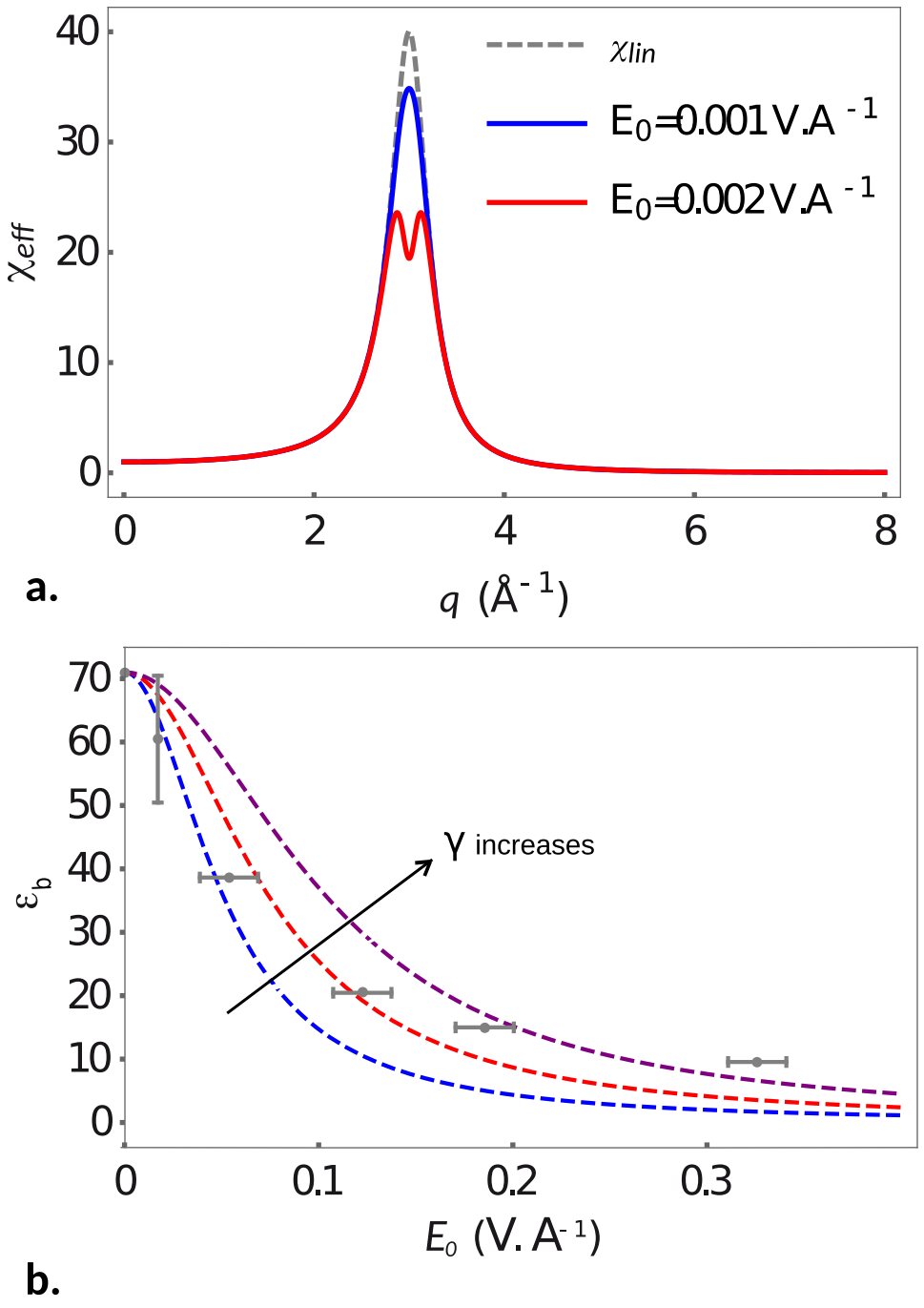

Figure 4.6: **a.** Susceptibility and effective response of a nonlinear dielectric medium. The dashed plot represents the susceptibility in the absence of an electrostatic field (Eq. (3.15)). The blue and the red curves represent the effective response given in Eq. (4.17) of a medium submitted to a small excitation, E_0, for parameters given in ref. [20]. **b.** Dielectric permittivity under constant field, $\epsilon_b(E_0)$ (Eq. (4.19)), for increasing values of γ compared to results obtained with Molecular Dynamics using SPC/E model for water (grey points and error bars). The molecular dynamics results are reproduced from Fig. 11 of Yeh I.-C. et al., J. Chem. Phys. **110** 7935-7942, 1999.

Chapter 5

Inclusion in water

5.1 Introduction

In the last few chapters we have introduced continuous models based on field functionals that describe the structure of water at the nanoscale. We have shown that, depending on the building blocks we use, we can describe the fluctuations of density and/or polarisation with tuned precision. We can also include non-linear effects in the response function of water. These models have been parameterised using MD simulations and microscopic models.

This chapter aims to study the perturbation of the solvent structure induced by the solvation of a punctal inclusion, which may be neutral or charged. Water is rarely pure and contains solutes that affect its properties. The modeling of the interaction between a solute and the liquid is therefore an important point in the description of aqueous solutions.

In this chapter, we study the density and polarization response given by the nonlocal Gaussian framework presented in Eq. (3.20). We then focus on the polarization response to a monovalent ion. Using a simple local model DL Eq. (4.7), we estimate the structure of the solvation zone that we decompose in a zone of saturated constant polarization, in a zone of nonlinear polarization where $\vec{P}$ scales as $\vec{D}^{1/3}$ and a linear regime. Finally, we study the polarization response of an ion described by a nonlinear nonlocal model given in Eq. (4.15). The last section is devoted to the conclusion.

5.2 Polarization and density response for a linear model

In this section, we consider a punctual inclusion solvated in water in $\vec{r} = \vec{0}$. The inclusion is modeled using two 'excitation' fields that are going to perturb the fluid, $\phi_n(r)$ a Lennard-Jones potential and $\vec{E}(r)$ an electrostatic field,

$$\phi_n(r) = 4\epsilon\left(\frac{\sigma^{12}}{r^{12}} - \frac{\sigma^6}{r^6}\right) \tag{5.1}$$

$$\vec{E}(r) = -\nabla\phi(r), \quad \text{with} \quad \phi(r) = \frac{Q}{4\pi\epsilon_0 r}, \tag{5.2}$$

where ϵ and σ are Lennard-Jones parameters characterizing the inclusion. Q is associated with its charge. The mean polarization and density induced in water by an inclusion will be obtained by minimizing the energy:

$$\mathcal{U}_{part} = \mathcal{U} + \int d^3r\rho(r)\phi_n(r) - \int d^3r\vec{P}(r)\vec{E}(r), \tag{5.3}$$

where the energy for bulk water $\mathcal{U}$ can be constructed using the examples we have described in Chapter 3. We consider here the coupled two-field $(\delta\rho, P)$ model which is given in Eq. (3.20).

The density and polarization response functions are presented in Fig. 5.1 to a chlorine atom ($\sigma_{cl} = 3.6$ Å, $\epsilon_{cl} = 9,6.10^{-22}$ J, Q_{cl}=0 C). The Lennard-Jones potential is represented in panel A. of the figure. The response of the medium to a chlorine atom ($\sigma_{cl} = 3.6$ Å, $\epsilon_{cl} = 9,6.10^{-22}$ J, Q_{cl}=0 C) and a chloride ($\sigma_{cl-} = 3.6$ Å, $\epsilon_{cl-} = 9,6.10^{-22}$ J, $Q_{cl-} = 1,6.10^{-19}$ C) are presented in Fig.5.1 Figure 5.1 Ba. represents the radial distribution function $g_{cl}(r) = 1 + \frac{\delta\rho_n(r)}{\rho_0}$, the density response of the medium to an atom of chlorine, while the figure 5.1 b. represents the distribution of polarization $P_n(r)/\mu_0\rho_0$, the polarization response of the medium to a chlorine atom. The dashed part of the plots corresponds to $r < \sigma_{cl}$. Both response functions show a structuration of the fluid around the inclusion associated with a period of about 2. 5 Åand decaying over one nm. The qualitative aspects of the responses are in agreement with the molecular dynamics results but the amplitude of the radial is overestimated. Moreover, the amplitude of the polarization response is similar to the molecular dynamics results given in ref. [44]. The Figure 5.1 B c and d. represents the response to a chloride ion associated with ($\sigma_{cl-} = 3.6$ Å, $\epsilon_{cl-} = 9,6.10^{-22}$ J, $Q_{cl-} = 1,6.10^{-19}$ C). The associated electrostatic potential is presented in the panel A (right plot). The plot 5.1 B c. shows the density response $g_{cl-} = 1 + \frac{\delta\rho_n(r)+\delta\rho_e(r)}{\rho_0}$. The plot 5.1 B d shows the polarization response $(P_n(r) + P_e(r))/\mu_0\rho_0$. We observe the structuration that was already visible for a neutral inclusion.

The density response is overestimated both in range and amplitude. We can mention several arguments to justify the poor results for the density response. The fitting of the structure factor is unsatisfactory (see Fig. 3.7); the density susceptibility is sharper than the ones of water. We do not take into account the excluded volume generated by inclusions embedded in the fluid that will affect the polarization and the density modes of the system. This could be taken into account in a Gaussian model[72, 73, 74]. Moreover, the density response also saturates as the polarization one and this is not included in a Gaussian model. The minimal Landau-Ginzburg model we introduced in Eq. (3.20) could be extended to include some of these effects. Landau-Ginzburg approach is not well developed to describe density in liquids and for a good reason. Determination of the density profile in a liquid is often approached using classical Density Functional Theory [34]. These functionals have been extensively developed in the last decade. The Molecular Density Functional Theory (MDFT) gives now good results for the solvation of non-charged, non-polar systems [40]. The structuration of water around polar or charged systems remains challenging for continuous methods such as DFT. Field theories as presented in this manuscript offer an alternative to address these questions. From now on, we will no longer consider the density response. We focus solely on the water polarization response induced by an ion.

5.3 Hydration shell of an ion for a nonlinear model of water

We have seen that a linear model overestimates the polarization response to a charge (section 5.2) In this section, we use the Dipole Langevin (DL) model (See for Eq. (4.7)- dipoles on a lattice, sketched in Fig.4.2 b. - presented in the Chapter 4. We study the response in the solvation shell calculated by this model and describe how the polarization scales with the excitation when approaching the ion, from linear scaling to saturation. For the moment, we do not consider the nonlocal nature of the material.

As in the previous section, we consider an inclusion, here a punctual ion in $\vec{r} = 0$, that generates an excitation field $\vec{D}_0 = e/4\pi r^2 \vec{u}_r$. The electrostatic energy of the system can be written as

$$\tilde{U}_{\rm ion,DL} = \tilde{U}_{\rm DL} - \frac{1}{\epsilon_0}\int d^3r\, \vec{D}_0(r)\vec{P} \quad \text{and} \quad \frac{\delta\tilde{U}_{\rm ion,DL}}{\delta P}[P_{\rm ion}] = 0 \tag{5.4}$$

where $U_{\rm DL}$ is given in Eq. (4.7). The mean polarization induced in water $P_{\rm ion,DL}(r)$ is purely radial and is obtained by minimizing the energy of the system $\tilde{U}_{\rm ion,DL}$. It gives the right equation in Eq. (5.4). We can also obtain the polarization $P_{\rm ion,i}$ corresponding to the i^{th} expansion of

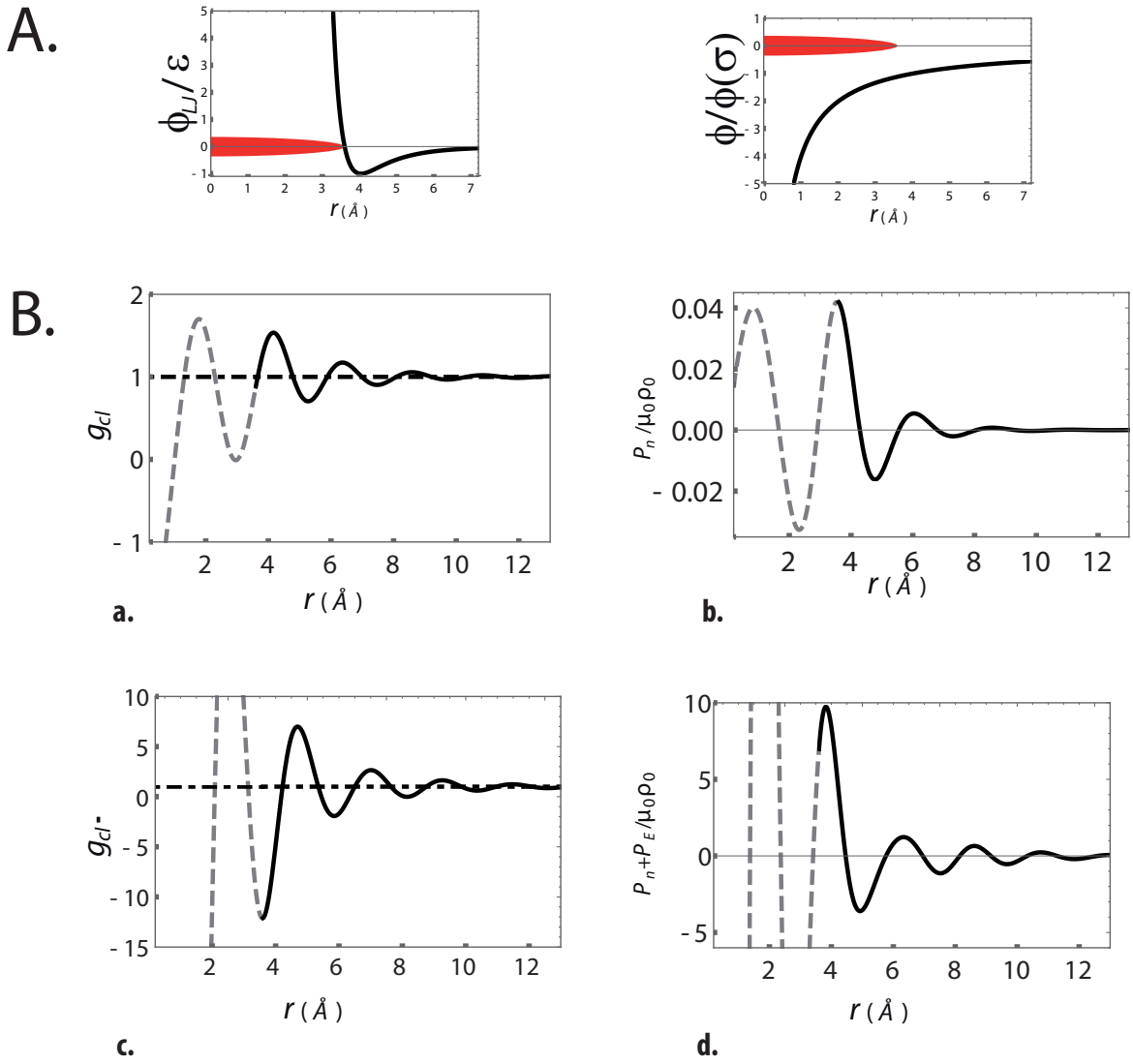

Figure 5.1: A. Representation of the Lennard-Jones potential generated by the chlorine/chloride atom and electrostatic potential generated by the chloride (atom represented by the red disk). B. a., b. Response of water in density and polarization to the chlorine. c., d. Response of water in density and polarization to the chloride. The dashed part of the plots corresponds to $r < \sigma_{cl}$.

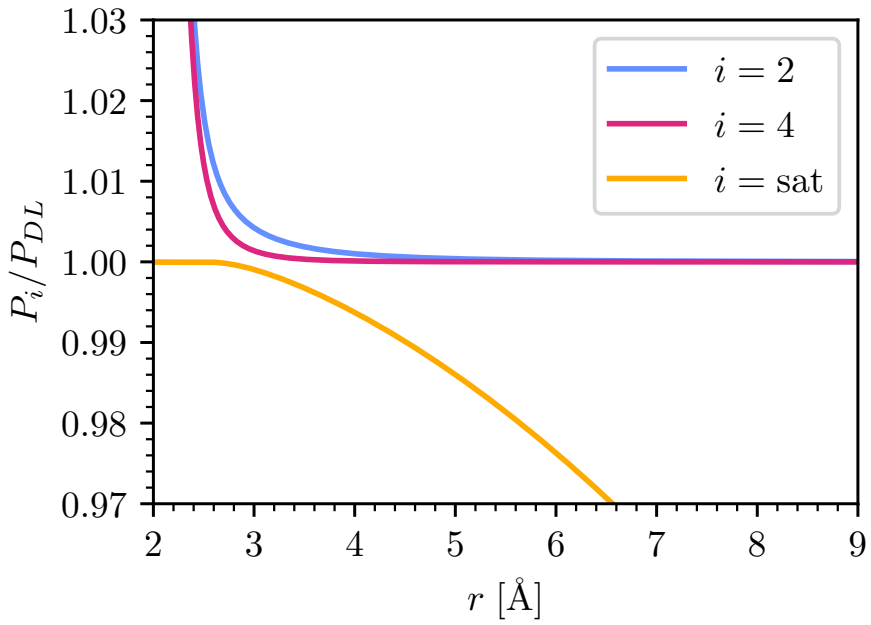

Figure 5.2: Rescaled polarization response to a monovalent ion calculated for low and high field regimes of the DL model. The rescaled linear polarization $P_{\text{ion},2}/P_{\text{ion,DL}}$ (Eq. (5.4)) is plotted in blue, the rescaled fourth-order polarization $P_{\text{ion},4}/P_{\text{ion,DL}}$ is plotted in pink and the rescaled saturated polarization $P_{\text{ion,sat}}/P_{\text{ion,DL}}$ is plotted in yellow. The parameters used are given in Fig. 4.4.

the DL model functional as detailed in the last chapter. We have shown in Eq. (4.11) that the polarization in the solvation shell of the ion, for low r and high excitation, saturates towards $P_{sat} = p_0/a^3$. At large r and low excitation, the response of the medium is homogeneous and linear and equal to $P_2(r) = \chi_b e/4\pi r^2$. Between these two regimes, for intermediate distance r, we can estimate the polarization by using the expansion of the free energy of the lattice model up to P^4 given in Eq. (4.10). The solution $P_{\text{ion},4}(r)$ is analytic and its expression is given in ref. ([23]).

The Figure (5.2) shows the polarization as a function of the distance r around an ion obtained for different approximations rescaled by the exact polarization given by the DL-model, $P_{\text{ion,DL}}(r)$, solution of Eq. (5.4). The linear regime is plotted in blue the 4th-order expansion response is plotted in pink and the saturation polarization is in yellow. We use the parameter values for the DL model estimated in the previous chapter to reproduce SPC/E water polarization under excitation - $p_0 = 9.62$ D and $a = 0.51$nm. As one sees, the linear model overestimates the response of the fluid for $r \leq 5$ Å. The fourth-order expansion brings a gain in the 3-5 Årange but fails to reproduce the first solvation shell. The saturation model succeeds in this range (r$\leq$ 3 Å) but is irrelevant outside of this zone. Note that the range of validity of the different expansions depends on the charge of the ion. Roughly, the size of the saturation shell can be estimated as the radius for which the linear response $P_{\text{ion},2}(r)$ equals the saturation polarization p_{sat} giving $r_{\text{sat}} = Q^{1/2} \times (ea^3/4\pi p_0)^{1/2}$, with Q the valence of the ion. This shell possesses a 2.3 Å radius for a monovalent ion and 4 Å radius for a trivalent ion.

In this shell, the polarization of water is "frozen", we can say that it is a layer of "electronically dead" water [64, 12]. Whatever extra excitation is applied to the medium, the polarization of this shell will remain constant. This corresponds to a vanishing permittivity/susceptibility.

5.4 Hydration shell of an ion for a nonlocal nonlinear medium

We have estimated the size of saturated polarization shell, attenuated polarization shell, and linear response regime around an ion. We now consider the nonlinear and nonlocal model for water presented in the last chapter (Eq. 4.15) and compute the polarization response to the excitation field generated by an ion in this case. We replace in Eq. (5.4) the electrostatic energy $U_{\rm DL}$ by a nonlocal non Gaussian functional given in Eq. (4.15). We perform a functional derivative of the energy and obtain a nonlinear differential equation that can be solved numerically to obtain the nonlocal polarization $P(r)$.

We define a characteristic distance $l = \sqrt{e\chi_b/4\pi P_m}$ defining the radius of the shell in which the response of water is attenuated (nonlinear regime). The polarization $P_m \approx P_0$ [1] is thus a threshold value distinguishing a regime of linear response and a regime of saturation extending over a length l around the ion.

The figure 5.3 shows the polarization obtained for boundary conditions adjusted on MD data published in ref.([44]). The Fig. 5.3 **a.** represents the results obtained with molecular dynamics simulations (red points) with a SPC/E model for water and a charged Lennard-Jones sphere for the chloride (see [44] for all the parameters), the local linear polarisation $P_2(r) = \chi_b e/4\pi r^2$ (dashed gray line) and the nonlocal nonlinear solution $P(r)$ for an attenuated shell of l=3.5 Å. It presents an oscillating decay over 1 nm before converging to the local polarisation $P_2(r)$. The model presented here reproduces both the oscillations and the range of the decay computed with MD simulations. Note that the nonlocal model is here parameterized to reproduce the $\chi_{\parallel}(q)$ of SPC/E.

The figure 5.3 **b** represents the polarization around the ion for increasing values of l. Close to the ion (r small) the polarization oscillates, indicating the arrangement of molecules in organized hydration layers. Far from the ion (r$\geq$ 1 nm) the medium responds as a homogeneous linear material characterized by its bulk susceptibility χ_b. The structuration propagates less for media associated with a large l, *i.e.* which saturates at low polarization. In this case, the response of the medium tends to the superposition of a saturated constant response at low r and a linear response at larger r. We have already noticed that these two regimes catch the response of simulated water in fig. (4.4).

We conclude this chapter by discussing the dielectric permittivity in the vicinity of the ion. As shown in the last chapter, the permittivity of water decreases under a strong electrostatic field (see Fig. 4.6). The static dielectric constant of an electrolyte is known to be a decreasing function of the salt concentration [75]. The intuitive comprehension of this phenomenon is that each ion generates a shell of vanishing permittivity around it [76]. Here, we consider an ion solvated in water and its polarizing given by $P(r)$ that we just discussed (Fig. 5.3). We perturb this system by submitting it to a radial constant static excitation D_0 that superposes to the ion field. We compute numerically the induced polarization $P(r, D_0)$. The response function is defined as follows:

$$\chi_{ion}(r) = \left.\frac{\partial P_{D_0}(r)}{\partial D_0}\right|_{D_0=0}. \tag{5.5}$$

The figure 5.4 shows in blue the dielectric susceptibility in the solvation shell of a monovalent ion. It shows in gray the susceptibility for nonlinear local medium described by a P^4 configurational energy ($\kappa_l = \alpha = 0$ in Eq. 4.15)) and in red the constant susceptibility associated with a linear nonlocal medium. The susceptibility depends on the distance r to the ion whereas the applied excitation is constant D_0. This is because the "degree" of saturation decreases with the field generated by the ion and thus with the distance r. For $r \ll l$, $\chi_{ion}(r)$ behaves as the susceptibility of a nonlinear local medium. The ion is surrounded by a zone of vanishing susceptibility indicating that the solvent molecules located in the first hydration shell of the ion are 'frozen' *i. e.* that they interact electrostatically only with the ion and do not respond to an

[1] $P_m = \pm P_0\sqrt{1 + 1/(2\gamma P_0^2)}$

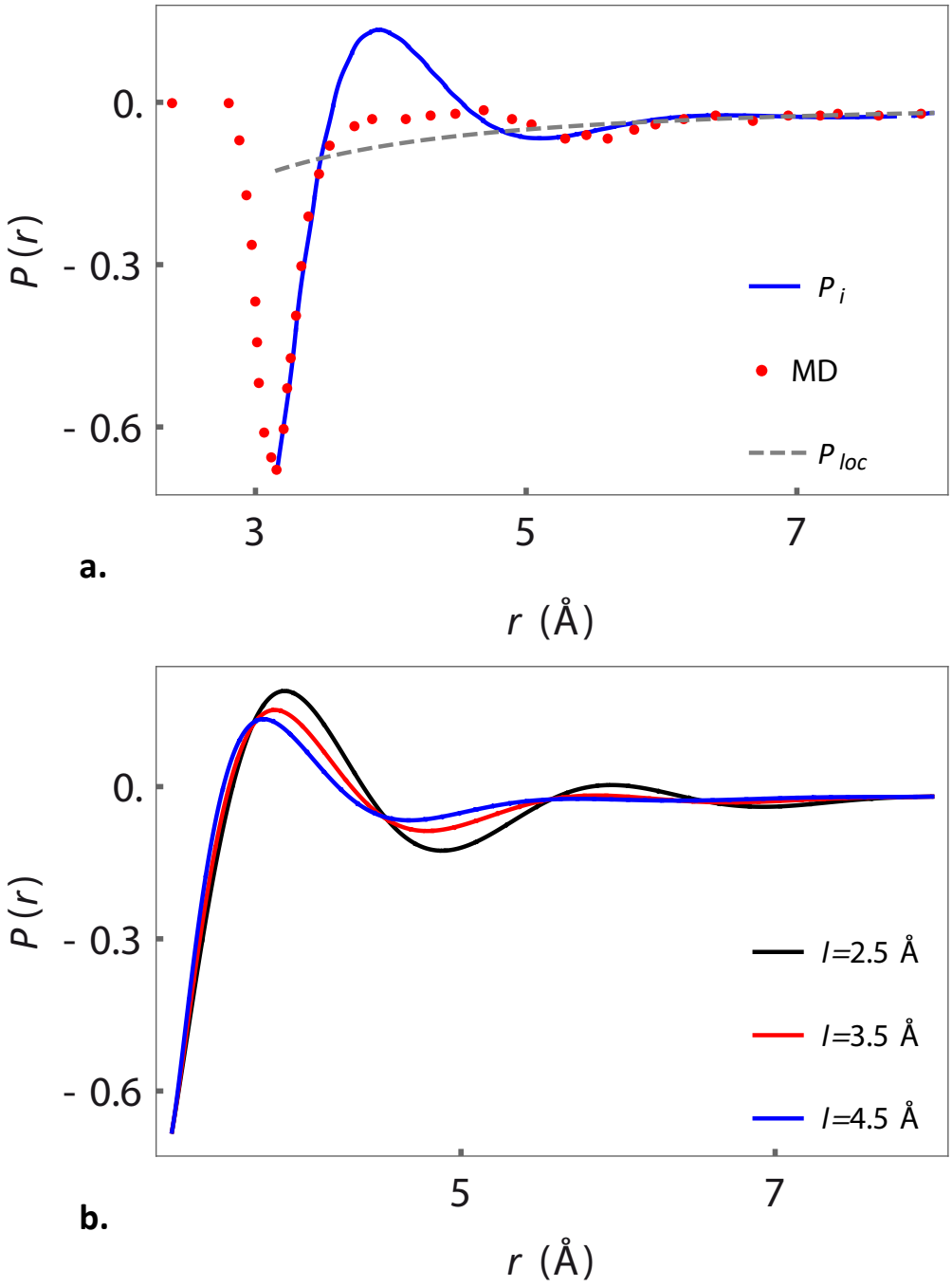

Figure 5.3: Polarisation response to the electrostatic field generated by a monovalent anion. (**a.**) The plain curve represents $P(r)$ as a function of r, for the set of parameters $2\gamma P_m^2 = 1.01$, $\kappa_l = -0.22$ Å^2, $\alpha = 0.012$ Å^4 and $l = 0.35$ nm. The local polarisation P_2 is represented by the gray dashed line and the molecular dynamics results are indicated with the red points, reproduced from Fig 11. of Jeanmairet, G. et al., J. Phys: Condens. Matter **28**. (2016) 244005. (**b.**). Polarisation response $P(r)$ (C.Å^{-2}) as a function of r, for increasing values of l.

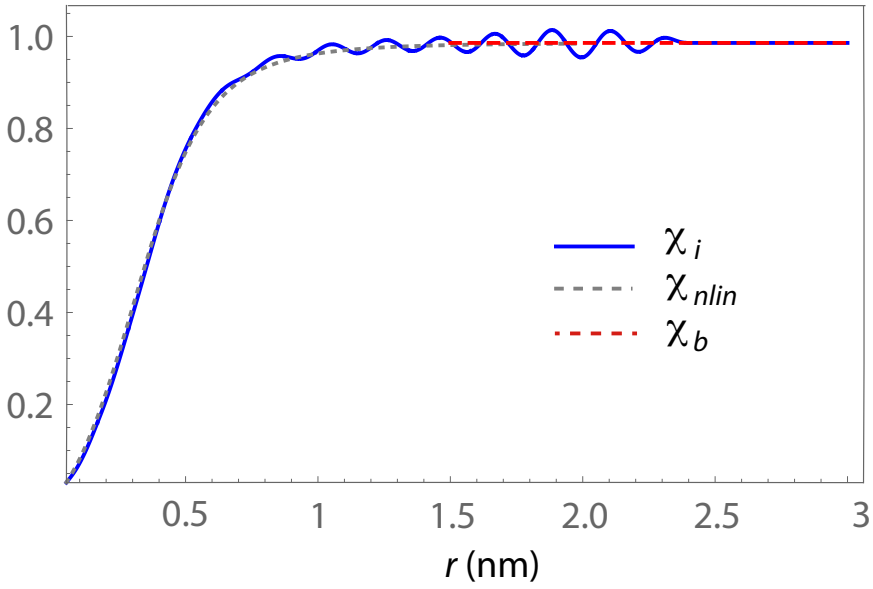

Figure 5.4: Susceptibility for a nonlinear nonlocal medium around an ion. The blue solid line represents $\chi_i(r)$ (relative to the bulk value) given in Eq. (5.5) for a monovalent ion and $P_m = 0.31$ C. Å^{-2}, $l = 0.2$ nm. The dotted line represents the susceptibility around an ion for a nonlinear local medium - see ref. ([20]) for detailed derivation - and the red dashed line represents the bulk susceptibility, $\chi_b \equiv \chi_{\parallel}(q = 0)$.

external field. For a nonlinear local medium, as one moves away from the ion, the molecules see a homogeneous medium associated with a given bulk dielectric susceptibility. For a nonlocal nonlinear medium, we observe an oscillating behavior of over-responses and under-responses around the bulk value due to the nonlocality of the medium. However the oscillations are weak and one distinguishes two zones, an "electronically dead" zone and a zone associated with the bulk permittivity.

5.5 Conclusion

In this chapter, we have computed the response of water to inclusions and focused on the polarization in response to an ion. We characterized the dielectric properties of the solvation shell of an ion and identified three zones. The first layer presents a saturation response, associated with a constant polarization and a vanishing permittivity/susceptibility. The second layer is associated with an attenuated response scaling in the excitation to the power 1/3, associated with a susceptibility lower than the bulk and showing the structural behavior of the fluid. Finally, at a large distance from the ion, water behaves as a linear local medium. We have studied and parameterized a nonlinear nonlocal functional of P (Eq. 4.15) reproducing the attenuated and linear zone observed in MD simulations. We continue this work by now considering electrolytes in the next chapter.

Chapter 6

Bulk electrolytes

In collaboration with Dominique Mouhanna, Douwe Bonthuis and Roland Netz

6.1 Introduction

The study of electrolytes at the nanoscale is exciting both for their ubiquity and for the theoretical challenge they bring [77, 78, 79]. The nanometer scale is the typical confinement size of technological and biological devices, the screening length of medium-concentrated ionic solutions, as well as the range at which water starts to behave as a discrete molecular medium [80, 12, 21]. In the Poisson-Boltzmann equation, water is described as a linear dielectric medium and its permittivity ϵ_b is wavenumber independent. This model cannot capture the complexity of water-ion interaction at the nanoscale.

As we have seen in Chapter 3, at the molecular scale, water is a correlated dielectric medium. This can be characterized by the wavenumber dependence of the susceptibility tensor $\chi(q)$. The figure (3.1) shows the longitudinal and transverse part of the tensor in Fourier space, simulated with Tip4pϵ [45].

The description of the nonlocal dielectric properties of electrolytes has been the subject of many experimental [81, 13, 82, 83] and simulation works [84, 85]. However, the qualitative effect of the salt on water structure, *i.e.* on the H-bond network is still discussed. Is it reinforcing or destroying the network? Contradictory trends have recently been published.

The coarse-grained theories that we have presented until now can provide a useful framework to describe correlated fluids [86, 87, 88, 39]. Nonlocal electrostatics functionals for a correlated fluid associated with a unique length (in the same framework as Eq. (3.12)) have been used to study the coupling between the correlation length of the fluid and the Debye length. by deriving a nonlocal linear PB equation [41, 89]. Recently, a general theory for electrolytes including electrostatic and structural interactions for the solvent has been derived [90, 91, 92]. However, a nonlocal field theory for aqueous electrolytes elucidating water-salt interaction at the nanoscale and validated by MD simulations is missing. In this chapter, we compute the Gibbs free energy and the nonlocal dielectric susceptibility of an aqueous electrolyte for which water is modeled in the Gaussian limit - Eq. (3.13). We perform MD simulations and compare the Gaussian model to a simulated system. We include nonlinear effects - Eq. (4.15). We determine the dependence of the bulk permittivity, and the longitudinal and transverse water correlations with the salt concentration. Finally, we identify the essential building blocks to construct a field theory modeling electrolytes at the nanoscale and reproducing MD simulations

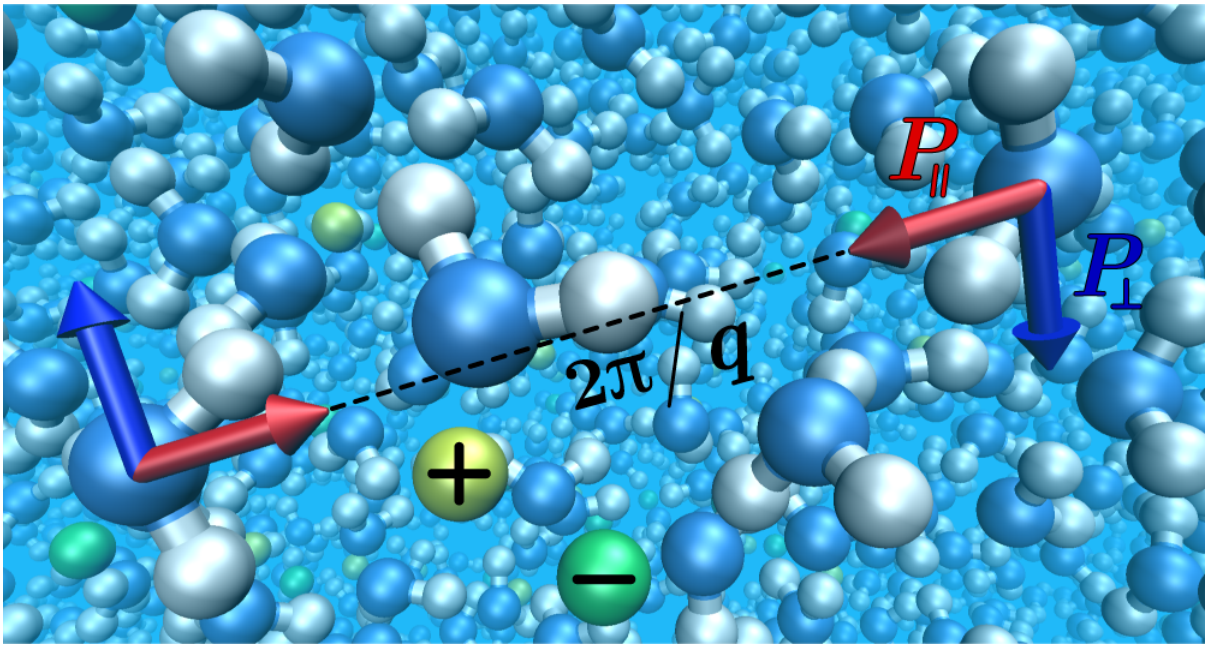

Figure 6.1: Sketch of the system under study. Water is described as a nonlocal nonlinear continuous dielectric medium and ions as point charges. We evaluate the ionic-strength effect on the water longitudinal $\boldsymbol{\mathcal{P}}_{\parallel}$ (red arrow) and transverse $\boldsymbol{\mathcal{P}}_{\perp}$ (blue arrow) polarization correlations and compare it with simulated response functions.

6.2 Model for an electrolyte

In this chapter, we write the electrostatic energy of the solvent as follows:

$$\mathcal{U}_{\rm el}[\boldsymbol{\mathcal{P}}] = \frac{1}{2}\int d\vec{r}d\vec{r}'\frac{\nabla\cdot\boldsymbol{\mathcal{P}}(\vec{r})\nabla\cdot\boldsymbol{\mathcal{P}}(\vec{r}')}{4\pi\epsilon_0|\vec{r}-\vec{r}'|} + \mathcal{U}_{\rm conf}[\boldsymbol{\mathcal{P}}]. \tag{6.1}$$

As previously explained, the first term corresponds to the bare Coulomb interactions between the partial charges $-\nabla\cdot\boldsymbol{\mathcal{P}}(\vec{r})$ of the fluid and the second term to a phenomenological configurational energy of the fluid [39]. We write the configurational energy as follows:

$$\begin{aligned}\mathcal{U}_{\rm conf}[\boldsymbol{\mathcal{P}}] &= \frac{1}{2\epsilon_0}\int d\vec{r}\Big[\gamma\boldsymbol{\mathcal{P}}(\vec{r})^4 + K\boldsymbol{\mathcal{P}}(\vec{r})^2 + \kappa_l(\boldsymbol{\nabla}\cdot\boldsymbol{\mathcal{P}}(\vec{r}))^2 \\ &+ \kappa_t(\boldsymbol{\nabla}\times\boldsymbol{\mathcal{P}}(\vec{r}))^2 + \alpha(\boldsymbol{\nabla}(\boldsymbol{\nabla}\cdot\boldsymbol{\mathcal{P}}(\vec{r})))^2\Big].\end{aligned} \tag{6.2}$$

We thus recover the Gaussian limit given in Eq. (3.13) and studied in chapter 3 for $\gamma = 0$ and the nonlinear model presented in chapter 4 - Eq. (4.15) - for $\gamma \neq 0$.

6.3 Gaussian linear model

We consider an electrolyte with N_+ punctual cations of charge e and N_- punctual anions of charge $-e$ solvated in water modeled with Eq. (3.13). The ionic charge density reads $\rho(\vec{r}) = \Sigma_{i=1}^{N+} e\delta(\vec{r}-\vec{r}_i^{+}) - \Sigma_{j=1}^{N-} e\delta(\vec{r}-\vec{r}_j^{-})$. In the canonical ensemble, the partition function of the system can be written as

$$\mathcal{Z} = \frac{1}{N_+!}\frac{1}{N_-!}\left[\prod_{i=1}^{N+}\int d\vec{r}_i^{+}\right]\left[\prod_{j=1}^{N-}\int d\vec{r}_j^{-}\right]\times\int\mathcal{D}[\boldsymbol{\mathcal{P}}]e^{-\beta\mathcal{U}_{\rm conf}[\boldsymbol{\mathcal{P}}]}e^{-\frac{\beta}{2}\int d\vec{r}d\vec{r}'\rho_{\rm tot}(\vec{r})v(\vec{r}-\vec{r}')\rho_{\rm tot}(\vec{r}')} \tag{6.3}$$

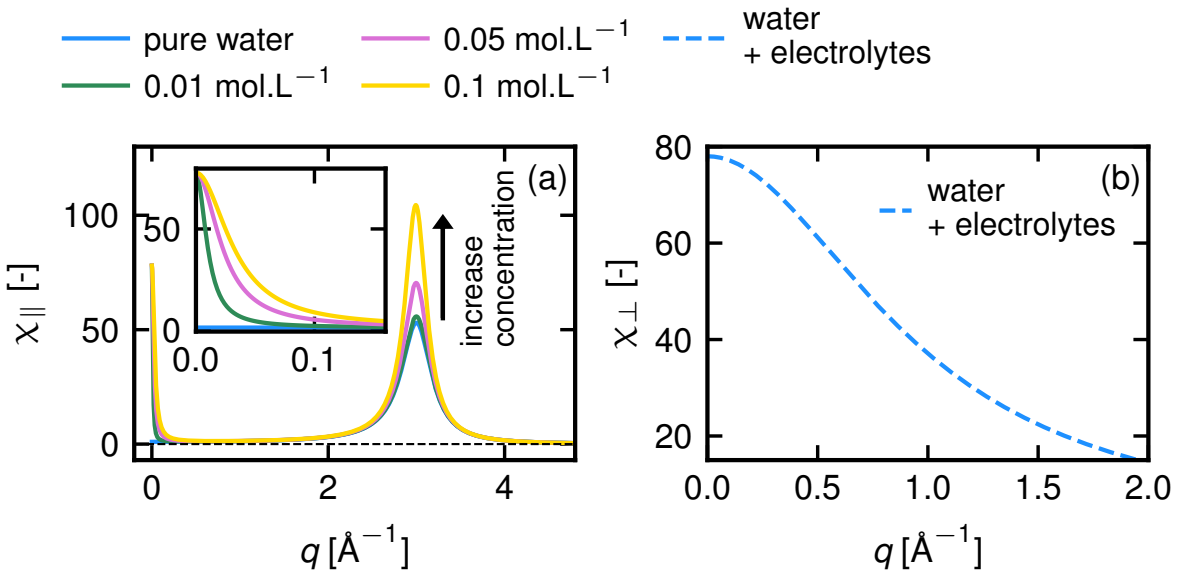

Figure 6.2: Dielectric susceptibility for electrolytes. (a) Longitudinal susceptibility $\chi_{\parallel}$ - Eq. (6.6) - as a function of q for water and solutions of increasing salt concentration. The arrow indicates the increase of the peak maximum with an increase of the concentration. The inset presents a zoom on the low q part of the plot. The inset zooms on the low q part of the plot. (b) Transverse susceptibility $\chi_{\perp} = \chi_{\perp}^{\mathrm{w}}$ given by Eq (3.15) as a function of q, which is identical for water and electrolytic solutions. The parameter values of the FT model given in Eq. (3.13) are K= 1/76, κ_l= -0.218 Å^2, α=0.012 Å^4 and κ_t=0.013 Å^2.

with $\rho_{\mathrm{tot}}(\vec{r}) = \rho(\vec{r}) - \nabla \cdot \boldsymbol{\mathcal{P}}(\vec{r})$ and $v(\vec{r}) = 1/4\pi\epsilon_0|\vec{r}|$. $\mathcal{Z}^{\mathrm{G}}$ includes the configurational degrees of freedom of the solvent and the Coulomb interactions between free and partial charges. Note that here the field $\boldsymbol{\mathcal{P}}$ is the thermally fluctuating polarization. Its mean value is written $\vec{P}$ consistently with the previous chapters. The figure 6.1 presents a schematic illustration of the system we are considering in this chapter.

Following the work of Orland and co-workers [64], we perform a Hubbard-Stratonivich transformation for $\mathcal{Z}^{\mathrm{G}}$ to get rid of the long-range potential v and we switch to the grand canonical ensemble for a more tractable expression of the partition function. The grand-canonical ensemble partition function,

$$\Xi = \int \mathcal{D}[\boldsymbol{\mathcal{P}}]\, \mathcal{D}[\Psi] e^{-\beta F_u^{\mathrm{G}}[\boldsymbol{\mathcal{P}},\Psi]} \tag{6.4}$$

takes a simple expression as a function of the action $F_u[\boldsymbol{\mathcal{P}}, \Psi]$, a functional of $\boldsymbol{\mathcal{P}}$ and of the electrostatic potential Ψ [64]. Assuming a 1:1 electrolyte and an ionic density n, we find:

$$F_u[\boldsymbol{\mathcal{P}}, \Psi] \;=\; \mathcal{U}_{\mathrm{conf}}[\boldsymbol{\mathcal{P}}] - \int d\vec{r}\Big(\frac{\epsilon_0}{2}(\nabla\Psi)^2 - \Psi\nabla\cdot\boldsymbol{\mathcal{P}} - \frac{2n}{\beta}\cosh(\beta\Psi e)\Big). \tag{6.5}$$

Details of the calculations are given in the supplementary material of ref ([46]). The associated susceptibility is calculated by from second functional derivatives of $F_u^{\mathrm{G}}[\boldsymbol{\mathcal{P}}, \Psi]$ and evaluated it in the mean-field point $(\vec{P}, \psi)$. The longitudinal polarization susceptibility is written in Fourier space as

$$\chi_{\parallel}^{\mathrm{G}}(q) = \frac{\frac{\epsilon_b}{\lambda_D^2} + q^2}{\left(\frac{\epsilon_b}{\lambda_D^2} + q^2\right)(K + \kappa_l q^2 + \alpha q^4) + q^2}. \tag{6.6}$$

λ_D is the Debye length and obeys $\lambda_D = \sqrt{\epsilon_0\epsilon_b/2\beta n e^2}$.

Fig. (**??**) a) shows $\chi_{\parallel}(q)$ for increasing salt concentration $c = n/\mathcal{N}_a$, where $\mathcal{N}_a$ is the Avogadro number. The Gaussian model predicts an enhancement of the water ordering with an increase of c, as indicated by the magnitude increase of the peak at q=3 Å^{-1}. This can be understood as follows. In the nonlocal Gaussian framework, an ion, located in $r = 0$ generates the electrostatic potential, $1/4\pi\epsilon_0\epsilon_b r$, and an extra potential oscillating in an exponentially decaying envelope over about one nanometer, as shown in Fig (5.1) [48]. This oscillating landscape leads to the organization of the charges and to longer-range correlations that increase with the salt concentration until a nonphysical crystallization of the system occurs, corresponding to a divergence of $\chi_{\parallel}(q)$.

In contrast, for a very diluted solution $\lambda_D \to \infty$, the longitudinal susceptibility can be approximated as the sum of two contributions:

$$\chi_{\parallel}(q) \approx \frac{\frac{\epsilon_b}{\lambda_D^2} + q^2}{K\frac{\epsilon_b}{\lambda_D^2}q^2 + q^2} + \chi_{\parallel}^{\mathrm{w}}(q). \tag{6.7}$$

The first term corresponds to the response of a local electrolyte associated with a Debye length λ_D and the second term is the unperturbed water spectrum given in Eq. (3.15). The green plot in Fig 6.2 (a). shows this very diluted regime: at low q, we see a decay corresponding to the Debye wavenumber $1/\lambda_D$ (see inset of Fig. 6.2 (a)), for q >2 Å the spectrum superposes with the pure water one. The transverse susceptibility $\chi_{\perp}(q)$ of electrolytes is unaffected by the presence of salt and obeys $\chi_{\perp}(q)$=$\chi^{\mathrm{w}}(q)$. Indeed, the coupling between the salt and the solvent occurs via the Coulomb interactions and involves only the longitudinal part of the polarization as seen in Eq. (6.3). Finally, we note that the Gaussian model predicts that the dielectric bulk properties of electrolyte solutions $\chi_{\parallel}(0) = \chi_{\perp}(0) = 1/K$ are independent of the salt concentration.

6.4 MD simulated response functions for electrolytes

To check the validity of the Gaussian model, we compare its predictions with the dielectric properties of simulated solutions of NaCl in TIP4p/ϵ water for concentrations c up to 1.5 mol.L^{-1} [45, 93]. We simulate a cubic water box of side size L=6.5 nm composed of N_w water molecules, N_w going from 9033 to 8527 for increasing salt concentration. See a snapshot of the simulated system in Fig. 6.3. The 0.15 mol.l^{-1} solution contains 25 ion pairs, the 0.75 mol.l^{-1} solution contains 124 ion pairs and the 1.5 mol.l^{-1} solution, 248 ion pairs. We perform simulations with TIP4p/ϵ ([45]) Production runs are performed in the NVT ensemble for 20 ns.

Bulk permittivity is calculated from the fluctuations of the total system dipole moment [94]. The longitudinal susceptibility is computed from the charge structure factor [46] and the transverse one following the method detailed in ref. [49]. For the longitudinal and transverse susceptibility, the error bars are derived following the reblocking method [95]. For the bulk permittivity, we cut the trajectory in 5 statistically independent blocks, compute the bulk permittivity of each block, estimate the sample variance σ^2 and define the error bar as $\sqrt{\sigma^2/5}$.

We compute the bulk permittivity and plot $\epsilon(c)$ in Fig. 6.4 (a). We observe a linear decay, which is not described by the Gaussian model that predicts a constant bulk (q=0) permittivity. The susceptibilities $\chi_{\perp}^{\mathrm{MD}}(q)$ and $\chi_{\parallel}^{\mathrm{MD}}(q)$ are shown in Fig 6.4 (b) and (c) for c=0.15 mol.L^{-1} - λ_D=7.8 Å-, c=0.75 mol.L^{-1} - λ_D=3.5 Å-, and c=1.5 mol.L^{-1} - λ_D=2.5 Å. The blue markers show the response for pure water. We observe a decay of the bulk value $\chi_{\perp}^{\mathrm{MD}}(0)$ for an increasing concentration, which is not captured by the Gaussian model. The longitudinal susceptibility plot, $\chi_{\parallel}^{\mathrm{MD}}(q)$, shows a decay at low q ($q \leq$2 Å^{-1}) corresponding to the Debye wavenumber and shows the spectrum of water (q >2 Å^{-1}), which remains almost unperturbed. At high salt concentration, the peak at $q \approx$3 Å^{-1} slightly increases and is flattened. The MD results indicate thus an effect of the salt opposite to the Gaussian model predictions that appear at a much higher concentration.

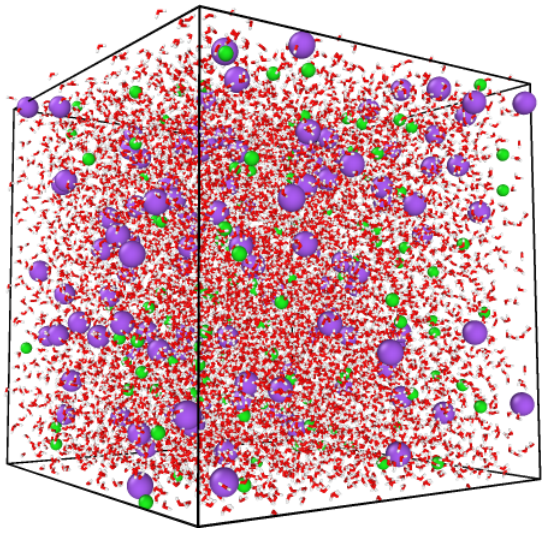

Figure 6.3: Snapshot of a simulation box of electrolytes. Red and white sticks represent TIP4p/ϵ water molecules, purple spheres chloride Cl^- ions and green spheres sodium Na^+ ions. This picture corresponds to a 0.75 mol.l^{-1} solution. Side size of the box: L=6.5 nm.

A Nonlinear model for the solvent - To get a better agreement between FT and MD simulations, we consider the nonlinear configuration energy $\mathcal{U}_{\rm conf}$ with $\gamma \neq 0$. The grand partition function obeys $\Xi = \int \mathcal{D}[\boldsymbol{\mathcal{P}}]\,\mathcal{D}[\Psi] e^{-\beta F_u[\boldsymbol{\mathcal{P}},\Psi]}$. The action contains here a non-quadratic term, $\gamma\boldsymbol{\mathcal{P}}^4$ and its effect on response functions can be estimated by using a *loop expansion*. This method allows to go beyond Gaussian partition functions. It is based on a systematic expansion of the action around the mean field [96] that we perform here at the first order, named *one loop expansion* [65]. The action F_u is expanded up to the second order in $(\boldsymbol{\mathcal{P}}, \Psi)$ around the mean field solution, $F_u[\boldsymbol{\mathcal{P}}, \Psi] \approx F_u[\boldsymbol{P}, \psi] + 1/2 \int d\vec{r} d\vec{r}' (\delta\vec{P}(\vec{r}), \delta\psi(\vec{r})) \cdot F_u^{(2)}(\boldsymbol{P}, \psi) \cdot (\delta\vec{P}(\vec{r}'), \delta\psi(\vec{r}'))$, with $F_u^{(2)}$ the second functional derivative of F_u with respect to $(\boldsymbol{\mathcal{P}}, \Psi)$ and $\delta\vec{P} = \boldsymbol{\mathcal{P}} - \boldsymbol{P}$, $\delta\psi = \Psi - \psi$. The mean fields $(\vec{P}, \psi)$, are vanishing. The partition function thus follows as

$$\Xi \approx \exp\left\{-\beta F_u[\vec{\boldsymbol{P}}, \psi] - \frac{1}{2}\ln\left[\det \beta F_u^{(2)}(\boldsymbol{P}, \psi)\right]\right\} \tag{6.8}$$

and the free energy is then written as $\mathcal{F} \approx F_u[\boldsymbol{P}, \psi] + \mathrm{Trln}(\beta F_u^{(2)}[\boldsymbol{P}, \psi])/\beta$. The inverse susceptibility follows as $\chi^{-1}(\vec{r}_1 - \vec{r}_2) = \chi^{-1}(\vec{r}_1 - \vec{r}_2) + \chi^{-1,1}(\vec{r}_1 - \vec{r}_2)$, with the one-loop correction term $\chi^{-1,1}(\vec{r}_1 - \vec{r}_2)$ defined as:

$$\chi_{i,j}^{-1,1}(\vec{r}_1 - \vec{r}_2) = \frac{1}{2\beta} \frac{\delta^2 \mathrm{Tr} \ln \beta F_u^{(2)}}{\delta\mathcal{P}_i(\vec{r}_1)\delta\mathcal{P}_j(\vec{r}_2)}(\boldsymbol{P}, \psi). \tag{6.9}$$

χ^{-1} is the inverse of the susceptibility in the Gaussian limit given in Eq. (6.6). Performing the field derivatives and calculating the trace in Eq. (6.9), one obtains

$$\begin{aligned} \chi_{i,j}^{-1,1}(\vec{r}_1 - \vec{r}_2) &= \delta K \delta(\vec{r}_1 - \vec{r}_2)\delta_{ij} \quad \text{with} \\ \delta K &= \frac{20\gamma\epsilon_0}{3\beta}\left(\chi_\parallel(r=0) + 2\chi_\perp(r=0)\right). \end{aligned} \tag{6.10}$$

The derivation of $\chi_{i,j}^{-1,1}$ is detailed in the supplementary material of the ref.([46]). Note that here $\chi_\parallel$ and $\chi_\perp$ are expressed in real space as Fourier transform of Eq. (6.6) and taken in $r = 0$. The first-order correction of the susceptibility is purely local and proportional to γ, which tunes the saturation regime of the model. More importantly, Eq. (6.10) shows that the correction

δK depends now on the salt concentration c. Indeed, δK is a function of $\chi_{\parallel}$ which depends on λ_D^2 (see Eq. (6.6)) and thus of c. δK is expanded linearly in c as $\delta K(c) = \delta K_w + \delta K_c c + \tau(c^2)$, where δK_w is the one-loop expanded correction to K for pure water and $\delta K_c c$ is the one induced by the salt. Their analytical expressions are derived in ref.([46]). The corrected permittivity, $\epsilon = 1+1/(K+\delta K)$ is now salt concentration dependent. Setting δK_w to zero as it is included in the fitted value of K, and performing a linear expansion in c of $\epsilon(c)$, we find for the permittivity:

$$\epsilon(c) \quad = \quad \epsilon_b - \frac{\delta K_c}{K^2} c. \tag{6.11}$$

Figure 6.4 (a) shows $\epsilon(c)$ for a value of δK_c adjusted to reproduce the MD data and given in the caption of Fig 6.4. The one loop expansion of a nonlinear polarization functional can thus reproduce the decrement of the bulk permittivity of electrolytes observed in MD simulations [64].

6.5 Susceptibility kernels for electrolytes

We now compare the simulated q-dependent susceptibilities with the nonlinear FT model ones, obtained by replacing K by $K + \delta K_c c$ in Eq. (6.6) for $\chi_{\parallel}$ and in Eq. (3.15) for $\chi_{\perp}$. The one-loop corrected transverse response,

$$\chi_{\perp}^{\mathrm{FT}}(q) = \frac{1}{K + \delta K_c c + \kappa_t q^2}, \tag{6.12}$$

is plotted in Fig. 6.4 (b) for c=0, 0.15, 0.75, 1.5 mol.L^{-1} and shows very good agreement with simulations. The one-loop corrected longitudinal response is plotted in Fig. 6.5. Similarly to the Gaussian limits, it foresees an enhancement of the longitudinal correlations and thus fails to reproduce MD data.

We thus propose an *ad hoc* longitudinal susceptibility based on the one of very diluted electrolytes given in Eq. (6.7). Taking into account the quasi-invariance of the water spectrum observed in the MD data, we write $\chi_{\parallel}^{\mathrm{FT}}$ as the sum of two decoupled terms as follows:

$$\begin{aligned} \chi_{\parallel}^{\mathrm{FT}}(q) \quad &= \quad \frac{\frac{\epsilon_b}{\lambda_D^2} + q^2}{(K + \delta K_c c)(\frac{\epsilon_b}{\lambda_D^2} + q^2) + q^2} \\ &+ \quad \frac{1}{1 + K + \delta K_c c + \kappa_l q^2 + \alpha q^4}. \end{aligned} \tag{6.13}$$

The first term corresponds to the susceptibility of a local electrolyte associated with the corrected permittivity $\epsilon(c)$ given in Eq. (6.11). The second term corresponds to the nonlocal susceptibility of pure water associated with this corrected permittivity. We plot $\chi_{\parallel}^{\mathrm{FT}}(q)$ for c=0, 0.15, 0.75, 1.5 mol.L^{-1} in Fig. 6.4 (d). It reproduces well the decay at low q and the flattening of the peak at q=3 Å^{-1} with an increase of the salt concentration. It thus catches the main effect of the salt on water correlation modes.

6.6 Interaction between the filaments in electrolytes at the nanoscale

In collaboration with Anne-Florence Bitbol, Serges Reynaud and Paolo Maia Neto.

Now that we have described the electrostatic correlations in electrolytes, we study briefly the interactions between objects solvated in electrolytes. The fluctuations of the electromagnetic field are responsible for an interaction between them called van der Waals or Casimir force depending on the system. It is broadly assumed that these interactions are short-ranged for objects immersed in electrolytes due to Debye screening. However, in the last section, we have shown that transverse electrostatic modes remain unscreened by salt.

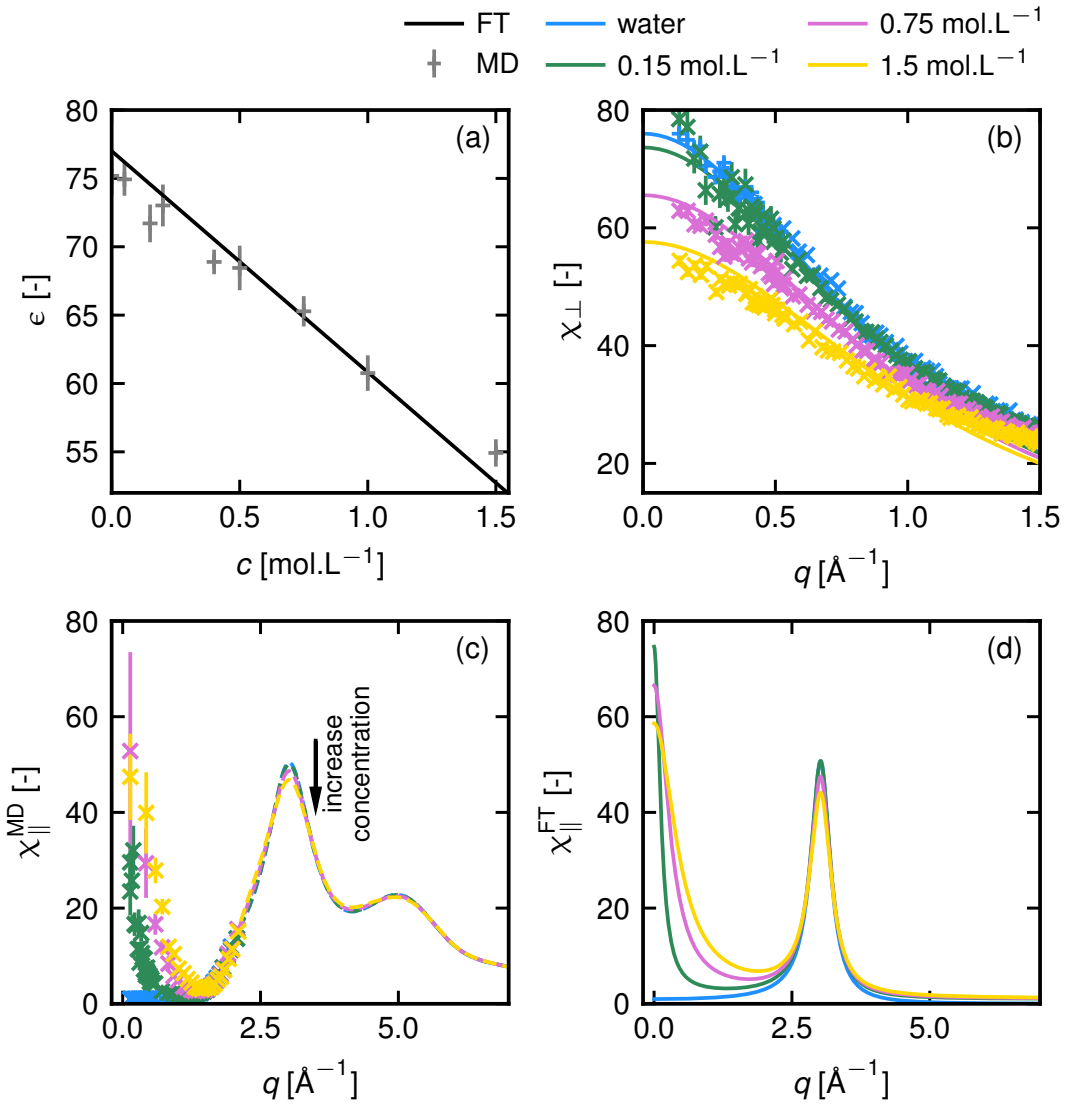

Figure 6.4: Comparison of FT-derived and MD simulated response functions of electrolytes. (a) Bulk permittivity as a function of c. The field theory expression is given in Eq. (6.11) and plotted for δK_c=0.0028 mol^{-1}.L, (b) Transverse permittivity - FT expression given in Eq (6.12), (c) MD simulated longitudinal susceptibility $\chi_\parallel^{\mathrm{MD}}$, (d) conjectured expression of the longitudinal susceptibility $\chi_\parallel^{\mathrm{FT}}$ given in Eq. (6.13).

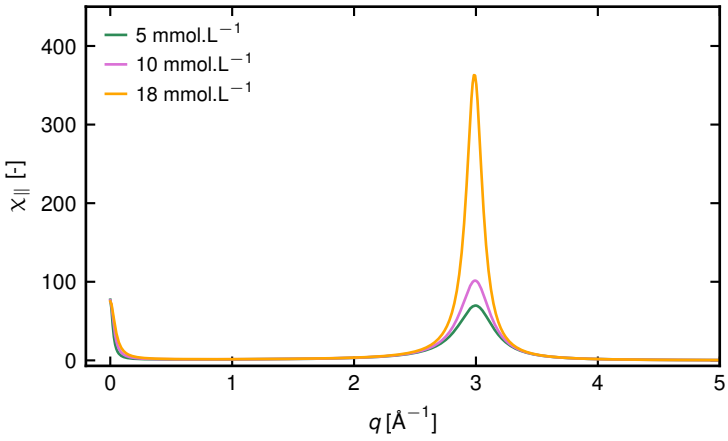

Figure 6.5: One-loop expanded longitudinal susceptibility of electrolytes. The susceptibility $\chi_{\parallel}(q)$ given in Eq. (6.12), for increasing concentration with δK_c=0.028 mol^{-1}.L.

In independent works, the Casimir interaction was recently shown to be stronger and of longer range than previously expected. This interaction was computed between two dielectric spheres and measured experimentally for colloids immersed in electrolytes, confirming the long range of the force. However, for the system considered, the interaction remains significantly lower than the thermal energy and could not play a structural role for such systems. As the filamentous structures are ubiquitous in cells, we compute here the Casimir interactions for such systems.

Cytoskeletal filaments, in particular actin filaments and microtubules, play crucial parts in maintaining the integrity of eukaryotic cell shape, in its deformations, as well as in multiple subcellular processes, by actively generating forces with the help of motor proteins [97, 98, 99]. Actin filaments form bundles, where filaments are cross-linked by specific proteins into parallel arrays. Microtubules, which are thicker and more rigid than actin filaments, also form bundles cross-linked by microtubule-associated proteins [100]. Both in the case of actin filaments [101, 102] and in that of microtubules [103, 104, 105], bundles of parallel filaments have been shown to form *in vitro* in the absence of cross-linkers under certain experimental conditions. Beyond the cytoskeleton, several enzymes form filaments in cells, with important biological functions, and these filaments also often self-assemble into larger assemblies, especially bundles [106].

To investigate whether a long-range Casimir interaction could play a role in the formation of these bundles, we first calculate the dielectric response for an electrolyte that mimics the cytosol. We have simulated a solution with a concentration of 0.2 mole per liter of potassium bromide (KBr) This is in the range of typical cytoplasmic concentrations and is thus relevant for our applications to bundles of biological filaments below. In agreement with the results shown in Fig. (6.4), we find that the longitudinal modes of the electrostatic polarization are screened whereas transverse modes remain unaffected.

We derive the Casimir free energy by using the scattering method. A detailed derivation is given in refs. ([107, 108]). We show that its magnitude largely exceeds the thermal energy scale for a large parameter range. This includes length scales relevant for actin filaments as shown in Fig. (6.6) and microtubule bundles in cells. Therefore, it could have important implications in the self-assembly and cohesion of bundles of filaments at the cell scale [99].

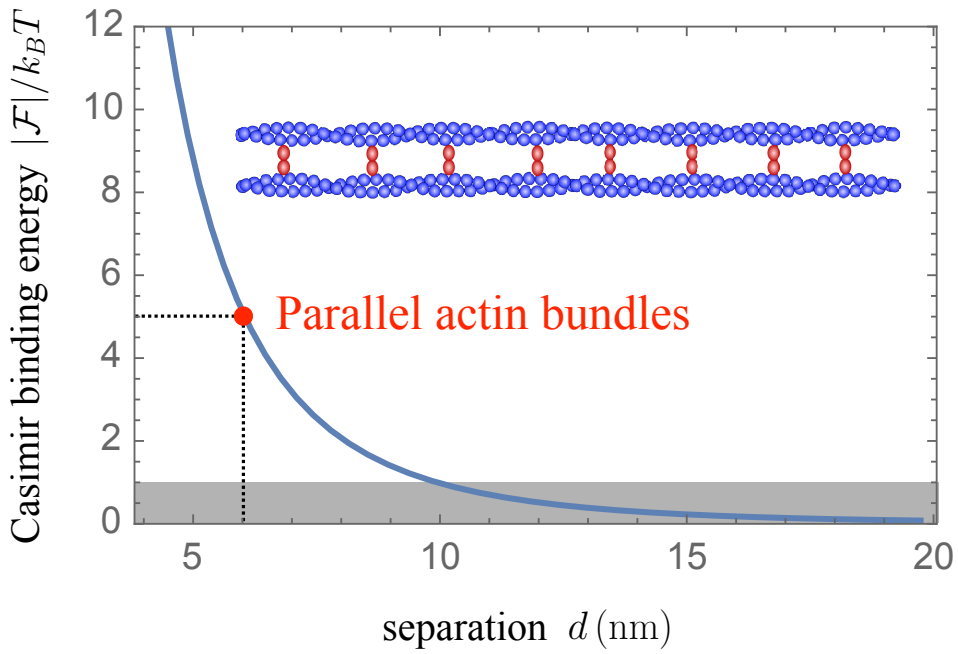

Figure 6.6: **Casimir binding free energy between actin filaments.** The Casimir binding free energy $|\mathcal{F}| = -\mathcal{F}$ is shown versus the separation distance d (nm) for two parallel actin filaments. Each filament has a radius 3 nm and length 15 μm. $|\mathcal{F}|$ is expressed in units of k_BT, and the zone where $|\mathcal{F}| < k_BT$ is shaded in gray. Casimir binding free energies above the gray zone are expected to matter in practice, including in the physiological case of parallel actin bundles (red marker). Inset: schematic of two actin filaments (blue) in a parallel actin bundle. Cross-linkers are shown in red.

6.7 Conclusion

In this chapter, we have analyzed how polarization correlations in water are affected by the addition of salt. To do so, we have compared susceptibilities calculated from a FT model including nonlocal and nonlinear behavior of water and with MD-derived ones, and identified the key effects of the salt on water organization. For the longitudinal modes, we highlight two length scales that do not couple to each other: for small q, $q \leq 2$ Å^{-1}, the medium can be described with a q-independent permittivity $\epsilon(c)$. This corresponds to long-range interactions for which the Debye screening occurs. At larger q, the water longitudinal susceptibility is similar to the one of pure water but associated with a corrected permittivity $\epsilon(c)$. These two decoupled q-domains could indicate two "types" of water molecules that are spatially separated: the one solvating ions are frozen in response to the ionic field, creating an "electrically dead" solvation shell [64]. Outside of this shell, the molecular water organization is remarkably unaffected by the ions [23, 82]. Moreover, our work reveals the absence of coupling between salt screening and transverse polarization modes of water. We have thus shown that the non-coupling with transverse modes could have important consequences on the interactions between filaments in biological cell electrolytes [107, 108].

This study gives us a clear picture of the nature and the range effect of the salt on water organization at the nanoscale for unconfined solutions. In the next chapter, we will discuss the properties of confined solutions, first neat water and then electrolytes.

Chapter 7

Nanoconfined aqueous solutions

7.1 Introduction

In this chapter, we show through 3 examples that the structure of water at the nanoscale has a strong impact on the properties of confined systems.

We first consider the permittivity of confined water. Interest in the dielectric properties of confined water has been boosted by the remarked measurement of the dielectric permittivity of nanometric water layer confined between hydrophobic surfaces [12]. Fumagali et al. reported an anomalously low dielectric constant in the direction perpendicular to the surface. [109] Water permittivity in the vicinity of a surface is inhomogeneous[47, 110] leading to a significant increase of the electrostatic interactions, as postulated in the 1950's by Schellman,[111] and observed experimentally and in simulations [112, 113, 114]. The stability of emulsions and colloidal solutions [115, 116], ion transport and reactivity in channels of proteins,[117], in subsystems of geological interest [118] or in nanotechnological devices [119] are strongly influenced by electrostatic properties of confined water. However, a fundamental analytic theory connecting the dielectric response to the properties of the confining surfaces, namely chemical composition, degree and geometry of confinement, is still outstanding.[120] We use the nonlocal electrostatic energy for water coupled to a surface interaction to study the dielectric properties of the interface. We define the size of the "interfacial water layer" and show how its dielectric properties are encoded both by bulk correlations and surface properties. This framework compares favorably to experiments and simulations and is versatile.

In the second part of this chapter, we study the interfacial properties of electrolytes. We investigate how the nonlocal dielectric properties of water at the nanoscale affect the ion profile in the electrical double layer by developing a nonlocal Poisson-Boltzmann equation which includes the effect of the ionic size. We observe an ion layering at the surface, which is in agreement with recent experiments characterizing these systems [121, 122].

Finally, we consider the forces mediated by water between macroscopic surfaces [123]. These hydration forces have been extensively studied experimentally. In this part of the manuscript, we explore the consequences of an extended phenomenological Landau-Ginzburg energy model for the nonlocal correlations in water. We show that this approach describes consistently the non-monotonic, oscillatory decay in the forces measured between molecularly smooth surfaces [124] and the quasi-exponential, monotonous decay between rough surfaces [125].

The last part of the chapter is devoted to the conclusion.

7.2 Dielectric properties of confined water

In collaboration with Geoffrey Monet, Fernando Bresme and Alexei Kornyshev

In this section, we use nonlocal electrostatics to describe the dielectric properties of a nanometric

water slab.

7.2.1 Field theory description

We consider water delimited by a planar interface infinite in the xy plane and located at $z = 0$ (See Fig. 7.1a). A static homogeneous external field $\vec{D}_0 = D_0\vec{u}_z$ is applied in the z-direction. According to the symmetry of the problem, this field excites exclusively the longitudinal polarization that depends on z: $\vec{P}(\vec{r}) = P(z)\vec{u}_z$. We write the energy of the system per unit area $U[P, D_0] = U_{\text{bulk}} + U_s$, the sum of the bulk-determined term, U_{bulk}, derived from (Eq. 3.13), and a surface term U_s as:

$$\begin{aligned} U_{\text{bulk}} &= \int_{z=0}^{\infty} \frac{dz}{2\epsilon_0} \left[(D_0 - P)^2 + KP^2 + \kappa_l \dot{P}^2 + \alpha \ddot{P}^2 \right] \\ U_s &= \frac{k_P}{2} \left(P(0) - P_0 \right))^2 + \frac{k_\rho}{2} \left(\rho(0) - \rho_0 \right))^2 \end{aligned} \tag{7.1}$$

where the upper dot stands for the spatial derivation along z. In the spirit of the Landau-Ginzburg development used to express the electrostatic energy (Eq. (3.13)), U_s is written as an expansion of elastic energies[126, 127] depending on the polarization field and its derivative $\dot{P}(z)$, equal to minus the bound charge, $\rho(z)$.[128] The major contribution promotes a surface polarization P_0 and the corrective second term favors a water charge density ρ_0 at the interface. The stiffness k_P and k_ρ quantify the strength of the boundary conditions. In the strong interaction limit $(k_P, k_\rho) \to \infty$, the surface fixes both polarization and charge density at the interface.

The partition function of the system, $\mathcal{Z}[D_0] = \int D[P_z] \exp\left[- \left(U_{\text{bulk}}[P, D_0] + U_s \right) / k_B T \right]$, can be split in the form

$$\mathcal{Z}[D_0] = \int d\bar{P} d\bar{\rho} \exp\left[-\frac{1}{k_B T} \left(\frac{k_P}{2} (\bar{P} - P_0)^2 + \frac{k_\rho}{2} (\bar{\rho} - \rho_0)^2 \right) \right] \int_{\substack{\dot{P}(0) = -\bar{\rho} \\ P(0) = \bar{P}}}^{\substack{\dot{P}(z\to\infty) = 0 \\ P(z\to\infty) = 0}} D[P] \exp\left[-\frac{1}{k_B T} U_{\text{bulk}}[P, D_0] \right]. \tag{7.2}$$

This includes a partition of the fields $P(z)$ satisfying the boundary conditions (right integral), then a sampling of the $z = 0$ boundary conditions $(\bar{P}, \bar{\rho})$ (left integral). We find the mean field solution, $P(z)$, by first minimizing $U_{\text{bulk}}[P, D_0]$ with respect to $P(z)$ leading to:

$$P(z) = \frac{D_0}{1 + K} \left(1 - e^{-\frac{z}{\lambda_d}} \left(\cos(q_o z) + \frac{q_d}{q_o} \sin(q_o z) \right) \right) + e^{-\frac{z}{\lambda_d}} \left(\bar{P} \left(\cos(q_o z) + \frac{q_d}{q_o} \sin(q_o z) \right) - \frac{\bar{\rho}}{q_0} \sin(q_o z) \right) \tag{7.3}$$

with $q_o = 2\pi/\lambda_o$ and $q_d = 1/\lambda_d$, the wavenumbers of the bulk correlations. Second, we extremalize the total energy of the system, $U = U_{\text{bulk}} + U_s$, with respect to $(\bar{P}, \bar{\rho})$. $U(\bar{P}, \bar{\rho})$ admits a minimum for strong enough stiffness k_P and k_ρ. A weak coupling leads to a nonphysical diverging polarization at the interface. The zone of interest (finite polarization) is defined for dimensionless stiffness $\bar{k}_P$ and $\bar{k}_\rho$ and is represented in Fig. 7.1b. Details are given in ref. ([21]).

To study the dielectric properties of interfacial water, we introduce the real space susceptibility, $\chi(z) = dP(z)/dD_0$. It quantifies the response to a homogeneous external field D_0 and is constant and equal to $\chi_b = \hat{\chi}(0)$ for bulk water. Fig. 7.1c, d show typical mean field polarization $P(z)$ and susceptibility $\chi(z)$ in the interfacial water. We observe a nonvanishing polarization and a nonconstant $\chi(z)$ that are oscillating functions of period λ_o in an exponentially decaying envelope of range λ_d. The surface induces a layering of the fluid that extends over about 1 nm, a length scale consistent with many previous simulations of interfacial water[47, 80]. The susceptibility shows alternation of "underresponding" ($\chi(z) \ll \chi_b$) and "overresponding" layers ($\chi(z) \gg \chi_b$), typical for "overscreening" effect. Whereas the amplitude of the polarization is a non-trivial function of the bulk properties, the four parameters of the surface interaction and

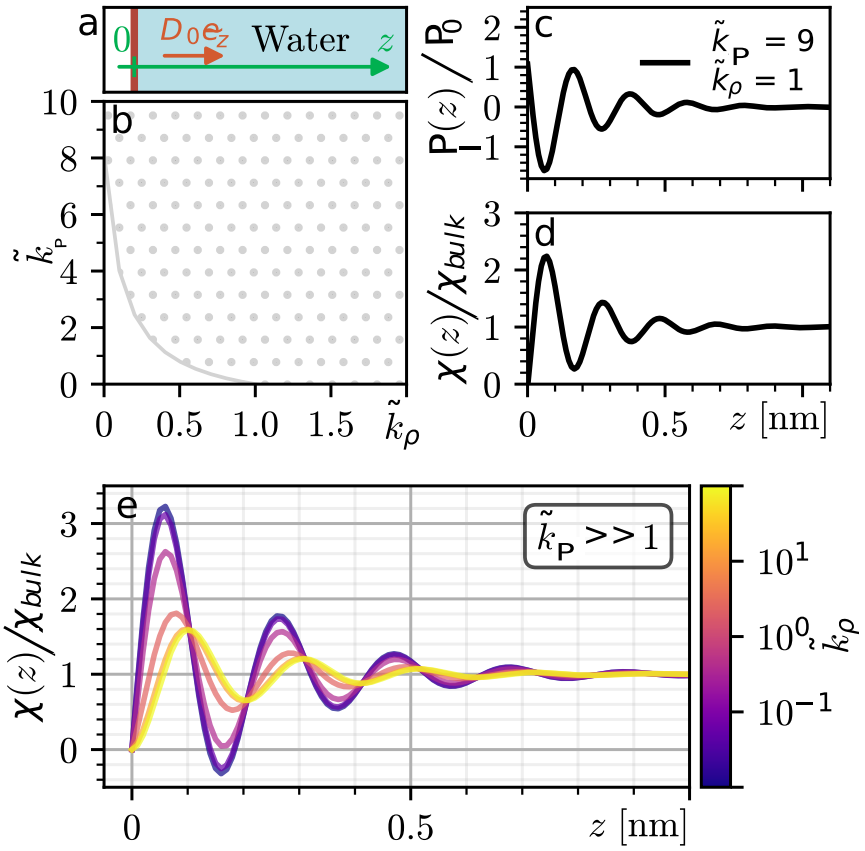

Figure 7.1: Dielectric properties of water in the vicinity of a surface. **a.** Sketch of the system. **b.** Diagram presenting the zone of finite minimum (dotted zone) as a function of $\tilde{k}_P$ and $\tilde{k}_\rho$. Profile of the polarization $P(z)$ **(c)** and the normalized susceptibility $\chi(z)$ **(d)** computed for $(\tilde{k}_P = 9, \tilde{k}_\rho = 1)$ and $(P_0 = -10\,\mathrm{V/nm}, \rho_0/q_o = -10\,\mathrm{V/nm})$. **e.** Susceptibility normalized to the bulk susceptibility with different values of $\tilde{k}_\rho$.

D_0, the amplitude of $\chi(z)$ does not depend on (P_0, ρ_0, D_0). The interface affects the dielectric properties of water only through the stiffnesses $(\tilde{k}_P, \tilde{k}_\rho)$.

The amplitude of $\chi(z)_{\tilde{k}_\rho=0}$ decreases with $\tilde{k}_m$ and tends to a finite value for $\tilde{k}_P \gg 1$. This case is represented in Fig. 7.1e (blue/dark curve).[1]. Then we consider the corrective effect of $\tilde{k}_\rho$ in the limit of a large $\tilde{k}_P$. An increasing $\tilde{k}_\rho$ induces a dephasing and an amplitude decrease up to a factor 2 of $\chi(z)$ (See 7.1e). The behavior of $\chi(z)$ as a function of $(\tilde{k}_P, \tilde{k}_\rho)$ illustrates that different surfaces, having a stronger or weaker influence on polarization and partial charge, induce different dielectric properties of interfacial water.

7.2.2 Comparison with MD simulations

We performed MD simulations of pure water confined in a slab geometry using the GROMACS MD simulation package.[129] Water molecules are described with the SPC/E model and the walls are made up of atoms of frozen positions. We considered graphene and hBN surfaces (Simulation method is described in ref. ([21]).

We analyze the polarization, $P_{\rm MD}(z) = -\int_0^z dz \rho_{\rm MD}(z) dz$, with $\rho_{\rm MD}$ the charge density of water, and the susceptibility $\chi_{\rm MD}(z) = (P_{\rm MD}(z, D_0 + \delta D_0) - P_{\rm MD}(z, D_0))/\delta D_0$ [47] with δD_0 = 0.5V/nm, in the vicinity of the surfaces. The profiles are similar for both surfaces (Fig. 7.4): first, a vacuum layer ($P_{\rm MD}(z) = 0$, $\chi_{\rm MD}(z) = 0$) between the surface and the liquid, due to the repulsive part of the surface-fluid Lennard-Jones (LJ) interaction, then decaying oscillations over about 1 nm before reaching the bulk value. Figure 7.3 shows log of the polarization for the two strategies we have considered to fit the longitudinal dielectric susceptibility of bulk water with a 4 order model given in Eq. (3.15), compared to the MD results (black curve). The first one aims at fitting the maximum of the susceptibility while the second one focuses on fitting the width of the susceptibility normalized to 1 (the aspect ratio) bearing in mind that in both cases $\hat{\chi}_\parallel(q = 0)$ is set by the value of the relative dielectric permittivity of the water SPC/E $\epsilon_b = (1 - \hat{\chi}_\parallel(q = 0))^{-1} \sim 71$. The corresponding susceptibilities are plotted in Fig. 7.2.

[1] Note that the diverging value $\tilde{k}_m = 1$ corresponds to the boundary of the stability region of the phase space parameter (see Fig. 7.1b)

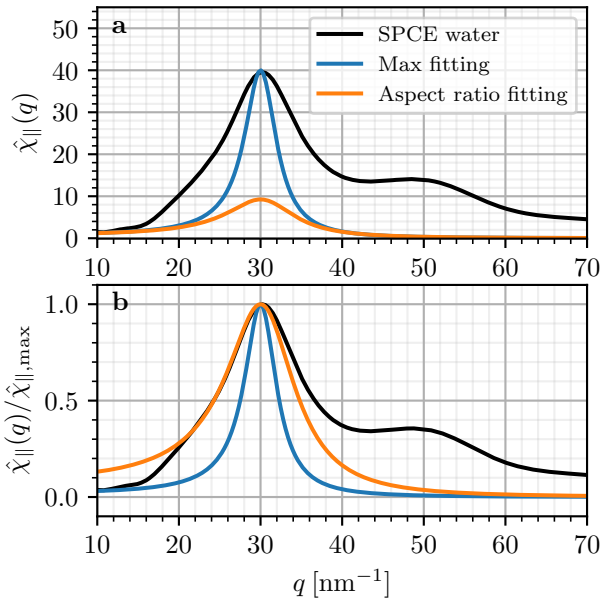

Figure 7.2: Susceptibility $\chi(q)$ (**a**) -labeled here $\hat{\chi}(q)$ - and normalized susceptibility $\chi(q)/\chi_{max}$ (**b**) computed from pure SPC/E water molecular dynamic simulation (black curve). The blue curve arises from the fit of the maximum of the first component of the susceptibility while the orange curve shows the result of the fit of the aspect ratio.

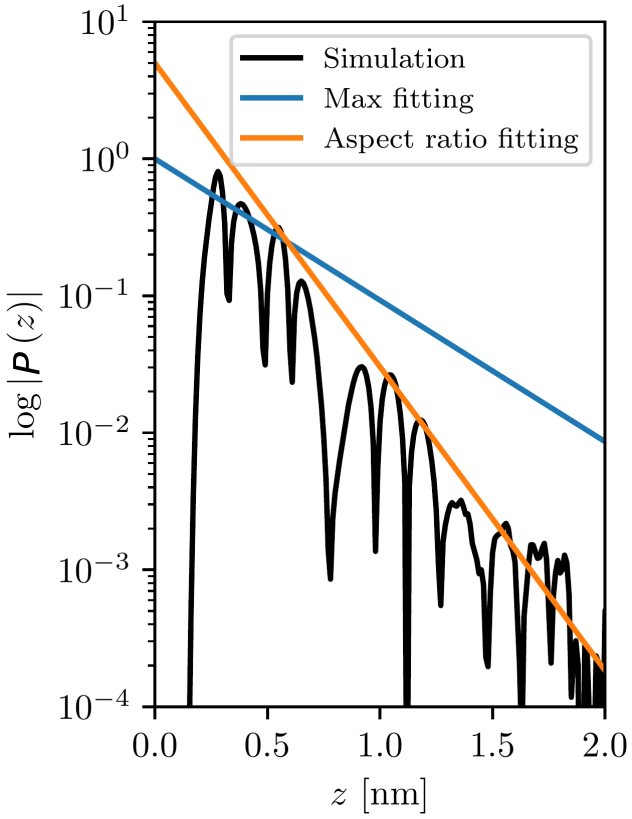

Figure 7.3: The black curve is the polarisation field computed from MD simulation of water in the vicinity of graphene layer at vanishing D_0. Color curves have the equation $P(z) = Ae^{-q_d z}$ where q_d is computed from the fitting of the bulk susceptibility $\hat{\chi}(q)$. The blue one arises from the fit of the maximum of the first component of the susceptibility while the orange curve shows the result of the fit of the aspect ratio. The parameter A is chosen to match the back curve.

Fig. 7.3 confirms that fitting the aspect ratio gives quantitative agreement between MD and field theory for evaluating the correlation lengths.

Indeed, Fig. 7.4 shows that the theoretical decay λ_d and the period λ_o are in very good agreement with the simulated ones. In MD simulations, the position of the interfaces is not as clear-cut as in theory due to thermal capillary fluctuations and the non-infinitely sharp repulsion of the surface-fluid LJ interaction.[130] This is taken into account by applying a smearing to the theoretical predictions to get a polarization labeled as $\tilde{P}$. The hBN surface is characterized by a deeper LJ potential and consequently a smaller smearing than the graphene. Correspondingly, $P_{\mathrm{MD}}(z)$ amplitude is smaller in interfacial water for graphene than for hBN (see Figs. 7.4a-b).

We validate the theoretical model in three steps. First, we adjust the simulated susceptibilities with the smeared, theoretically computed $\tilde{\chi}(z)$. If we choose ($\tilde{k}_m \gg 1$, $\tilde{k}_\rho = 0$) for graphene and ($\tilde{k}_P \gg 1$, $\tilde{k}_\rho = 0.2$) for hBN, we obtain a good agreement between the calculated and the simulated value of the susceptibilities as shown in figures 7.4c-d. Next, we fit the simulated polarization for graphene surface with $\tilde{P}(z)$ by fixing P_0, the single left unknown parameter for graphene as $\tilde{k}_\rho = 0$. Finally, we fit the simulated polarization for a hBN surface. Taking the surface polarization P_0 previously determined in the case of graphene, we fix ρ_0. The comparison between theoretical and simulated polarization is presented in Figs. 7.4a-b. The dotted part of the simulated curves corresponds to the vacuum gap and the contribution of hydrogen located in $z < z_0$. The theoretical model describes this zone as a vacuum gap.

Graphene and hBN surfaces are parameterized by $\tilde{k}_P \gg 1$, thus both surfaces freeze the interfacial polarization to $P(z_0) = P_0$ which doesn't respond to D_0. At the microscopic scale,

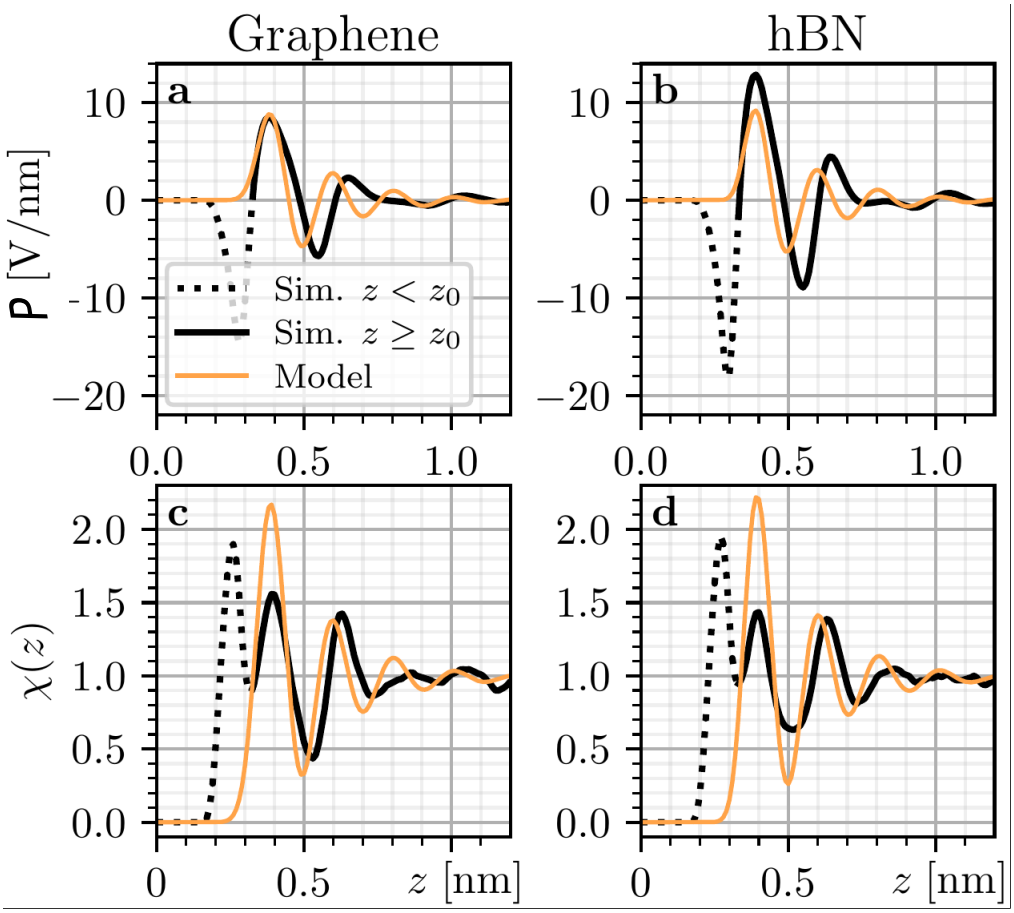

Figure 7.4: Comparison between model (in orange/light grey) and MD simulations (in black) for a graphene layer (left panels) and a hBN layer (right panels). Top (respectively bottom) panels show the polarization (respectively the susceptibility). Simulation curves for $z \leq z_0$ are represented with dotted lines.

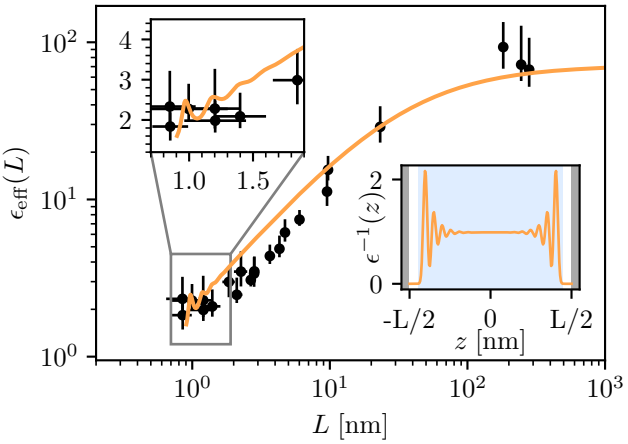

Figure 7.5: Effective dielectric permittivity ϵ_{eff} of water nanoconfined in a channel of width L. Comparison between experimental measurements reproduced from [12] and theoretical model.

this result can be interpreted as the effect of the vacuum gap on the organization in the first layer of water which optimizes the number of H-bonds [131]. Most likely, $\tilde{k}_P$ is very large for a wide variety of surfaces, both hydrophobic and hydrophilic, as they impose a layout in the first hydration layer.[47, 132]. For a non-vanishing corrective term $\tilde{k}_\rho$, the surface has an effect on the interfacial charge, $\rho_s(z_0)$, and its variation under D_0.

We investigate the microscopic origin of this effect by performing MD simulations for artificial surfaces associated with hybrid properties between graphene and hBN surfaces. The simulations are presented in ref. [21]. We find out that it is induced by a large mean depth of the LJ minimum. A non-vanishing $\tilde{k}_\rho$ is related to important variations of the interaction energy between the surface and a water molecule in the (xy) plane for $z = z_0$ that constrains the position of water molecules in this plane.

7.2.3 Nanoconfined water

We use now this theoretical model to derive the dielectric properties of a confined water layer. The experimental measurements report an effective dielectric permittivity up to $\epsilon_{\text{eff}} = 2$ for a channel of about 1 nm [12] (reported on Fig. 7.5). The authors suggest the existence in the channel of three water layers of homogeneous dielectric properties: two interfacial layers ($\epsilon = 2.1$, thickness: 0.7 nm) and a layer of bulk water ($\epsilon = 78$). We compute the effective permittivity $\epsilon_{\text{eff}} = L/\int_0^L (1-\chi(z))dz$ as a function of L for two graphene surfaces. Our model can be seen as two vacuum gaps and an inhomogeneous water layer. This inhomogeneity is not implemented *ad hoc* but is the signature of the nonlocal dielectric properties of water, revealed by the boundary conditions. The results are presented in Fig. 7.5. The model reproduces the experimental measures and catches in particular a non-homogeneous behavior of the permittivity as a function of L for small L as shown in the insert that cannot be described by a three homogeneous layer model.[133, 12, 110]

7.3 Distribution of ions near surfaces

In collaboration with Jonathan Hedley and Alexei Kornyshev

As seen in the last section, interfacial water presents a structured dielectric response alternating layers of high susceptibility and low one, even for a non-charged confining surface. See fig. (7.4). This inhomogeneous profile raises the question of the non-homogeneous distribution of ions at

an interface. There is currently much debate on how water structuring could influence ion distribution near the interface. The interest in this question however has a long history, based either on the earlier exploration of nonlocal electrostatic effects described within the concept of Lorentzian correlations [134] which explains how this structuring of water will influence the way ions are distributed close to the surface.

Nonlocal electrostatics furnishes a convenient platform to study this question provided that the interaction between ions and water is appropriately modeled. We have shown in the last chapter that a nonlocal linear model for water and punctual ions interacting via Coulomb interactions fails to reproduce the behavior of bulk electrolytes. Nonlinear effects have to be included. In the last chapter, we have considered an attenuated response of water to high fields. Here, we are going to take into account another source of nonlinearity. We describe water as a nonlocal linear "overscreening" medium for water - described using the double polarization functional given in Eq. (3.18) and consider the electrostatic interactions with the ions. We do not model the ions as punctual charges but take into account their spacial expansion. This approach is often referred to as Poisson-Fermi due to the Fermi-Dirac-like nature of the ion distributions and has been implemented several times in the past for electrolyte / ionic liquid systems [135, 136, 137, 138]. The full approach corresponds to a nonlocal nonlinear (induced by nonvanishing ion size) Poisson-Boltzmann formalism.

We compute at the mean-field level the electrostatic potential and the ion concentration in the vicinity of a charged surface. The results are plotted in Fig. 7.6. Note that all Hamiltonians and technical details for mean field derivation are given in ref. ([22]). The Figure 7.6 shows the concentration profile of anions (blue curve) and cations (red curves) close a surface positively charged. We consider varying boundary conditions given by the polarization value at the surface (one column per condition: $\bar{P}_0$) and two distinct concentrations (1 mMol first row of plot, 10 mMol second row of plot). All insets show the convergence to Gouy-Chapman behavior - dashed lines - at long distances. The last line of the plot (b) indicates the electrostatic potential ϕ for both conditions of concentrations. We see in Fig. 7.6 that even in a very diluted electrolyte, ions do get trapped in the potential wells created by the "overscreening" dielectric response of water to the charge of the electrode, known also as the layering of water molecules, as we see in the first row of panels in Fig. 5. Such 'water wells' are deep enough to keep ions in, against the entropic drive to spread them around. Moreover, ions do not follow the potential profiles due to pure water literally, as their presence disturbs their corresponding potential wells, albeit not much. Ion concentration in the wells is limited by the effect of 'excluded volume' (finite ion size), so that the first 3-4 wells have the same maximum possible concentrations of cations or anions, as seen by the plateauing profiles in Fig. 5a. We thus cannot see the effect of concentration of ions in the bulk, as the occupation of the wells is very much close to the limit determined by the excluded volume of ions

Recently, the Garcia group [139], which uses the 3D-AFM experimental techniques studies the structuration of diluted electrolytes (down to 10 mM concentration) in contact with mica surfaces. Even at such a low concentration, they show evidence of distinct layers of water (hydration layers) and cations in the normal direction to the surface. This is in line with the results we have obtained for a sharp interface (Fig. 7.6).

As a conclusion of this part, we have shown that nonlocal dielectric properties could affect the ion distribution in the double layer. Layering of the ions appears for atomically flat surfaces. This prediction is in agreement with experimental observation.

7.4 The hydration Force

The last section of this manuscript is devoted to the consequence of the dielectric nanometric structure of the fluid on macroscopic observable *i.e.* the hydration force. Hydration forces have had a long history since their first experimental discovery [123, 140]. These forces have been

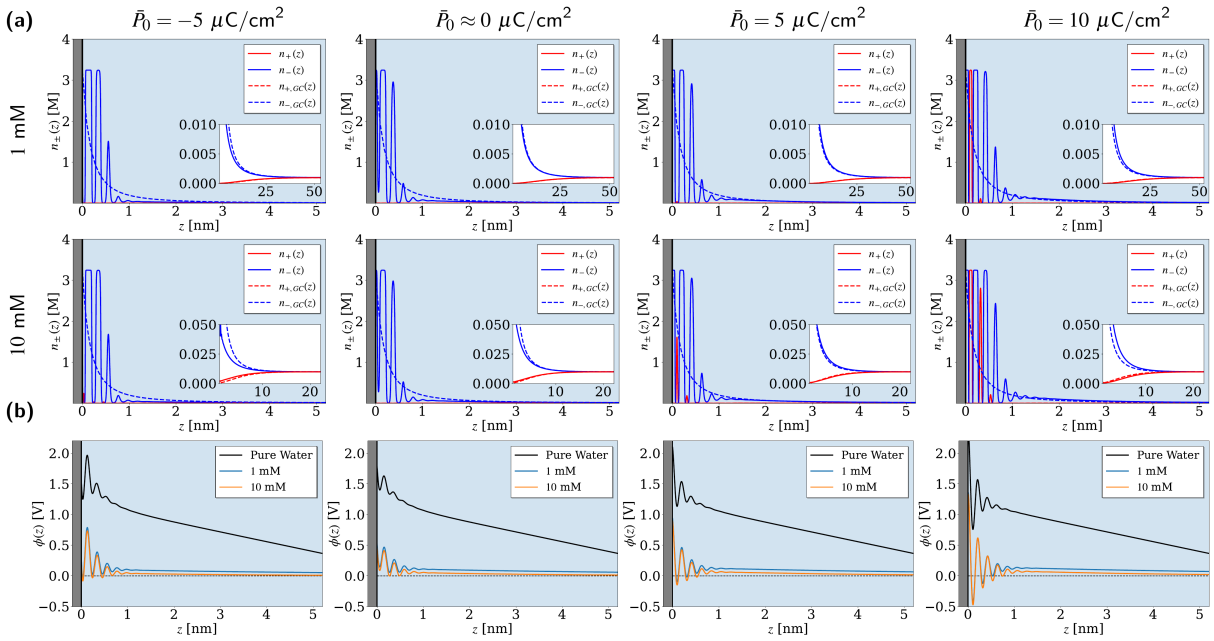

Figure 7.6: Double layer structure and electrostatic potential profiles from an ideally sharp surface. In all plots, the surface charge density $\bar{\sigma}_0 = +10\ \mu C/cm^2$, and the lattice gas cell length $a = 0.8$ nm. (a) shows the ion distributions from the positively charged surface with the indicated bulk concentrations, and the mean polarisation density of water at the surface, $\bar{P}_0$. Greater values of $\bar{P}_0$ indicate stronger water structuring at the surface, and hence deeper potential wells. All insets show the convergence to Gouy-Chapman behaviour at long distances, but very different behaviours near the surface. It is also seen that counterions (anions here) tend to reside at the maxima of the electrostatic potential profiles that would have been seen in pure water, whereas co-ions (cations) tend to sit in the minima of those profiles, as demonstrated in (b). For easy comparison, the potential profiles for pure water are plotted between two oppositely charged surfaces at a distance of $L = 15$ nm.

experimentally and numerically studied between soft [141] and solid surfaces [123, 142], and even between macromolecules such as polysaccharides, collagen, and DNA [125, 143]. Between solid surfaces, these force measurements were initially based on Surface Force Apparatus (SFA) [144], and later, Atomic Force Microscopes (AFM) [145] were also used to measure forces rather than just for drawing surface landscapes. The general understanding of the origin of hydration forces was that hydrophilic surfaces perturb the structure of water or affect its polarization at the boundaries and that these perturbations propagate from one surface to another through the correlations of the perturbed quantities in water. Thus, beyond their typical correlation lengths, such forces should vanish. Since many of the studied surfaces are charged, hydration forces are usually perceived as an additional force emerging at short distances on top of the forces described by DLVO theory – the force determined by the repulsion of electrical double layers (the so-called electrostatic force) and Van der Waals attractions [146].

The mathematical description of such a liquid-mediated force was pioneered by Marčelja and Radić [147]. They postulated a simple gradient expansion of a free energy functional of the liquid (water), quadratic in the 'order parameter' (often interpreted as the orientation of the molecules), where the coefficients determine the correlation length.

In the 'primitive' gradient expansions representing the Landau free-energy functional of bulk water, the hydration forces were always exponentially decaying with the distance. However, experimental crossed-cylinder SFA measurements of the forces between ideally smooth mica surfaces have shown sharp decaying oscillations, with a period on the order of the diameter of a water molecule [124, 148]. These oscillating patterns have to be described by going beyond the simple gradient expansion of the free energy, or by using resonance-containing forms of the nonlocal dielectric function [149]. However, for atomically rough surfaces, these oscillations disappear [150, 151]. Including the resonance alone does not explain why for some interacting surfaces the forces in the experiments decay exponentially, whereas for many others we see these oscillations. Wisely, it was suggested that smearing of the interfaces due to surface roughness leads to oscillation dysphasia, eliminating these oscillations. The question remained open, how large must the smearing be for this, and what would remain of the force after such smearing?

In the spirit of Marčelja-Radič [147], we calculate the indirect solvent contribution to the hydration force by finding the derivative of the energy obtained from the configurational energy we have detailed in Chapter 3. In particular, we consider the simplest functional capturing the "overscreening" effect in water, given in Eq. (3.13), and the more complex functional introducing two polarizations and focusing on the low-q/long-range structure of water given in Eq. (3.18). We model the roughness of the surface by a Gaussian probability distribution for the interface position. Details of the calculations are given in ref. ([22]).

The computed hydration force profile and the effect of smearing the force is shown in Fig. 7.7 for the model of two polarizations given in Eq. (3.18). For sharp interfaces, we see an oscillatory force profile - blue plots -, but when the surface is smeared, the oscillations rapidly disappear - red plots. A surface roughness corresponding to the size of a water molecule ($2\delta \approx 2.5$ Å) is enough to completely remove oscillations from the profile, leaving only an exponentially decaying force. This reproduces thus the experimental "force oscillation-non-oscillation" observations.

Interestingly, the computed hydration force with Eq. (3.13) shows oscillations for vanishing smearing but vanishes for rough surfaces.

As a summary of this section: we have used two nonlocal models - Eq(3.13), purely resonant and Eq. (3.18) - to compute hydration forces between flat and rough surfaces. Explanation of experimental observations appears only possible for the second model. This two modes of polarization model for water - Eq. (3.18) - is consistent with the low-q behavior of the response function. It is constant at small and resonance-like at higher wavenumbers as shown in Fig (3.5).

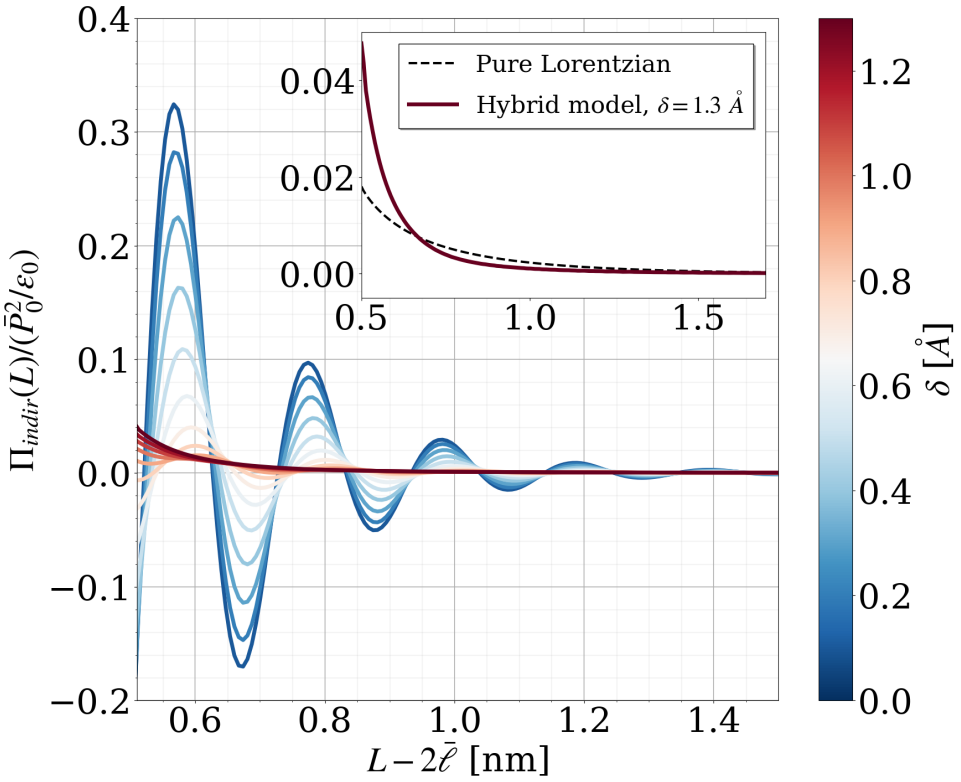

Figure 7.7: Hydration force profiles as a function of surface roughness. We see suppression of oscillations in the profile leading to a fully repulsive, exponential force as the surface roughness is increased. A roughness of $2\delta \approx 2.5$ Å is required to fully suppress oscillations, corresponding to the diameter of a water molecule. Inset shows the comparison between the pure Lorentzian mode of decay for hydration forces historically proposed by Marčelja-Radič [147] with what is left of the force after smearing in our 2-polarisation hybrid model; inset axes are the same as in the full picture.

7.5 Conclusion

In this last chapter we have considered examples of confined water and electrolytes and have studied the dielectric properties of the interfacial layer and the macroscopic properties of the system. To do this, we have proposed an interfacial energy equation (7.1) in the spirit of the Landau-Ginzburg functionals for the bulk energy. We have validated our approach by comparing our results with simulations and/or experiments. The developed model provides a framework that can be tailored to any type of confinement characterised by its geometry and surface physicochemical properties. Thus, it can be used to consider different confinement conditions, such as soft interfaces.

Chapter 8

Perspectives

I have presented a versatile framework for studying the dielectric properties of confined water and electrolytes at the nanoscale. However, this framework is still incomplete. Soon, I will be working on two missing pieces of the static description of these systems: (i) a complete theory for the bulk electrolyte response, (ii) a study of the ion-surface interaction. In the meantime, I will work on the description of charge transport in structured electrolytes. In the more distant future, I will use these methods to study the transport of ions in *in cellulo* compartments, focusing on the description of the powerhouse of the cell: the mitochondrion. I describe this research perspective in this chapter.

8.1 Bulk electrolytes

In collaboration with Jonathan Hedley and Alexey Kornyshev

As shown in Chapter 6, the response function of electrolytes cannot be captured by Gaussian theory for water nonlocality. We have proposed an ad-hoc expression for the longitudinal susceptibility (Eq. (6.13) that reproduces qualitatively the MD simulations. However, a consistent description of ions and ion-water interaction leading to such a result is still missing. The work in section 7.3 shows that a model taking into account nonlocality of water and spacial extension of the ions reproduces the ion layering along the confining surface observed experimentally for very diluted electrolytes.

8.1.1 Effect of the finite size of the ions - ion-ion interaction

In future work, we will study more in detail how to couple the size of ions and nonlocality of water to describe bulk electrolytes. We first consider the electrostatic interaction between two ions. We use a charge distribution taking into account the finite size of an ion: we can consider a Born sphere and a smeared Born sphere ([70]). The Fourier transform of the ion density for two models can be written as follows:

$$\rho_{BS}(q) = e\frac{\sin(qa)}{qa}, \quad \rho_{SBS} = \frac{e}{1+(\zeta/a)^2(2-e^{-a/\zeta})}\left(\frac{\sin(qa)}{qa}\frac{1}{\zeta^2q^2} + \frac{\zeta^2}{a^2}\frac{(2\cos(qa)-e^{-a/\zeta})}{(1+\zeta^2q^2)^2}\right). \tag{8.1}$$

For the Born sphere (BS) model, the charge ρ_{BS} is uniformly distributed over a sphere of radius a which is the ion radius. The first distribution may lead to an overestimation of the water response which could be corrected by the second distribution. For the Smeared Born sphere model, the charge density is radially inhomogeneous and has a maximum at a distance a from the center of the sphere; from this distance, it decreases exponentially (both outside and inside the sphere) with decay length ζ. In the limit of $\zeta \to 0$, it reduces to the Born sphere distribution. This model is thus characterized by 2 length scales instead of one for the BS model.

We will start this work by characterizing the polarization induced in a nonlocal medium by these charge distributions and the related charge-charge interaction as done in ref. ([48]) for punctual charges. The relevant characteristic sizes of this system are not clear. Is it only the size of the ion modeled as a Lennard-Jones sphere? or the size of the ion and the first water layer? It could depend on the chemical nature of the ion. The theoretical results will be compared to MD simulated charge-charge interactions that we will perform. For weak charges - MD simulations allow partial charges for ions - the linear response of water will be a good approximation. For higher charges, we will introduce nonlinear terms and discuss the threshold between the linear and nonlinear regimes.

8.1.2 Effect of the finite size of the ions - bulk electrolytes

After the characterization of the effect of the ion size on electrostatic interactions in water, we will consider the response of bulk electrolytes. We will rederive the partition function as in Eq. (6.3), the free energy of the system and the response function for an updated ion-water interaction and taking into ion size effect. We will compare the results to MD simulations.

8.2 Solvated ion-surface interaction

In textbooks on electrostatics, the surface-charge interaction is treated by the "image charge" method. It consists of replacing the surface by a fictitious ion generating in water the same potential as the surface. The charge carried by the ion is deduced from the continuity of the electrostatic and excitation field at the interface. This framework has been extended for nonlocal media [152, 88, 153]. However, for "overscreening" media, such as water, this method leads to an nonphysical diverging response of the medium [154, 26]. The potential mean force of an ion interacting with a graphene surface was lately addressed with MD simulations[155]. In this case, the atoms of the surface are described as LJ spheres and their electronic response is not included. It was recently shown that the coupling between water and electron modes could drastically influence the response of the system [30]. The results of such simulations have to be questioned. The problem of charges in confinement can be addressed mainly with heavy numerical simulations based on the Born Oppenheimer approximation of the electrons [156]. In addition, sophisticated classical MD simulation methods are being developed to bridge the gap between pure classical and full quantum description at reasonable computational cost [157]. The minimal ingredients to add to a nonlocal "image charge" description to get a good precision on electrostatic interactions is still an open question.

8.2.1 Dielectric properties of water including electronic degrees of freedom

In collaboration with Darka Labavić, Roland Netz and Marie-Laure Bocquet

We will start this part of the project by characterizing the dielectric properties of pure water simulated using the electronic Density functional theory (DFT) [158]. We will calculate the charge structure factor for electronic densities including the electrons and obtain information on the dielectric spectrum at high q. We remember that for classical MD simulations, the high-q part of the spectrum is irrelevant as the atoms are described as LJ spheres. We will use this result as an input for a three polarization field P_1, P_2, P_{el}, in the spirit of Eq. (3.18) but including electronic degrees of freedom. We will first quantify the coupling between the "resonant" polarization field P_1, the polarization field associated with a nanometric decaying length P_2 and the electronic structure captured by P_{el} in bulk water. In a second time, we will consider the polarization in water induced by a confinement between two plates - using the framework presented in section 7.1. We will compare the response obtained for a field theory

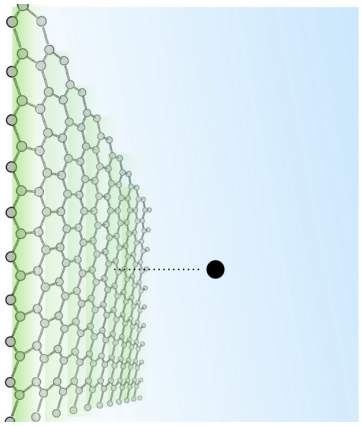

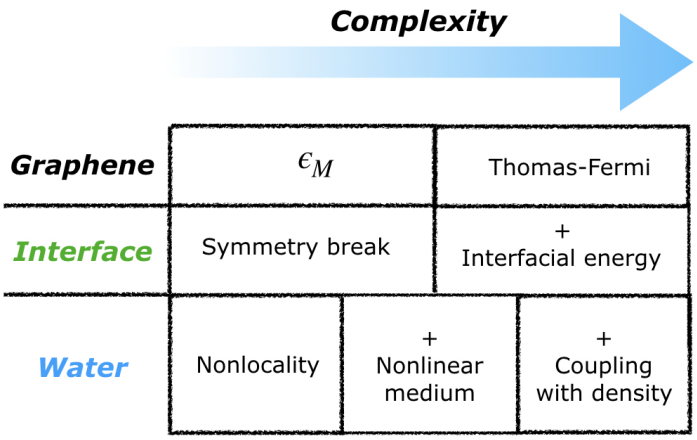

Figure 8.1: (left) Schematic description of a solvated charge-graphene interaction. (right) Table presenting an increase of the complexity of the theoretical model addressing this problem.

parameterized with classical MD simulations and electronic DFT. We will focus on the response at a small scale - 0.5 nm - that should differ for the two approaches. We will discuss the role of nonbonding lone electron pairs of the system in surface hydration.

8.2.2 Image charge

Then we extend the textbook "image charge" framework to this "electronic-water" nonlocal medium plus a confining medium interacting with a harmonic surface energy as introduced in Chapter 7. See sketch in Fig 8.1. With this approach, we could compute the surface charge in the solid material for different types of interface energies. This can be done by varying the spring constants k_P and k_ρ encoding the stiffness of the water/surface interaction. For the confining medium, we consider graphene and we will describe using a Thomas-Fermi model. More complex and realistic descriptions for the graphene [26, 159], nonlinear response of water or coupling with the density could be envisaged in the second time. See the table in Fig 8.1.

To discuss the validity of such a framework, we will compare the analytical results to simulations. As already mentioned, Classical MD simulations are irrelevant for these questions and we will perform *ab initio* simulations [160, 156].

8.3 Ion transport

In collaboration with Vincent Demery

Until now, we have considered exclusively static properties of electrolytes. In the future, I will use the tools developed in this manuscript to study charge transport in complex dielectric media.

Ion transport in confined systems is a key process for energy production both in technological devices such as supercapacitors or batteries and in biological organelles such as mitochondria. With Vincent Demery, we plan to study the transport of ions in a structured dielectric medium such as water. To do so, we use the stochastic Density Functional Theory (sDFT) [27]. We consider a 1:1 electrolyte composed of cations of density ρ_+ and anions of density ρ_-. In this framework, the dynamic of the cation density ρ_+ is governed by a the stochastic equation as

follows:

$$\partial_t \rho_+ = -\nabla \cdot \vec{j}_+ \quad (8.2)$$
$$\vec{j}_+ = -k_B T \kappa_+ \nabla \rho_+ + \kappa_+ \rho_+ \vec{f}_+ + (\kappa_+ \rho_+)^{1/2} \vec{\eta}_+ \quad (8.3)$$

κ_+ is the mobility of cations, $\vec{\eta}_+$ is a white noise. The force $\vec{f}_+$ is the force generated by an external potential and the interactions between ions. The conductivity of such a system when submitted to a constant electric field has been studied for ideal electrolytes, *i.e* a local medium associated with a q-independent permittivity, responding linearly to the field and punctual ions. This framework reproduces the Wien effect which is the increase of the conductivity under a high electric field. Indeed the electric field kills out the Debye screening between the ions that thus behave as independent charge carriers.

We plan to modify the description of the solvent in this equation to get closer to real systems. In the first time, we start by considering the saturation of water permittivity under a constant field using the DL model for water, which we have described earlier (see sketch 4.1, and 4.2). In this case, the application of an electric field both decorates the ions by killing off the screening and re-correlates them by decreasing the permittivity of the solvent. We discuss the dominant effect. We will compare the analytical results for the conductivity with MD simulations. In the second, we will consider the effect of the water structure on the conductivity of an ionic solution using nonlocal electrostatics for a q-dependent description of the permittivity...

8.4 Electrolytes *in vivo*: transport in mitochondria

I finish this perspective chapter by presenting a long-term objective of the present work on the properties of confined electrolytes. It is the study of the charge transport in nanoconfined biological systems. I focus on the description of mitochondria.

Mitochondrion organelle is named the "powerhouse" of the living cell as it is the place of ATP synthesis. It is formed of numerous nanometric tubular membrane invaginations named the cristae - see Fig. (8.2) for a representation of the organelle - that are the location of this synthesis. The energy needed to synthesize ATP is furnished by a proton flux along these membrane tubes established by transmembrane proteins. The respiratory complex plays the role of proton source and the ATPsynthaze consumes H^+ to synthetize ATP. The description of this energy supply is important to understand the efficiency of this organelle and also its dysfunction which is responsible for numerous diseases. The existing models describing driving force are based on macroscopic descriptions of the components of the system [161].

The confinement properties, the nonlocal dielectric properties of water, and the ion current are intimately coupled. The pH flux is assumed to be localized along the surface by the nonlocal dielectric properties of water [162, 163], this flux affects the protonation state of the lipid membrane and thus modifies its surface charges and its mechanical properties. In turn, this mechanical modification affects the tension and bending forces exerted by the membrane on the transmembrane proteins and modifies their rate of proton injections. In previous works [24, 25], I focused on the membrane mechanics and described the pH flux as a constant input. I will now work on a more precise description of the ion distribution in the mitochondria cristae taking into account the dielectric properties of water at small scales. I will take into account the effect of surface charge on the membrane on its mechanical properties and introduce a coupling between the rates of proton injection and consumption by the proteins and the local membrane shape to get a description of the system at the nanoscale and derive its efficiency. Part of these questions will be addressed during the PhD of Yorgos Chatziantoniou.

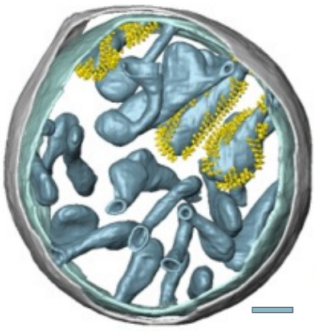

Figure 8.2: Reproduction from ref. [164] of a graphical scheme of a mitochondron. The tubes represent the crista of the organelle. The yellow points are the ATPsynthaze. scale bar =100 nm.

8.5 Conclusion

The first perspective of this work is to model at negligible computer cost and with a precision comparable to quantum simulations of liquid/solid and interfaces prototyping aqueous electrolytes. I will also work on the transport properties of these systems. In the longer term, I will apply these tools to biological systems.

Appendix A

List of publications

Publications

1. B. Spreng, H. Berthoumieux, A. Lambrecht, A-F. Bitbol, P. A. Maia Neto, S. Reynaud, Universal Casimir attraction between filaments at the cell scale, arXiv:2306.14059 (2023)

2. M. R. Becker, P. Loche, D. J. Bonthuis, D. Mouhanna, R. R. Netz, H. Berthoumieux*, Dielectric properties of aqueous electrolytes at the nanoscale, arXiv:2303.14846, (2023)

3. J. Hedley, H. Berthoumieux, A. Kornyshev, The dramatic effect of water structure on hydration forces and the electrical double layer, J. Phys. Chem. C, 128, (2023)

4. A. Robert, H. Berthoumieux*, M.-L. Bocquet*, Coupled interactions at the ionic graphene/water interface, Phys. Rev. Lett. 130 076201, (2023).

5. T. V. Mendes, J. Ranft, H. Berthoumieux*, A model of membrane deformations driven by a surface pH gradient, Phys. Rev. E. 108, 014113 (2023)

6. G. Monet, F. Bresme, A. Kornyshev, H. Berthoumieux*, Nonlocal dielectric response of water in nanoconfinement, Phys. Rev. Lett. 126 216001, (2021).

7. H. Berthoumieux, G. Monet, R. Blossey, Dipolar Poisson models in a dual view, J. Chem Phys. 155, 024112 (2021).

8. A. Senoussi, Y. Vyborna, H. Berthoumieux, J-C Galas J-C, A. Estevez-Torres, Learning from embryo development to engineer self-organizing materials, in Out-of-equilibrium supramolecular systems and materials, eds N. Giuseppone and A. Walther (Wiley-VCH), 2021

9. M. Vatin, A. Porro, N. Sator, JF. Dufreche, H. Berthoumieux*, Electrostatic interactions in water: nonlocal electrostatic approach, Mol. Phys. e1825849, (2020).

10. N. Patil, S. Bonneau, F. Joubert, AF Bitbol, H. Berthoumieux*, Mitochondrial cristae modeled as an out-of-equilibrium membrane driven by a proton field, Phys. Rev. E, 102 022401, (2020).

11. F. Paillusson, H. Berthoumieux*, Dielectric response in the vicinity of an ion: A nonlocal and nonlinear model of the dielectric properties of water, J. Chem. Phys., 150, 094507 (2019).

12. H. Berthoumieux*, Gaussian field model for polar fluids as a function of density and polarization: Toward a model for water, J. Chem. Phys., 10, 104504 (2018).

13. H. Berthoumieux*, Fluctuations in reactive networks subject to extrinsic noise studied in the framework of the chemical Langevin equation, Phys. Rev. E, 102, 012310 (2016).

14. H. Berthoumieux* and A. C. Maggs, Fluctuation-induced forces governed by the dielectric properties of water, a contribution to hydrophobic interactions, J Chem Phys., 143, 104501 (2015).

15. H. Berthoumieux, J-L. Maître, C-P. Heisenberg, E. K. Paluch, F. Jülicher and G.Salbreux, Active elastic thin shell theory for cellular deformation, New Journal of Physics, 16, 065005 (2014).

16. J-L. Maître, H. Berthoumieux, S. F. G. Krens, G. Salbreux, F. Jülicher, E. Paluch, C- P. Heisenberg, La mecanique de l'adhesion cellulaire dans la gastrulation du poisson zebre, Medecine sciences, 29, 147-150 (2013).

17. J-L. Maître, H. Berthoumieux, S. F. G. Krens, G. Salbreux, F. Jülicher, E. Paluch, C-P. Heisenberg, Adhesion function in cell sorting by mechanically coupling the cortices of adhering cells, Science, 338, 253-256 (2012).

18. A. Lemarchand, H. Berthoumieux, L. Jullien, C . Gosse, Chemical mechanism identification from frequency responce to small temperature modulation, J. Chem. Phys, 116, 8455-8463, (2012)

19. K. Zrelli, T. Barilero, E. Cavatore, H. Berthoumieux, T. Le Saux, V. Croquette, A. Lemarchand, C Gosse, L. Jullien, Temperature modulation and quadrature detection for selective titration of two-state exchanging reactants, Anal. Chem, 83, 2476-2484 (2011).

20. K. Zrelli, T. Barilero, H. Berthoumieux, T. Le Saux, C. Gosse, A. Lemarchand and L. Jullien, Kinetic and Thermodynamic Characterisation by Heating in a Microfluidic Cell, Sensor Lett. 9, 2332 (2011)

21. H. Berthoumieux, A. C. Maggs, Collective dispersion forces in the fluid state, EurophysLett., 91, 56006 (2010).

22. H. Berthoumieux, C. Antoine, A. Lemarchand, Determination of the six rate constants of a three-state enzymatic network and a noninvasive test of detailed balance, J. Chem. Phys., 131, 084106 (2009).

23. H. Berthoumieux, C. Antoine, A. Lemarchand, L. Jullien, Resonant response to temperature modulation for enzymatic dynamics characterization, Phys. Rev. E, 79, 021906 (2009).Selected by the Virtual Journal of Biological Physics Research, Feb. 15, Vol. 17(4), (2009).

24. H. Berthoumieux, A. Lemarchand, L. Jullien, Response to a temperature modulation as a signature of chemical mechanisms, Phys. Rev. E, 76, 056112 (2007). Selected by the Virtual Journal of Biological Physics Research, Nov. 15, Vol. 14(10), (2007).

25. A. Estevez-Torres, C. Gosse, T. Le Saux, J.-F. Allemand, V. Croquette, H.Berthoumieux, A. Lemarchand, and L. Jullien, Fourier analysis to measure diffusion coefficients and resolve mixtures on a continuous electrophoresis chip, Anal. Chem., 79, 8222 (2007).

26. H. Berthoumieux, A. Lemarchand, L. Jullien, Temporal modulation of a spacially periodic potential for kinetically governed oriented motion, J. Phys. Chem. B, 111, 2045 (2007).

27. J. Pilme, H. Berthoumieux, V. Robert, P. Fleurat-Lessard, Unusual bond formation in aspartic protease inhibitors : A theoretical study, Chemistry, 13, 5388, (2007).

*, corresponding author

Proceedings

1. K. Zrelly, T. Barilero, E. Cavatore, H. Berthoumieux, V. Croquette, A. Lemarchand, L. Jullien, T. Le Saux, C. Gosse, Temperature modulation and phase sensitive imaging to detect point mutations, Proceddings of the 14th International conference on miniaturized systems for chemistry and life sciences (2010).

2. K. Zrelli, T. Barilero, T. Le Saux, L. Jullien, H. Berthoumieux, A. Lemarchand, and C. Gosse, Thermal modulation and filtered video acquisition to image reactive species among non reactive ones, Proceedings of the 13th International conference on miniaturized systems for chemistry and life sciences. T. S. Kim, Y.-S. Lee, T.-D. Chung, N. L. Jeon, S.-H. Lee, K.-Y. Suh, J. Choo, Y.-K. Kim, eds., 1, 948 (2009).

3. A. Estevez-Torres, T. Le Saux, H. Berthoumieux, A. Georges, S. Fernandez, J.-F. Allemand, V. Croquette, A. Lemarchand, L. Jullien, and C. Gosse, Point mutation detection by on-chip diffusion coefficient measurement, Proceedings of the 11th International conference on miniaturized systems for chemistry and life sciences, J.-L. Viovy, P. Tabeling, S. Descroix, and L. Malaquin, eds., 1, 236 (2008).

Appendix B

Supervision

Postdoctoral student

- Geoffrey Monet, jan. 2020-av. 2021, "Dielectric properties of nanoconfined water", co-supervised with Alexei Kornyshev

- Darka Labavič, jun. 2023-nov. 2024, "Electrolytes in confinement : a field theory approach".

PhD students

- Yorgos Chantziantoious (2023-...) starting a PhD on "Mitochondria: modelisation of the mechanical properties and ion fluxes".
- Jonathan Hedley (2020-2024) co-supervised with Alexei Kornyshev
- Anton Robert (2019-2022) participation of the supervision with Marie-Laure Bocquet.

Master students

Master students : Yorgos Chantziantoious (M2 2023), Julien Wychovaniak (M1, 2022) co-supervised with Laura Messio (LPTMC, Sorbonne) Morgane Berkane (M1, 2020), Toni Mendes (M2, 2020), Nirbhay Patil (M1, 2019), co-supervised with Anne-Florence Bitbol (LJP, Sorbonne), Andrea Porro, (M2, 2019), Marin Vatin, (M2, 2018).

Appendix C

Teaching and animation of research

Teaching

- 2013 Thermodynamics, Undergraduate level, Sorbonne Université, Paris, (40h/an).
- 2015-2018 Mathematical methods for physicists, Undergraduate level, Sorbonne Université, Paris, (40h/an).
- 2015-2018 Statistical Physics, Undergraduate level, ESPCI, Paris (16h/an)
- 2021- Theoretical chemistry and kinetics, Undergraduate level, ENS, Paris. (18h/an)
- 2022 - Mathematics, Master 1 ESPCI (12h/an)

Animation of research

Administration of research

Member of the laboratory board (conseil de laboratoire) of the LPTMC

Referee

referee for Phys. Rev. E, Biophysical Journal, Journal of Fluids Mechanics, ...

Committee

Selection committee for assistant professor : in 2019 for LPTMC, in 2020 pour MSC, Paris. Participation to PhD jury (Anis Senoussi, 2020; Sohvi Luukkonen, 2020; Valentin Dru, 2020; Marin Vatin 2022; Jean-François Olivieri, 2022; Theo Hannequin, 2022)

Organization of a workshop

Organization with Maximilien Levesque (CR at Dep. Chemistry ENS and CEO of Aquemia) of a parisien workshop 'Physique des Liquides'. 3 editions: Mai 2018 at ENS, Paris, December 2018 at LPTMC, Sorbonne and June 2019 at PHENIX, Sorbonne.

Appendix D

Miscellaneous research topics

Active surfaces applied to mitochondria membranes

Many cellular organelles are membrane-bound structures with complex membrane composition and shape. Their shapes have been observed to depend on the metabolic state of the organelle, and the mechanisms that couple biochemical pathways and membrane shape are still actively investigated. We propose and study Helfrich models for inhomogeneous membrane and show a rich phase diagram of inhomogeneity induced shapes that are consistent with *in vivo* orgnelle shape. We apply this model to describe the shape change of mitochondria membrane. This organelle is named the power house of the cell as it is the place of ATP synthesis Cristae membrane changes shape with the metabolic state and we show that this can be modeled by a coupling between the mechanical properties of the membrane and a surface pH flux established by the transmembrane proteins of the organelle (publications 1 and 7 of the list). In the previous works, we modeled the pH gradient as an input generated the proteins which are unaffected by the mechanical shape of the membrane. We will introduce a coupling between the rates of proton injection and consumption by the proteins and the local membrane shape. This coupling has been measured in *in vitro* system and coud explain the interplay between shape and function for this organelle.

Analytical chemistry

This is a new work started one year ago in collaboration with L. Messio (LPTMC), and Robba Moumné (LBM). Dynamic combinational chemistry is an efficient way to synthetize peptides via grafting aminoacids (AA) on a well-ordered backbones. However, it can be difficult to determine the composition of the reactive mixture as its complexity overtakes the performances of analysis methods available in labs. Here, we are developing a method based on statistical physics to describe the reactive mixture. The backbones are modeled as grids, the AA are spins associated with self energy and coupling energy between two sites. The energy of all the possible peptides can be expressed as a function of a limited number of parameters which are inferred to reproduce partial analysis data furnished by experimentalists. The preliminary results are encouraging.

Bibliography

[1] A. C. Fogarty, E. Duboué-Dijon, F. Sterpone, J. T. Hynes, and D. Laage. Biomolecular hydration dynamics: a jump model perspective. *Chem. Soc. Rev*, 42:5672–5683, 2013.

[2] M.-C. Bellissent-Funel, A. Hassanali, R. Henchman, P. Pohl, F. Sterpone, D. van der Spoel, Y. Xu, and A. E. Garcia. Water determines the structure and dynamics of proteins. *Chem. Rev.*, 116:7673–7697, 2016.

[3] D. T. Limmer, C. Merlet, M. Salanne, D. Chandler, P. A. Madden, R. V. Roij, and B. Rotenberg. Charge fluctuations in nanoscale capacitors. *Phys. Rev. Lett.*, 111:106102, 2011.

[4] B. Cabane and S. Hénon. *Liquides. Solutions, dispersions, émulsion, gels.* Dumas-Titoulet, 2003.

[5] P. A. Bopp, A. A. Kornyshev, and G. Sutmann. Static nonlocal dielectric function of liquid water. *Phys. Rev. Lett.*, 76:1280, 1996.

[6] I-C. Yeh and M. L. Berkowitz. Ewald summation for systems with slab geometry. *The Journal of Chemical Physics*, 111(7):3155–3162, August 1999.

[7] A. A. Kornyshev, A. I. Rubinshtein, and M. A. Vorotynstev. Model of non local electrostatics. I. *J. Phys. C: Solid State Physics*, 11:3307–3321, 1976.

[8] A. A. Kornyshev. Nonlocal screening of ions in a structurized polar liquid — new aspects of solvent description in electrolyte theory. *Electrochimica Acta*, 26:1–20, 1981.

[9] A. A. Kornyshev. Nonlocal electrostatics of solvation. In R. R. Dogonadze, E. Kalman, A. A. Kornyshev, and J. Ulstrup, editors, *The Chemical Physics of Solvation, Part A*, page 77. Elsevier, 1985.

[10] L. Bocquet and E. Charlaix. Nanofluidics, from bulk to interfaces. *Chem. Soc. Rev.*, 3:1073–1095, 2010.

[11] A. Siria, P. Poncheral, A-L. Biance, R. Fulcrand, X. Blase, S. T. Purcell, and L. Bocquet. Giant osmotic energy conversion measured in a single transmembrane boron nitride nanotube. *Nature*, 494:455–458, 2013.

[12] L. Fumagalli, A. Esfandiar, R. Fabregas, S. Hu, P. Ares, A. Janardanan, Q. Yang, B. Radha, T. Taniguchi, K. Watanabe, G. Gomila, K. S. Novoselov, and A. K. Geim. Anomalously low dielectric constant of confined water. *Science*, 360(6395):1339–1342, 2018.

[13] Y. Chen, H. I. Okur, N. Gomopoulos, C. Macias-Romero, P. S. Cremer, P. B. Petersen, G. Tocci, D. M. Wilkins, C. Liang, M. Ceriotti, and S. Roke. Electrolytes induce long-range orientational order and free energy changes in the H-bond network of bulk water. *Sci. Adv.*, 2:e1501891, 2016.

[14] M. Grechko, T. Hasegawa, F. D'Angelo, H. Ito, D. Turchinovich, Y. Nagata, and M. Bonn. Coupling between intra- and intermolecular motions in liquid water revealed by two-dimensional terahertz-infrared-visible spectroscopy. *Nature Communications*, 9(32):885, 2018.

[15] H. Berthoumieux, C. Antoine, A. Lemarchand, and L. Jullien. Resonant response to temperature modulation for enzymatic dynamics characterization. *Phys. Rev. E*, 79:021906, 2009.

[16] K. Zrelli, T. Barilero, E. Cavatore, H. Berthoumieux, T. Le Saux, V. Croquette, A. Lemarchand, C. Gosse, and L. Jullien. Temperature modulation and quadrature detection for selective titration of two-state exchanging reactants. *Anal. Chem.*, 83:2476–2484, 2011.

[17] H. Berthoumieux and A. C. Maggs. Fluctuation-induced forces governed by the dielectric properties of water- a contribution to the hydrophobic interaction. *J. Chem. Phys.*, 143:104501, 2015.

[18] J.-L. Maître, H. Berthoumieux, S. F. G. Krens, G. Salbreux, F. Jülicher, E. Paluch, and C-P. Heisenberg. Adhesion function in cell sorting by mechanically coupling the cortices of adhering cells. *Science*, 33:253–256, 2012.

[19] H. Berthoumieux, J.-L. Maître, C-P. Heisenberg, E. Paluch, F. Jülicher, and G. Salbreux. Active elastic thin shell theory for cellular deformation, New Journal of Physics. *Science*, 16:065005, 2014.

[20] F. Paillusson and H. Berthoumieux. Dielectric response in the vicinity of an ion: A nonlocal and nonlinear model of the dielectric properties of water. *J. Chem. Phys.*, 150:094507, 2019.

[21] G. Monet, F. Bresme, A. Kornyshev, and H. Berthoumieux. Nonlocal dielectric response of water in nanoconfinement. *Phys. Rev. Lett.*, 126:216001, 2021.

[22] J. G. Hedley, H. Berthoumieux, and A. A. Kornyshev. The dramatic effect of water structure on hydration forces and the electrical double layer. *J. Phys. Chem. C*, 127:3604, 2023.

[23] H. Berthoumieux, G. Monet, and R. Blossey. Dipolar Poisson modeels in a dual view. *J. Chem Phys.*, 155:024112, 2021.

[24] N. Patil, S. Bonneau, A-F. Bitbol F. Joubert, and H. Berthoumieux. Mitochondrial cristae modeled as an out-of-equilibrium membrane driven by a proton field. *Phys. Rev. E*, 102(11):0224401, 2020.

[25] T. Mendes, J. Ranft, and H. Berthoumieux. Model of membrane deformations driven by a surface ph gradient. *Phys. Rev. E*, 108:014113, 2023.

[26] A. Robert, H. Berthoumieux, and M.-L. Bocquet. Coupled interactions at the ionic graphene/water interface. *Phys. Rev. Lett.*, 157:184801, 2023.

[27] V. Démery and D. S. Dean. The conductivity of strong electrolytes from stochastic density functional theory. *J. Stat. Mech.*, 16:023106, 2016.

[28] P. Mark and L. Nilsson. Structure and dynamics of the TIP3P, SPC, and SPC/E water models. *J. Phys. Chem. A*, 43:9954–9960, 2001.

[29] E. Lambros and F. Paesani. How good are polarizable and flexible models for water: Insights from a many-body perspective. *J. Chem. Phys.*, 153:060901, 2020.

[30] N. Kavokine, M-L. Bocquet, and L. Bocquet. Fluctuation-induced quantum friction in nanoscale water flows. *Nature*, 602(7895):84–90, February 2022.

[31] A. A. Hassanali, V. Cuny, J. Verdolino, and M. Parrinello. Aqueous solutions: state of the art in ab initio molecular dynamics. *Phil. Trans. R. Soc. A*, 372:2012482, 2014.

[32] V. Kapil, C. Schran, A. Zen, J. Chen, C. J. Pickard, and A. Michaelides. The first-principles phase diagram of monolayer nanoconfined water. *Nature*, 609:512–516, 2022.

[33] D. Chandler. Gaussian field model of fluids with an application to polymeric fluids. *Phys. Rev. E*, 48:2898, 1993.

[34] R. Evans. The nature of the liquid-vapour interface and other topics in the statistical mechanics of non-uniform, classical fluids. *Advances in Physics*, 28:143–200, 1979.

[35] K. Lum, D. Chandler, and J. D. Weeks. Hydrophobicity at small and large length scales. *Journal of Physical Chemistry B*, 103:4570–4577, 6 1999.

[36] D. Chandler. Interfaces and the driving force of hydrophobic assembly. *Nature*, 437:640–647, 9 2005.

[37] A. P. Willard and D. Chandler. Instantaneous liquid interfaces. *J. Phys. Chem. B*, 114:6704–6709, 2001.

[38] A. A. Kornyshev, S. Leikin, and G. Sutmann. Overscreening in a polar liquid as a result of coupling between polarization and density fluctuations. *Electrochimica Acta*, 42:849–865, 1 1997.

[39] A. C. Maggs and R. Everaers. Simulating nanoscale dielectric response. *Phys. Rev. Lett.*, 96:230603, 2006.

[40] G. Jeanmairet, M. Levesque, R. Vuilleumier, and D. Borgis. Molecular density functional theory of water. *Journal of Physical Chemistry Letters*, 4:619–624, 2 2013.

[41] F. Paillusson and R. Blossey. Slits, plates, and poisson-boltzmann theory in a local formulation of nonlocal electrostatics. *Phys. Rev. E*, 82(5):052501, November 2010.

[42] P. A. Bopp, A. A. Kornyshev, and G. Sutmann. Frequency and wave-vector dependent dielectric function of water: Collective modes and relaxation spectra. *J. Chem. Phys.*, 109(5):1939–1958, 1998.

[43] A. K. Soper and M. A. Ricci. Structure of high-density and low-density water. *Phys. Rev. Lett*, 84:2881, 2000.

[44] G. Jeanmairet, N. Levy, M. Levesque, and D. Borgis. Molecular density functional theory of water including density-polarization coupling. *J. Phys.: Condens. Matter*, 16:244005, 2016.

[45] R. Fuentes-Azcatl and J. Alejandre. Non-Polarizable Force Field of Water Based on the Dielectric Constant: TIP4P. *J. Phys. Chem. B*, 118:1263–1272, 2014.

[46] R. M. Becker, P. Loche, D. J. Bonthuis, D. Mouhanna, R. R. Netz, and H. Berthoumieux. Dielectric properties of aqueous electrolytes at the nanoscale. *ArXiv*, page 2303.14846, 2023.

[47] D. J. Bonthuis, S. Gekle, and R. R Netz. Profile of the static permittivity tensor of water at interfaces: Consequences for capacitance, hydration interaction and ion adsorption. *Langmuir*, 28(20):7679–7694, 2012.

[48] M. Vatin, A. Porro, N. Sator, J.-F. Dufrêche, and H. Berthoumieux. Electrostatic interactions in water: a nonlocal electrostatic approach. *Mol. Phys.*, 119:e1825849, 2021.

[49] P. A. Bopp, A. A. Kornyshev, and G. Phys. Rev. Lett. Frequency and wave-vector dependent dielectic function of water: Collective modes and relaxation spectra. *J. Chem. Phys.*, 109:1940–1958, 1998.

[50] A. A. Kornyshev and G. Sutmann. The shape of the nonlocal dielectric function of polar liquids and the implications for thermodynamic properties of electrolytes: A comparative study. *J. Chem. Phys.*, 104(4):1524–1544, 1996.

[51] A. Levy, M. Bazant, and A. A. Kornyshev. Ionic activity in concentrated electrolytes: Solvent structure effect revisited. *Chem. Phys. Lett.*, 738:136915, 2020.

[52] H. J. Liebe, G. A. Hufford, and T. Manabe. A model for the complex permittivity of water at frequencies below 1 thz. *International Journal of Infrared and Millimeter Waves*, 12:659–675, 7 1991.

[53] R. Buchner, J. Barthel, and J. Stauber. The dielectric relaxation of water between 0°c and 35°c. *Chemical Physics Letters*, 306:57–63, 6 1999.

[54] D. C. Elton. The origin of the debye relaxation in liquid water and fitting the high frequency excess response. *PCCP*, 19:18739–18749, 2017.

[55] A. De Ninno, E. Nikollari, M. Missori, and F. Frezza. Dielectric permittivity of aqueous solutions of electrolytes probed by thz time-domain and ftir spectroscopy. *Physics Letters A*, 384:126865, 12 2020.

[56] K. T. Wikfeldt, A. Nilsson, and L. G. M. Pettersson. Spatially inhomogeneous bimodal inherent structure of simulated liquid water. *PCCP*, 13:19918–19924, 11 2011.

[57] A. Nilsson and L. G. M. Pettersson. The structural origin of anomalous properties of liquid water. *Nat. Commun.*, 6:1–11, 12 2015.

[58] D. Pines. *The Many-Body Problem*. W. A. Benjamin, inc., 1962.

[59] H. Berthoumieux. Gaussian field model for polar fluids as a function of density and polarization: Toward a model for water. *J. Chem. Phys.*, 148:104504, 3 2018.

[60] Y. S. Badyal, S.-L. Saboungi, D. L. Price, S. D. Shastri, D. K. Haeffner, and A. K. Soper. Electron distribution in water. *J. Chem. Phys.*, 112:9206–9208, 2000.

[61] A. A. Kornyshev and G. Sutmann. Nonlocal dielectric saturation in liquid water. *Phys. Rev. Lett.*, 79:3435, 1997.

[62] A. Abrashkin, A. Andelman, and H. Orland. Dipolar poisson-boltzmann equation: Ions and dipoles close to charge interfaces. *Phys. Rev. Lett.*, 99:077801, 2007.

[63] D. Frydel. Mean-field electrostatics beyond the point-charge description. *Adv. Chem. Phys.*, 160:209–260, 2016.

[64] A. Levy, D. Andelman, and H. Orland. Dielectric constant of ionic solutions: A field-theory approach. *Phys. Rev. Lett.*, 108:227801, 2012.

[65] A. Levy, D. Andelman, and H. Orland. Dipolar poisson-boltzmann approach to ionic solutions: A mean field and loop expansion analysis. *J. Chem. Phys.*, 139:164909, 2013.

[66] A. C. Maggs. A minimizing principle for the poisson-boltzmann equation. *Europhys. Lett.*, 98:16012, 2012.

[67] J. Pujos and A. C. Maggs. *Legendre transforms for electrostatic energies.*

[68] G. Monet, F. Bresme, A. A. Kornyshev, and H. Berthoumieux. The nonlocal dielectric response of water in nanoconfinement. *Phys. Rev. Lett.*, 126:216001, 2 2021.

[69] H. E. Alper and R. M. Levy. Field strength dependence of dielectric saturation in liquid water. *J. Chem. Phys.*, 94:8401–8403, 1990.

[70] M. V. Fedorov and A. A. Kornyshev. Unravelling the solvent response to neutral and charged solutes. *Molecular Physics*, 105:1–16, 1 2007.

[71] P. Bopp, G. Jancsó, and K. Heizinger. An improved potential for non-rigid water molecules in the liquid phase. *Chem. Phys. Lett.*, 98:129–133, 1983.

[72] H. Li and M. Kardar. Fluctuation-induced forces between rough surfaces. *Phys. Rev. Lett.*, 67:3275–3279, 1991.

[73] H. Li and M. Kardar. Fluctuation-induced forces between two manifolds immersed in correlated fluids. *Phys. Rev. A.*, 46:6490–6500, 1991.

[74] X. Song, D. Chandler, and R. A. Marcus. Gaussian Field Model of Dielectric Solvation Dynamics. *J. Phys. Chem.*, 100:11954–11959, 1996.

[75] J. B. Hasted, D. M. Ritson, and C. H. Collie. Dielectric properties of aqueous ionic solutions. part i and ii. *J. Chem. Phys.*, 16:1–21, 1948.

[76] N. Gavish and K. Promislow. Dependence of the dielectric constant of the electrolyte solutions on ionic concentration: a microfield approach. *Phys. Rev. E*, 94:012611, 2016.

[77] O. Björneholm, M. H. Hansen, A. Hodgson, L-M. Liu, D. T. Limmer, A. Michaelides, P. Pedevilla, J. Rossmeisl, H. Shen, G. Tocci, E. Tyrode, M.-M. Walz, J. Werner, and H. Bluhm. Water at interfaces. *Chem. Rev.*, 116:7698–7726, 2016.

[78] N. Kavokine, R. R. Netz, and L. Bocquet. Fluids at the nanoscale: From continuum to subcontinuum transport. *Annual Review of Fluid Mechanics*, 53:377–410, 2020.

[79] G. Gonella, E. H. G. Backus, Y. Nagata, J. D. Bonthuis, P. Loche, A. Schlaich, R. R. Netz, A. Künle, I. A. McCrum, M. T. M. Kopper, M. Wolf, B. Winter, G. Meijer, R. Kramer Campen, and M. Bonn. Water at charged interfaces. *Nature Reviews Chemistry*, 5:466–485, 2021.

[80] A. Schlaich, E. W. Knapp, and R. R. Netz. Water dielectric effects in planar confinement. *Phys. Rev. Lett.*, 117(4):048001, 2016.

[81] A. W. Omta, M. F. Kropman, S. Woutersen, and H. J. Bakker. Negligible effect of ions on the hydrogen-bond structure in liquid water. *Science*, 301:347–349, 2003.

[82] C. Zhang, S. Yue, A. Z. Panagiotopoulos, M. L. Klein, and X. Wu. Dissolving salt is not equivalent to applying pressure on water. *Nat. Commun.*, 13:822, 2022.

[83] V. Balos, N. K. Kaliannan, H. Elgabarty, M. Wolf, T. D. Kühne, and M. Sajadi. Time-resolved terahertz–raman spectroscopy reveals that cations and anions distinctly modify intermolecular interactions of water. *Nat. Chem.*, 14:1031–1037, 2022.

[84] A. P. Gaiduk and G. Galli. Local and global effects of dissolved sodium chloride on the structure of water. *J. Phys. Chem. Lett.*, 8:1496–1502, 2017.

[85] E. Pluhařova, D. Laage, and P. Jungwirth. Size and origins of long-range orientational water correlations in dilute aqueous salt solutions. *J. Chem. Phys. Lett.*, 8:2031–2035, 2017.

[86] A. A. Kornyshev. On the non-local electrostatic theory of hydration force. *Journal of Electroanalytical Chemistry and Interfacial Electrochemistry*, 204:79–84, 1986.

[87] M. V. Basilevsky and D. F. Parsons. Nonlocal continuum solvation model with exponential susceptibility kernels. *J. Chem. Phys.*, 108(21):9107–9113, 1998.

[88] A. Hildebrandt, R. Blossey, S. Rjasanow, O. Kohlbacher, and H.-P. Lenhof. Novel formulation of nonlocal electrostatics. *Phys. Rev. Lett.*, 93:108104, Sep 2004.

[89] D. Ben-Yaakov, D. Andelman, R. Podgornik, and D. Harries. Ion-specific hydration effects: Extending the poisson-boltzmann theory. *Current Opinion in Colloid & Interface Science*, 16:542–550, 2011.

[90] R. Blossey and R. Podgornick. Continuum theories of structured dielectrics. *EPL*, 139:27002, 2022.

[91] R. Blossey and R. Podgornick. Field theory of structured liquid dielectrics. *Phys. Rev. Research*, 4:023033, 2022.

[92] R. Blossey and R. Podgornick. A comprehensive continuum theory of structured liquids. *J. Phys. A Math. Theor.*, 56:025002, 2023.

[93] P. Loche, P. Steinbrunner, S. Friedowitz, Netz R. R., and D. J. Bonthuis. Transferable Ion Force Fields in Water from a Simultaneous Optimization of Ion Solvation and Ion–Ion Interaction. *J. Phys. Chem. B*, 125:8581–8587, 2021.

[94] M. Neumann. Dipole moment fluctuation formulas in computer simulations of polar systems. *Mol. Phys.*, 50:841–858, 1983.

[95] H. Flyvbjerg and H. G. Peetersen. Error estimates on averages of correlated data. *J. Chem. Phys.*, 91:461, 1989.

[96] R. R. Netz and H. Orland. Beyond poisson-boltzmann: Fluctuation effects and correlation functions. *EPJE*, 1:203–214, 2000.

[97] G. Salbreux, G. Charras, and E. Paluch. Actin cortex mechanics and cellular morphogenesis. *Trends Cell Biol*, 22(10):536–545, 2012.

[98] M. Murrell, P. W. Oakes, M. Lenz, and M. L. Gardel. Forcing cells into shape: the mechanics of actomyosin contractility. *Nat. Rev. Mol. Cell Biol.*, 16(8):486–498, 2015.

[99] F. Burla, Y. Mulla, B. E. Vos, A. Aufderhorst-Roberts, and G. H. Koenderink. From mechanical resilience to active material properties in biopolymer networks. *Nature Reviews Physics*, 1:249–263, 2019.

[100] L. Balabanian, A. R. Chaudhary, and A. G. Hendricks. Traffic control inside the cell: microtubule-based regulation of cargo transport. *The Biochemist*, 40(2):14–17, 2018.

[101] J. X. Tang and P. A. Janmey. The polyelectrolyte nature of F-actin and the mechanism of actin bundle formation. *J. Biol. Chem.*, 271(15):8556–8563, Apr 1996.

[102] S. Deshpande and T. Pfohl. Hierarchical self-assembly of actin in micro-confinements using microfluidics. *Biomicrofluidics*, 6(3):34120, 2012.

[103] D. J. Needleman, M. A. Ojeda-Lopez, U. Raviv, H. P. Miller, L. Wilson, and C. R. Safinya. Higher-order assembly of microtubules by counterions: from hexagonal bundles to living necklaces. *Proc. Natl. Acad. Sci. USA*, 101(46):16099–16103, 2004.

[104] L. Hamon, P. Savarin, P. A. Curmi, and D. Pastré. Rapid assembly and collective behavior of microtubule bundles in the presence of polyamines. *Biophys J*, 101(1):205–216, 2011.

[105] P. J. Chung, C. Song, J. Deek, H. P. Miller, Y. Li, M. C. Choi, L. Wilson, S. C. Feinstein, and C. R. Safinya. Tau mediates microtubule bundle architectures mimicking fascicles of microtubules found in the axon initial segment. *Nat Commun*, 7:12278, 07 2016.

[106] C. K. Park and N. C. Horton. Structures, functions, and mechanisms of filament forming enzymes: a renaissance of enzyme filamentation. *Biophys Rev*, 11(6):927–994, 2019.

[107] L. B. Pires, S. B. Ether, B. Spreng, G. R. S. Araújo, R. S. Decca, R. S. Dutra, M. Borges, F. S. S. Rosa, G.-L. Ingold, M. J. B. Moura, S. Frases, B. Pontes, H. M. Nussenzveig, S. Reynaud, N. B. Viana, and P. A. Maia Neto. Probing the screening of the casimir interaction with optical tweezers. *Phys. Rev. Research*, 3:033037, 2021.

[108] B. Spreng, H. Berthoumieux, A. Lambrecht, A-F. Bitbol, P. A. Maia Neto, and S. Reynaud. Universal casimir attraction between filaments at the cell scale. *arXiv*, page 2306.14059, 2023.

[109] S. V. Kalinin. Feel the dielectric force. *Science*, 360(6395):1302–1302, 2018.

[110] C. Zhang. Note: On the dielectric constant of nanoconfined water. *J. Chem. Phys.*, 148(15):156101, 2018.

[111] J. A. Schellman. The application of the bjerrum ion association theory to the binding of anions by proteins. *Journal of Physical Chemistry*, 57(4):472–475, 1953.

[112] V. Ballenegger and J.-P. Hansen. Dielectric permittivity profiles of confined polar fluids. *J. Chem. Phys.*, 122(11):114711, 2005.

[113] S. Chen, Y. Itoh, T. Masuda, S. Shimizu, J. Zhao, J. Ma, S. Nakamura, K. Okuro, H. Noguchi, K. Uosaki, and T. Aida. Subnanoscale hydrophobic modulation of salt bridges in aqueous media. *Science*, 348(6234):555–559, 2015.

[114] T. Sato, T. Sasaki, J. Ohnuki, K. Umezawa, and M. Takano. Hydrophobic surface enhances electrostatic interaction in water. *Phys. Rev. Lett.*, 121(20):206002, 2018.

[115] V. Bergeron. Forces and structure in thin liquid soap films. *J. Phys.: Condens. Matter*, 11(19):215–238, 1999.

[116] N. E. Levinger. Water in confinement. *Science*, 298(5599):1722–1723, 2002.

[117] E. Gouaux. Principles of selective ion transport in channels and pumps. *Science*, 310(5753):1461–1465, 2005.

[118] P. Fenter, S. Kerisit, P. Raiteri, and J. D. Gale. Is the calcite–water interface understood? direct comparisons of molecular dynamics simulations with specular x-ray reflectivity data. *J. Phys. Chem. C*, 117(10):5028–5042, 2013.

[119] A. Siria, M-L. Bocquet, and L. Bocquet. New avenues for the large-scale harvesting of blue energy. *Nature Reviews Chemistry*, 1(11):91, 2017.

[120] D. Muñoz Santiburcio and D. Marx. Nanoconfinement in slit pores enhances water self-dissociation. *Phys. Rev. Lett.*, 119:056002, 2017.

[121] D. Martin-Jimenez, E. Chacon, P. Tarazona, and R. Garcia. Atomically resolved three-dimensional structures of electrolyte aqueous solutions near a solid surface. *Nat. Commun.*, 7:1–7, 2016.

[122] S. S. Lee, A. Koishi, I. C. Bourg, and P. Fenter. Ion correlations drive charge overscreening and heterogeneous nucleation at solid-aqueous electrolyte interfaces. *Proc. Natl. Acad. Sci. USA*, 118:e2105154118, 8 2021.

[123] S. Leikin, V. A. Parsegian, D. C. Rau, and R. P. Rand. Hydration forces. *Annual Review of Physical Chemistry*, 44:369–395, 11 1993.

[124] J. N. Israelachvili and R. M. Pashley. Molecular layering of water at surfaces and origin of repulsive hydration forces. *Nature*, 306:249–250, 1983.

[125] V. A. Parsegian, R. P. Rand, N. L. Fuller, and D. C. Rau. Osmotic stress for the direct measurement of intermolecular forces. In *Biomembranes Part O: Protons and Water: Structure and Translocation*, volume 127 of *Methods in Enzymology*, pages 400–416. Academic Press, 1986.

[126] R. Lipowsky and W. Speth. Semi-infinite systems with first-order bulk transitions. *Physical Review B*, 28(7):3983–3993, 1983.

[127] A. Ajdari, B. Duplantier, D. Hone, L. Peliti, and J. Prost. "pseudo-casimir" effect in liquid crystals. *Journal de Physique II*, 2(3):487–501, 1992.

[128] John David Jackson. *Classical electrodynamics*. Wiley, New York, 1975.

[129] Lindahl, Abraham, Hess, and Spoel Van Der. Gromacs 2019 source code, 2018.

[130] P. Yang, Z. Wang, Z. Liang, H. Liang, and Y. Yang. A constant potential molecular dynamics simulation study of the atomic-scale structure of water surfaces near electrodes. *Chinese Journal of Chemistry*, 37(12):1251–1258, 2019.

[131] S. Varghese, S. K. Kannam, J S Hansen, and S P. Sathian. Effect of hydrogen bonds on the dielectric properties of interfacial water. *Langmuir*, 35(24):8159–8166, 2019.

[132] Q. A. Besford, A. J. Christofferson, J. Kalayan, J-U. Sommer, and R. H. Henchman. The attraction of water for itself at hydrophobic quartz interfaces. *J. Phys. Chem. B*, 124(29):6369–6375, 2020.

[133] P. Loche, C. Ayaz, A. Wolde-Kidan, A. Schlaich, and R. R. Netz. Universal and nonuniversal aspects of electrostatics in aqueous nanoconfinement. *J. Phys. Chem. B*, 124(21):4365–4371, 2020.

[134] A. A. Kornyshev and J. Ulstrup. Solvent structural effects on the diffuse double layer capacitance of metal electrolyte interfaces. *Chemica Scripta*, 25:58–62, 1985.

[135] J. J. Bikerman. Structure and capacity of the electrical double layer. *The London, Edinburgh, and Dublin Philosophical Magazine and Journal of Science*, 33(220):384–397, 1942.

[136] M. Z. Bazant, M. S. Kilic, B. D. Storey, and A. Ajdari. Towards an understanding of induced-charge electrokinetics at large applied voltages in concentrated solutions. *Advances in Colloid and Interface Science*, 152:48–88, 11 2009.

[137] I. Borukhov, D. Andelman, and H. Orland. Steric effects in electrolytes: A modified poisson-boltzmann equation. *Phys. Rev. Lett.*, 79:435, 7 1997.

[138] A. A. Kornyshev. Double-layer in ionic liquids: Paradigm change? *J. Phys. Chem. B*, 111:5545–5557, 5 2007.

[139] D. Martin-Jimenez, E. Chacon, P. Tarazona, and R. Garcia. Atomically resolved three-dimensional structures of electrolyte aqueous solutions near a solid surface. *Nat. Commun.*, 7:1–7, 7 2016.

[140] V. A. Parsegian and T. Zemb. Hydration forces: Observations, explanations, expectations, questions. *Current Opinion in Colloid & Interface Science*, 16:618–624, 2011.

[141] M. Kanduč, A. Schlaich, E. Schneck, and R. R. Netz. Hydration repulsion between membranes and polar surfaces: Simulation approaches versus continuum theories. *Adv. Colloid Interface Sci.*, 208:142–152, 2014.

[142] S. Perkin, L. Chai, N. Kampf, U. Raviv, W. Briscoe, I. Dunlop, S. Titmuss, M. Seo, E. Kumacheva, and J. Klein. Forces between mica surfaces, prepared in different ways, across aqueous and nonaqueous liquids confined to molecularly thin films. *Langmuir*, 22:6142–6152, 7 2006.

[143] C. Stanley and D. C. Rau. Evidence for water structuring forces between surfaces. *Current opinion in colloid & interface science*, 16:551, 2011.

[144] J. N. Israelachvili. *Intermolecular and surface forces.* Academic Press, 2nd edition, 1992.

[145] H. J. Butt. Measuring electrostatic, van der waals, and hydration forces in electrolyte solutions with an atomic force microscope. *Biophys. J.*, 60:1438–1444, 1991.

[146] B. V. Derjaguin, N. V. Churaev, and V. M. Muller. *Surface Forces.* Springer New York, NY, 1987.

[147] S. Marčelja and N. Radić. Repulsion of interfaces due to boundary water. *Chem. Phys. Lett.*, 42:129–130, 1976.

[148] R. M. Pashley and J. N. Israelachvili. Molecular layering of water in thin films between mica surfaces and its relation to hydration forces. *Journal of Colloid and Interface Science*, 101:511–523, 1984.

[149] D. A. Cherepanov. Force oscillations and dielectric overscreening of interfacial water. *Phys. Rev. Lett.*, 93:266104, 2004.

[150] R. M. Pashley. Hydration forces between mica surfaces in aqueous electrolyte solutions. *Journal of Colloid and Interface Science*, 80:153–162, 1981.

[151] R. G. Horn, D. T. Smith, and W. Haller. Surface forces and viscosity of water measured between silica sheets. *Chemical Physics Letters*, 162:404–408, 1989.

[152] A. A. Kornyshev, M. A. Vorotyntsev, and J. Ulstrup. The effect of spatial dispersion of the dielectric permittivity on the capacitance of thin insulating films: Non-linear dependence of the inverse capacitance on film thickness. *Thin Solid Films*, 75(2):105–118, 1981.

[153] V. Kaiser, J. Comtet, A. Nigues, A. Siria, B. Coasne, and L. Bocquet. Electrostatic interactions between ions near thomas–fermi substrates and the surface energy of ionic crystals at imperfect metals. *Faraday Discuss.*, 199:129–158, 2017.

[154] M. Vatin, A. Porro, N. Sator, J.-F. Dufrêche, and H. Berthoumieux. Electrostatic interactions in water: a nonlocal electrostatic approach. *Mol. Phys.*, page e1825849, 2020.

[155] P. Loche, C. Ayaz, A. Schlaich, Y. Uematsu, and R. R. Netz. Giant axial dielectric response in water-filled nanotubes and effective electrostatic ion–ion interactions from a tensorial dielectric model. *The Journal of Physical Chemistry B*, 123(50):10850–10857, 2019.

[156] L. Joly, R. H. Meißner, M. Iannuzzi, and G. Tocci. Osmotic transport at the aqueous graphene and hbn interfaces: Scaling laws from a unified, first-principles description. *ACS Nano*, 15:15249–15258, 2021.

[157] A. Coretti, C. Bacon, R. Berthin, A. Serva, L. Scalfi, I. Chubak, K. Goloviznina, M. Haefele, A. Marin-Laflèche, B. Rotenberg, S. Bonella, and M. Salanne. Metalwalls: Simulating electrochemical interfaces between polarizable electrolytes and metallic electrodes. *J. Chem. Phys.*, 157:184801, 2021.

[158] S. Carlson, F. N. Brünig, P. Loche, D. J. Bonthuis, and R. R. Netz. Exploring the absorption spectrum of simulated water from mhz to infrared. *J. Phys. Chem. A*, 124:5599–5605, 2020.

[159] T. Hennequin, M. Manghi, A. Noury, F. Henn, V. Jourdain, and J. Palmeri. Quantum capacitance governs electrolyte conductivity in carbon nanotubes. *arXiv:2307.12071*, 2023.

[160] G. Tocci, L. Joly, and A. Michaelides. Friction of water on graphene and hexagonal boron nitride from ab initio methods: Very different slippage despite very similar interface structures. *Nano Letters*, 14(12):6872–6877, 2014.

[161] P. Mitchell. Coupling of phosphorylation to electron and hydrogen transfer by a chemiosmotic type of mechanism. *Nature*, 191(4784):144–148, 1961.

[162] J. Heberle, J. Riesle, G. Thiedemann, D. Oesterhelt, and N. A. Dencher. Proton migration along the membrane surface and retarded surface to bulk transfer. *Nature*, 370:379–382, 1994.

[163] D. A. Cherepanov, B. Feniouk, W. Junge, and A. Y. Mulkidjanian. Low dielectric permittivity of water at the membrane interface: effect on the energy coupling mechanism in biological membranes. *Biophys. J.*, 85(2):1307–1316, 2003.

[164] T. B. Blum, A. Hahn, T. Meier, K. M. Davies, and W. Kühlbrandt. Dimers of mitochondrial atp synthase induce membrane curvature and self-assemble into rows. *Proc. Nat. Acad. Soc. USA*, 116:4250–4255, 2019.

RÉSUMÉ

Ce mémoire d'habilitation à diriger les recherches présente un cadre de théorie statistique des champs pour étudier les propriétés diélectriques de l'eau et des électrolytes à petite échelle. Le nanomètre est la taille de confinement typique des dispositifs technologiques et biologiques, la longueur de Debye des solutions ioniques faiblement concentrées, ainsi que l'échelle à laquelle l'eau commence à se comporter comme un milieu moléculaire. Les simulations sont souvent utilisées pour étudier ces systèmes, mais elles ne fournissent pas "l'équation maîtresse" qui les gouverne. Nous décrivons ici l'eau comme un milieu diélectrique corrélé. Nous développons des fonctionnelles de la polarisation pour modéliser la structure moléculaire du fluide et nous construisons un cadre analytique minimal pour étudier les propriétés des solutions aqueuses. Nous incluons une modélisation du confinement et nous identifions les éléments qui gouvernent l'interaction entre la structure des électrolytes et les propriétés de la surface de confinement. Nous proposons ainsi une approche systématique pour étudier les électrolytes à l'échelle nanométrique.

MOTS CLÉS

Electrostatique aux échelles nanométriques - Eau et électrolytes - Théorie statistique des champs

ABSTRACT

This habilitation manuscript presents a framework based on statistical field theory to study the dielectric properties of water and electrolytes at small scale. The nanometer scale is the typical confinement size of technological and biological devices, the screening length of low-concentrated ionic solutions, as well as the range at which water starts to behave as a discrete molecular medium. Simulations are often used to study these systems, but they do not provide the "master equation" that governs them. Here, we describe water as a correlated dielectric medium. We develop functionals of the polarization to capture the molecular structure of the fluid and build a minimal analytical framework to study the properties of aqueous solutions. We include a modelization of the confinement and identify the key elements that govern the interplay between the structure of the electrolytes and the properties of the confining surface. We thus provide a versatile approach to studying electrolytes at the nanoscale.

KEYWORDS

Electrostatics at the nanoscale - Water and electrolytes - Statistical field theory